

Università degli Studi di Genova

Facoltà di Scienze M.F.N.

Tesi di Dottorato in Fisica

XVIII ciclo

**Analytical models of turbulence:
from large scales to small scales,
and beyond**

Relatori: Prof. Roberto Festa
Dott. Andrea Mazzino

Relatore esterno: Prof. Guido Boffetta

Candidato: Marco Martins Afonso

Acknowledgements - Ringraziamenti

Chi mi conosce, sa che non sono molto bravo in questo compito, né portato a dilungarmi. E chi, non conoscendomi, non lo sa... beh, lo scoprirà adesso! Ritengo opportuno ringraziare innanzitutto i miei relatori: Roberto Festa, che mi ha permesso di scoprire quanto interessante sia la fluidodinamica, e Andrea Mazzino, che mi ha costantemente seguito e guidato da vicino in questo lavoro. Ringrazio inoltre Guido Boffetta, che ha accettato l'incarico di relatore esterno.

Insieme a loro, ringrazio tutti quelli che hanno collaborato dal punto di vista scientifico alle diverse pubblicazioni: in particolare Antonio Celani, che è stato l'ispiratore di gran parte di esse. E naturalmente, tutti i componenti del gruppo di Fisica dell'Atmosfera e dell'Oceano, con cui ho lavorato fianco a fianco in questi anni: mi sia permesso, anche in questo caso, di non elencarli tutti.

Desidero inoltre ringraziare Grisha Falkovich e tutto lo staff del Weizmann Institute of Science di Rehovot, che mi ha accolto in Israele durante l'ultimo periodo di scrittura di questa tesi.

Infine, un grazie a tutti coloro che, negli anni, mi hanno permesso di raggiungere questo traguardo: insegnanti, amici e soprattutto i miei familiari, per avermi sempre supportato nella mia carriera; grazie sia a quelli che ci sono ancora, sia a quelli che non ci sono più.

Contents

Introduction	ix
Publications	xv
I Turbulence at mesoscopic scales	1
1 Is the inertial-range scaling a genuine property of turbulence?	3
1.1 Introduction: the four-fifths law and its implications	4
1.2 Multifractal and multiplicative models	5
1.3 Large-deviation theory and saddle-point approximation	8
1.3.1 Classical multifractal results	10
1.3.2 How spurious logarithmic corrections generate	12
1.3.3 The way to solve the paradox of logarithmic corrections	12
1.3.4 Other ways to produce spurious logarithms and how to rule them out	13
1.4 Conclusion: back to multifractal turbulence	14
1.5 Appendix: the Novikov–Stewart model	15
2 Exact results for nonideal turbulence	19
2.1 Introduction	21
2.2 The two-point equal-time scalar correlation function	22
2.2.1 Homogeneous isotropic case	22
2.2.2 Extension to the inhomogeneous anisotropic case	25
2.2.3 Analysis of the inhomogeneous isotropic case	31
2.3 Random point-source emission	37
2.4 Conclusions	42

2.5	Appendix on calculation details	43
2.6	Appendix on constant point-source emission	46
II	Turbulence at macroscopic scales	51
3	Analytical models for closures	53
3.1	Introduction	54
3.2	Large-eddy simulation for passive scalar turbulence	55
3.2.1	Basic equation and phenomenology	55
3.2.2	Definition of the filtering process	56
3.2.3	The problem of closure in the large scale	56
3.2.4	Structure of small-scale contributions	57
3.3	An example of exact closure	58
3.4	Kraichnan advection model	59
3.4.1	Basic properties and known results	59
3.4.2	Second-order correlation function of the coarse-grained passive scalar	60
3.4.3	Properties of the filtered velocity and forcing	61
3.4.4	Analysis of the filtered equation	61
3.5	Examples of analytical closures	63
3.5.1	Importance of small-scale contributions	63
3.5.2	Constant-eddy-diffusivity closure	64
3.5.3	Improved closure	66
3.5.4	An alternative closure	68
3.5.5	Absence of eddy diffusivity	69
3.5.6	Absence of second-order correction	69
3.6	Conclusions	70
3.7	Appendix on exact analytical expressions	72
3.7.1	Coarse-grained passive scalar	72
3.7.2	Coarse-grained velocity	74
3.8	Appendix on limit cases	74
3.8.1	Purely diffusive flow	74
3.8.2	Smooth flow	75
3.9	Appendix on small-scale correlations	76

4	Numerical results for the statistics of large excursions	79
4.1	Introduction	81
4.2	Global scale invariance and its violation	83
4.3	Fronts: mature vs nonmature objects	86
4.3.1	An example from passive scalar advection	86
4.3.2	A quantitative definition of mature and nonmature fronts	87
4.4	Weak events: cancelled vs uncanceled objects	89
4.5	The large-eddy simulation model	91
4.6	The simulated convective boundary layers	92
4.6.1	The quasi-steady state for the simulated boundary layers	94
4.7	Analysis of results and discussions	95
4.7.1	Statistics of large temperature fluctuations	95
4.7.2	Dominance of nonmature fronts	110
4.7.3	Statistics of weak temperature fluctuations	112
4.7.4	Characterizing weak temperature excursions	112
4.8	Sensitivity test at higher resolution	113
4.9	Conclusions and perspectives	117
III	Toward the turbulence of complex fluids	121
5	The role of inertia: heavy particles and bubbles	123
5.1	Introduction	124
5.2	Basic equations and multiscale technique	125
5.3	Second-quantization algorithm	128
5.4	Equations for the falling velocity	132
5.5	Future work	133
6	Polymer relaxation time in FENE model	135
6.1	Introduction	136
6.2	Coil-stretch transition	138
6.2.1	Stationary regime	139
6.2.2	Relaxation to the stationary regime	142
6.3	Fokker–Planck equation	143
6.4	Relaxation time	144
6.5	Summary and discussion	146
	Bibliography	149

Summary - Riassunto

161

Introduction

This thesis collects the work performed during my Ph.D. activity, concerning the study of turbulence mainly from the analytical point of view. The manuscript is subdivided into three parts, containing two chapters each. Citations consisting in numbers between square braces are relative to the general bibliography at the end of the manuscript. Capital letters between round braces refer to the list of my own publications, placed after this introduction.

The guideline of my work consisted in the consideration that, despite a huge range of scales of motion are excited and nonlinearly coupled in turbulent flows, it is nevertheless possible to individuate at which scales different phenomena take place and other effects are negligible, and at the same time one can extract a whole range of scales, extending for several orders of magnitude, where universal behaviours are expected, independently of external intervention and boundary constraints.

The study of turbulence has a greater and greater relevance in the framework of fluid dynamics, also because it is connected to mathematical concepts of chaos dynamics which developed only in these last few decades (one may think, in way of example, to fractal and multifractal theories [1]). The most relevant contribution was however given by Kolmogorov at the half of the last century (the famous theory K41, expressed in 1941 [2]), even if Leonardo da Vinci already had a precise idea of the physical phenomena taking part in turbulence [1].

A very important role, in defining the different sceneries emerging in the study of turbulent flows, is played by the “Reynolds number” (Re), defined as the adimensional ratio $Re = UL/\nu$, U , L and ν being the typical velocity and size of the flow and the kinematic viscosity of the fluid, respectively. In way of example, if one considers the flow around a cylinder, its radius may be identified as the typical length L , while a characteristic speed U can be defined as the mean value of the velocity over the whole volume.

For values $Re \ll 1$, the linear terms are dominant in the equations describing the flow dynamics: laminar flows are expected, showing “simple” behaviours which can often be described by exact solutions.

In the intermediate region, $Re \approx O(1)$, nonlinear effects act in competition with purely dissipative ones: the flow develops nonstationary behaviours, the velocity field gets complicated, the Fourier analysis of its frequency spectrum shows a growing number of excited modes, until a critical value Re_c (strongly dependent on geometry and external forcing, thus nonuniversal).

For $Re > Re_c$ the fluid shows a sharp transition: the spectrum becomes continuous, the flow turns highly nontrivial (at least in its temporal characteristics), features related to transport are sensibly amplified.

For $Re \rightarrow \infty$ (that is, $Re \gg Re_c$, such a regime is known as “fully-developed turbulence”), the (apparent) aleatory character also extends to the spatial behaviour of the velocity field: the number of excited temporal frequencies and spatial scales tends to infinity, and the same is for the number of degrees of freedom necessary to correctly describe the flow dynamics. Apart from some considerations in chapter 5, which apply to general flows (also laminar ones), I will exclusively focus my attention on this regime.

From the phenomenological point of view, fully-developed turbulence consists in a hierarchy of turbulent eddies on different spatial and temporal scales. The instability of large-scale eddies generates smaller-scale eddies which, becoming themselves unstable, give rise to similar structures on scales even smaller, and so on. The basic idea, on which Kolmogorov built up his K41 theory, derives from Richardson’s concept of turbulent cascade. According to this vision, the energy injected into the system at a large scale creates strong correlations in the velocity fields between points distant this same scale from each other, and such correlations are associated with the presence of eddies. Energy thus flows from large scales (small wavenumbers) to small scales (large wavenumbers, where dissipative terms become relevant and stop the cascade), through a process of eddy fragmentation. Such a process is local, in the sense that eddies at each scale are generated by the fragmentation of eddies at a scale just larger, and is self-similar, i.e. it does not depend on the observation scale.

Part I: Turbulence at mesoscopic scales

Self-similarity at different scales is a key point in fully-developed turbulence, in the sense that it accounts for the existence of a wide range of scales where

universal behaviours are expected and the “matching” with large- and small-scale constraints is reducible to the knowledge of some parameters, as the external energy input rate. This range of scales is called *inertial* and presents some universal features, like the scaling exponents of the velocity structure functions. Chapter 1 is meant to clarify some points about this degree of universality, in particular the absence of logarithmic corrections in scaling power laws. The analysis presented here is essentially based on an article written together with Uriel Frisch, Andrea Mazzino and Victor Yakhot (A).

When under investigation is not the flow itself, but a physical quantity transported by it, one may however find the analogous of the inertial range. Specifically, in chapter 2, I will focus on *passive scalar advection*, i.e. I will study scalar fields which are advected by the surrounding turbulent flow but that do not affect it. A common example is provided by the concentration of a tracer (by definition) or even of a pollutant, if its density is sufficiently similar to the one of the fluid and the feedback on the flow is negligible: this means, e.g., the absence of both chemical reactions and “mechanical” modification of the streamlines. Analogously, the temperature field can be assumed as passive if buoyancy effects are negligible.

The *convective* range (the passive scalar counterpart of the inertial one) shows universal scaling properties in ideal situations, for instance in the presence of homogeneity and isotropy. When these conditions are not satisfied by the large-scale constraints (as usually is in practical situations), the question of a possible small-scale restoration of homogeneity or isotropy arises. In a context similar to passive scalar transport, provided by magnetohydrodynamics (the study of magnetic field advection), it has been shown [3, 4, 5, 6, 7] that anisotropy persists at small scales. The objective of the chapter will be the study of situations in which inhomogeneities play a significant role (first from a generic point of view and later focusing on a specific case, the point-source emission), and the investigation of their effect on universality. I will report results discussed in two articles, the former — already published — with Mauro Sbragaglia (B) and the latter — in preparation — with Antonio Celani and Andrea Mazzino (C).

Part II: Turbulence at macroscopic scales

From a quantitative point of view, in principle it would be possible to build the statistical mechanics of turbulence starting from first principles (i.e. the equations for the turbulent flow); unfortunately, any such analytical the-

ory of turbulence necessarily faces “closure” problems. Indeed, writing the equations for a statistical n -th order moment, one immediately notices the appearance of moments of order $n + 1$; the equations for the latter present moments of order $n + 2$, and so on. Such difficulties, typical of nonlinear systems, also hold for turbulent systems linear in the unknown field but nonlinearly interacting with the velocity field. On the other hand, the strongly non-Gaussian character of the flow in fully-developed turbulence makes any perturbative approach useless.

From a conceptual point of view, one can build a numerical approach, which amounts to numerically solve (with a powerful computer) the partial differential equations ruling turbulent flows. Despite the typical space-time irregularity of velocity, derivatives are well-defined: thanks to viscosity, velocity differences at very small scales are indeed “smooth”. However, a direct simulation of a turbulent flow must explicitly take into account all excited scales of motion, ranging from the largest, whose size is typically imposed by boundary conditions (the so-called “integral scale”), to the smallest, associated with dissipative effects due to molecular motion (“Kolmogorov scale”). For instance, a direct simulation of the atmosphere would require the description of $\sim 10^{27}$ degrees of freedom, whose number scales as $Re^{3/4}$ in each spatial direction for large Re : such numbers are clearly too large also for any modern, powerful computer. Consequently, for a small-viscosity fluid, it is not possible, now or in a near future, to explicitly simulate all active scales for a turbulent flow.

Nevertheless, such a problem does not exclude the possibility of a numerical description. Back to Richardson’s concept of turbulent cascade, one is often not interested in describing the complete dynamics down to small scales. The idea is then to artificially stop the energy flux at an intermediate scale, much smaller than the integral one (so as not to be affected by large-scale, boundary details) but much larger than the Kolmogorov dissipative scale. In this way, only eddies larger than such a “cutoff” scale are dynamically described, while the remaining, smaller ones are “parameterized” (i.e. dealt with statistically): as a result, the number of degrees of freedom is drastically reduced. This strategy is called “large-eddy simulation”. In view of what previously stated, it is easy to find the critical point of such a scheme. Indeed, in the absence of closed equations for the small scales of motion, most of nowadays parameterizations are empirical, and thus not based on first principles. It is then difficult, if not impossible, to quantify the impact of the closure on large-scale fields.

The situation is even more difficult when different turbulent systems are supposed to interact with each other. One of the best-known example is the temperature field in a turbulent flow, which, depending on the role of buoyancy, may (as already said) behave as an active or a passive scalar. If very few exact results on the closure problem are known for non interacting turbulent systems, the situations is even worst in the presence of interaction. The aim of chapter 3 is to provide some exact results for a particular class of turbulent systems: the passive scalar turbulence. This problem is *per se* interesting in connection, e.g., to numerical studies of atmospheric pollutants in the atmosphere, but it might also give useful suggestions on how to generalize the results to active scalar fields and, hopefully, to hydrodynamic turbulence (this latter point is however, at the present stage, far from being achieved). The parameterization of small scales will be derived from first principles, thus allowing one to completely keep under control the statistical effect of closures on the large, dynamically described scales of motion, and to rigorously justify the large-eddy simulation strategy.

I will report the analysis based on my Laurea thesis (D) and later presented in two articles and two proceedings — in both cases, one already published (E,F) and the other submitted (G,H) — in collaboration with Antonio Celani, Roberto Festa and Andrea Mazzino.

Once the closures are well established and justified from the analytical point of view, the following step is obviously provided by their application to the numerical study of real situations, as (in way of example) flows of geophysical relevance. In chapter 4 I will show the results of several numerical simulations performed on the atmospheric boundary layer, aiming to quantitatively verify some of the aspects discussed in the first part, and published in an article (I) by Marta Antonelli, Andrea Mazzino and Umberto Rizza.

Part III: Toward the turbulence of complex fluids

Everyday experience shows the relevance of understanding the behaviour of small particles advected by (turbulent or regular) flows. Beside the study of the evolution of the velocity field itself, and of a passive scalar transported by it, it is therefore necessary to consider complex, or nonideal, fluids. The complexity may arise, e.g., from inertial effects, when the particle mass cannot be neglected also in relation to gravity, or from the internal structure of such particles, which are often far from being modelled as point masses. The last word of the title of this manuscript, which refers to its last part, is meant

to indicate that a different degree of complexity in the physical description of these phenomena is required; the minimal-complexity approach being the one used in this work, where any feedback of such particles on the advecting flow is disregarded. And the word “beyond” also stands to indicate that these phenomena take place at small scales, even smaller than those described in the first part of the manuscript: but no other collocation different from a final one would be possible, in view of the aforementioned refinement needed in the physical description.

In chapter 5 I will therefore deal with inertial particles, whose non-negligible mass makes them deviate from the streamlines of the surrounding flow. On the one side, this can cause aggregation and formation of clusters, even in incompressible flows. On the other hand, falling velocity in the presence of gravity is also modified in a non trivial way: this will constitute the main subject of this chapter, in which use is made of mathematical tools like multiscale techniques and second-quantization algorithm.

Lastly, I will move to the study of polymers, i.e. long chains of molecules, inside turbulent flows. In particular I will investigate their dynamics in terms of probability density functions, both in the stationary state and in the relaxing toward it, with relation to the characteristics of the flow and of the modelled particle. As in most of the previous sections, I will analyse the problem mainly from an analytical point of view, but I will also exploit numerical facilities to show quantitative results. The material in chapter 6 refers to a published article (J) deriving from a collaboration with Dario Vincenzi.

Publications

- (A) *Does multifractal theory of turbulence have logarithms in the scaling relations?*
U. Frisch, **M. Martins Afonso**, A. Mazzino and V. Yakhot
Journal of Fluid Mechanics **542**, 97–103 (2005).
- (B) *Inhomogeneous anisotropic passive scalars*
M. Martins Afonso and M. Sbragaglia
Journal of Turbulence **6**, no. 10, pp. 1–13 (2005).
- (C) *Passive scalar turbulence from a point source*
A. Celani, **M. Martins Afonso** and A. Mazzino
to be submitted to *Journal of Fluid Mechanics*.
- (D) *Un modello risolubile analiticamente di Large-Eddy Simulation di campi scalari passivi*
M. Martins Afonso
Laurea Thesis, University of Genova (2002).
- (E) *Large-eddy-simulation closures of passive scalar turbulence: a systematic approach*
M. Martins Afonso, A. Celani, R. Festa and A. Mazzino
Journal of Fluid Mechanics **496**, 355–364 (2003).
- (F) *Closures for large-eddy simulations of passive scalars*
M. Martins Afonso, A. Celani and A. Mazzino
In: *Advances in Turbulence X, Proceedings of the Tenth European Turbulence Conference, Trondheim (Norway), June 29–July 2, 2004*, pp. 319–322, ed. by H.I. Andersson and P.A. Krogstad, CIMNE, Barcelona.

-
- (G) *Coarse-grained scalar transport: closures and large-eddy simulations*
A. Celani, **M. Martins Afonso** and A. Mazzino
In: Proceedings of the iTi Conference on Turbulence, Bad Zwischenahn
(Germany), September 25–28, 2005, Springer–Verlag, Berlin (in press).
- (H) *Coarse-grained description of a passive scalar*
A. Celani, **M. Martins Afonso** and A. Mazzino
submitted to *Journal of Turbulence*.
- (I) *Structure of temperature fluctuations in turbulent convective boundary layers*
M. Antonelli, **M. Martins Afonso**, A. Mazzino and U. Rizza
Journal of Turbulence **6**, no. 35, pp. 1–34 (2005).
- (J) *Nonlinear elastic polymers in random flows*
M. Martins Afonso and D. Vincenzi
Journal of Fluid Mechanics **540**, 99–108 (2005).

Part I

Turbulence at mesoscopic scales

Chapter 1

Is the inertial-range scaling a genuine property of turbulence?

The multifractal theory of turbulence uses a saddle-point evaluation in determining the power-law behaviour of structure functions. This could lead to the presence of logarithmic corrections, thereby violating known exact relations such as the four-fifths law. Using the theory of large deviations and calculating subdominant terms, I explain here why such corrections need not be present.

The chapter is organized as follows: in the introduction § 1.1 I recall some basic features of turbulence, like Kolmogorov's four-fifths law and its implications. In section § 1.2 I introduce multifractal and multiplicative models, related to each other by the concept of cascade. In section § 1.3 I recall some basic aspects of the large-deviation theory and of the saddle-point approximation and I provide some results, paradoxes and consequent explanations deriving from their application to these models. In section § 1.4 conclusions are provided by summarizing the main results, returning to the general multifractal formalism beyond the specific random multiplicative model, showing that the four-fifths law allows one to obtain the first subleading correction to the usual multifractal probability and rapidly quoting different situations where logarithms can actually appear. The appendix § 1.5 is devoted to the analysis of a specific multiplicative model, where analytical calculations can be performed in order to extend these results up to higher orders.

1.1 Introduction: the four-fifths law and its implications

In fully-developed turbulence there is now fairly good evidence for anomalous scaling, that is scaling exponents which cannot be predicted by dimensional analysis. Some of this evidence is reviewed in [1]. This reference also contains a detailed presentation of the multifractal formalism in the formulation of Parisi and Frisch [8, 9], henceforth PF, in which anomalous scaling for structure functions (moments of velocity increments) is connected by a Legendre transformation to the distribution of singularities of the velocity field. An earlier and alternative formalism for anomalous scaling was introduced by the Russian School of Kolmogorov [10, 11, 12]. In its simplest version it uses random multiplicative models for calculating the statistical fluctuations of the energy dissipation on various scales; the fractal properties of these models were discovered by Mandelbrot [13]. The bridging of the two formalisms is discussed in [1] in the light of the theory of large deviations for the sums of independent identically distributed random variables, discovered in the thirties by Cramér [14].

It must be stressed that, in its original formulation, PF gives an integral representation of the structure functions which are then evaluated by the method of steepest descent through a saddle point. When doing that, taking the leading contribution for the expression of the probability, P , of being within a certain distance from a fractal set of singularities, logarithmic corrections in the scaling relations do appear. This is clearly inconsistent with the four-fifths law of Kolmogorov [15], one of the very few exact results in high-Reynolds number turbulence, which imposes a strict constraint on any turbulent theory by fixing the behaviour of the third-order longitudinal (i.e. involving the component of the velocity \mathbf{v} parallel to the separation) structure function. In homogeneous and isotropic turbulence, defining $\Delta_\ell v \equiv [\mathbf{v}(\mathbf{x} + \boldsymbol{\ell}) - \mathbf{v}(\mathbf{x})] \cdot \boldsymbol{\ell} / \ell$, one has indeed $S_p(\ell) \equiv \langle (\Delta_\ell v)^p \rangle$ independently of the point \mathbf{x} and of the direction of $\boldsymbol{\ell}$. Namely, the four-fifths law states that

$$S_3(\ell) = -(4/5)\varepsilon\ell$$

in the stationary state of fully-developed turbulence, where ε is the mean energy dissipation per unit mass. On the contrary, a naïve application of the saddle-point technique would imply that, at small separations, $S_p(\ell)$ varies as ℓ^{ζ_p} but *with a logarithmic prefactor* $(\ln \ell)^{-1/2}$ stemming from the Gaussian

integration near the minimum ζ_p of the PF integrand exponent.

The above-mentioned logarithmic corrections are often sloppily ignored, or the difficulty is handled writing

$$\lim_{\ell \rightarrow 0} \frac{\ln S_p(\ell)}{\ln \ell} = \zeta_p .$$

Indeed, by taking the logarithm of the structure function, one changes the *multiplicative* logarithmic correction into an *additive* log-log correction which, after division by $\ln \ell$, becomes *subdominant* as $\ell \rightarrow 0$. But if one does not take the logarithm of the structure function, is there a logarithmic correction in the leading term, whose presence, for $p = 3$, would invalidate the standard multifractal formalism?

It is well established that such logarithmic corrections are definitely absent also in the random multiplicative model. Actually, the latter will turn out to give the key allowing one to understand why logarithmic corrections are unlikely and are definitely ruled out in the third-order structure function.

It is the main aim of the present chapter to resolve the paradox of the spurious presence of logarithms. In particular, I will compute the first sub-leading contribution in the expression for the logarithm of the probability P and show how its incorporation in the exploitation of the saddle-point method to evaluate the velocity structure functions cancels the leading-order logarithmic corrections. For a specific multiplicative model it will be shown that logarithmic corrections actually disappear also at higher orders.

1.2 Multifractal and multiplicative models

Turbulence is one of the main subject areas that has provided the physical intuition for the development of a theory of multifractals. This is reviewed in [16], where mention is also made of the strict relationship between multifractals and other phenomena described by chaotic dynamical systems, such as rainfall fields, earthquake modelling, global climate and self-similar auxiliary stochastic processes.

Focusing on turbulence, it is in order to briefly recall some basic phenomenology linking the idea of “cascade” to the one of multifractals [1]. To do that, consider a given laminar flow, the typical velocity of which is increased till some irregularities in the flow start to appear. This is the very initial stage of turbulence, which eventually becomes completely developed

6 Is the inertial-range scaling a genuine property of turbulence?

(i.e. exciting many temporal/spatial degrees of freedom) as the typical flow velocity is further increased. Cascade models have been introduced to provide a phenomenological description of the latter regime.

These models are based on the assumption that kinetic energy is introduced into the system on large scales, but can only be dissipated in the form of heat on very small scales, where the effect of viscosity becomes important. Cascade models moreover assume that energy is driven through a sequence of eddies of decreasing size (just a cascade), until it reaches sufficiently small eddies where the energy is dissipated as heat, thus leading the process to a stationary state. The crucial point is that the rate of energy dissipation per unit time and volume has a highly-sensitive dependence on space position and scale of observation. The phenomenological description of this fact and the important consequences on the phenomena of intermittency and anomalous scaling can be given in terms of multiplicative random cascade models [1].

These models are based on the hypothesis that, starting from a uniform nonrandom dissipation ε per unit mass in an initial cube of side ℓ_0 (corresponding to the integral scale of the problem), the “local” dissipation per unit mass in each of the eight cubes with half the previous side is equal to εW , where W is a random variable (with independent realizations in each cube) subject to the constraints $W \geq 0$, $\langle W \rangle = 1$ and $\langle W^p \rangle < \infty$ for all $p > 0$. Repeating the generation process, after n steps the local dissipation in a cube of side $\ell = 2^{-n}\ell_0$ is given by

$$\varepsilon_\ell = \varepsilon W_1 \cdots W_n ,$$

with independent and identically distributed W_i 's. The ensemble average $\langle \varepsilon_\ell \rangle$ is thus still equal to ε , but the cascade is nonconservative. Since one is interested in describing the inertial-range scaling properties ($\ell \ll \ell_0$), attention will mainly be focused on situations of highly-repeated generation, i.e. on large values of n . As a consequence, the formalism of multiplicative variables leads to the presence of very large fluctuations. The parallelism between multifractality and the probabilistic theory is expressed by the relationship

$$n = -\log_2 \frac{\ell}{\ell_0} = -\frac{1}{\ln 2} \ln \frac{\ell}{\ell_0} . \quad (1.1)$$

In other words, expression (1.1) shows the two meanings of n , relating the number of factors W_i determining the local dissipation to the number of steps

performed in the generation process, i.e. to the ratio between the current scale ℓ and the initial “injection” length ℓ_0 .

The moments of the local dissipation are elementarily given by

$$T_p(\ell) \equiv \langle \varepsilon_\ell^p \rangle = \langle (\varepsilon W_1 \cdots W_n)^p \rangle = \varepsilon^p \langle W^p \rangle^n = \varepsilon^p \left(\frac{\ell}{\ell_0} \right)^{-\log_2 \langle W^p \rangle}. \quad (1.2)$$

Following the suggestion originally made by Obukhov [10], one calculates the velocity structure functions at separation ℓ by the Kolmogorov expression [15], replacing the mean dissipation by its local random value. A relation with the T_p 's thus arises by means of the simple dimensional scaling property $\Delta_\ell v \approx (\ell \varepsilon_\ell)^{1/3}$, so

$$S_p(\ell) \approx \langle (\ell \varepsilon_\ell)^{p/3} \rangle = \ell^{p/3} T_{p/3}(\ell) = \varepsilon^{p/3} \ell^{p/3} \langle W^{p/3} \rangle^n, \quad (1.3)$$

and consequently one gets the power law $S_p(\ell) \propto \ell^{\zeta_p}$, with $\zeta_p = p/3 - \log_2 \langle W^{p/3} \rangle$. For $p = 3$ these models satisfy the constraint imposed by the four-fifths law [1] and none of the structure functions has any multiplicative logarithmic factor.

For later convenience, the above expression can be rephrased exploiting the formalism of additive random variables. This is easily done by performing the substitution $W = 2^{-m}$. In this way, the moments of the local dissipation (from which the velocity structure functions can be derived) are expressed by:

$$\begin{aligned} T_p(\ell) &= \langle (\varepsilon 2^{-m_1} \cdots 2^{-m_n})^p \rangle = \varepsilon^p \langle 2^{-m_1 p} \cdots 2^{-m_n p} \rangle \\ &= \varepsilon^p \langle 2^{-n x p} \rangle = \varepsilon^p \int dx e^{-n x p \ln 2} P_n(x), \end{aligned} \quad (1.4)$$

where

$$x \equiv \frac{m_1 + \cdots + m_n}{n} \quad (1.5)$$

is the partial average of n independent and identically distributed random variables.

In the multifractal language, (1.4) can be rewritten in the form

$$T_p(\ell) = \varepsilon^p \int d\mu(h) \left(\frac{\ell}{\ell_0} \right)^{(3h-1)p+3-D(h)} = \varepsilon^p \int dh \mu'(h) e^{[(3h-1)p+3-D(h)] \ln(\ell/\ell_0)}, \quad (1.6)$$

8 Is the inertial-range scaling a genuine property of turbulence?

where the exponent $3h - 1$ corresponds to x , $\mu(h)$ is a measure expressing the weight of a local value of h and $(\ell/\ell_0)^{3-D(h)}$ plays the role of the probability density function (PDF), $D(h)$ being the Hausdorff fractal dimension of the support of the h spectrum.

Equation (1.4) provides an alternative and somewhat roundabout way of evaluating the moments of the local dissipation, and thus the structure functions, for the random multiplicative model. Of course, it must give the same final result (1.2). In order to see whether this is really the case, it is necessary to recall the main aspects of the large-deviation theory.

1.3 Large-deviation theory and saddle-point approximation

Starting from the probability distribution for a single random variable m , $P(m)$, one defines [1]

$$Z(\alpha) \equiv \int dm e^{-\alpha m} P(m) = \langle e^{-\alpha m} \rangle .$$

$Z(\alpha)$ is equal to the characteristic function evaluated for an imaginary argument and exists $\forall \alpha$ if $P(m)$ decreases faster than exponentially for large m . In this case one is interested in the behaviour of the probability distribution $P_n(x)$ of the variable x defined in (1.5), when n is large. In way of example, if $P(m)$ is the Bernoullian distribution in the coin-tossing problem [17], then $P_n(x)$ can be identified as the probability distribution of the normalized sum of each result after n trials.

It is easily proved that

$$\begin{aligned} Z_n(\alpha) &\equiv \int dx e^{-\alpha x} P_n(x) = \langle e^{-\alpha x} \rangle = \langle e^{-\alpha(m_1 + \dots + m_n)/n} \rangle \\ &= \langle e^{-\alpha m_1/n} \dots e^{-\alpha m_n/n} \rangle = \langle e^{-\alpha m/n} \rangle^n = Z^n\left(\frac{\alpha}{n}\right). \end{aligned}$$

Consequently, inverting the above Laplace transform through a Fourier integral, one gets the expression

$$P_n(x) = \frac{1}{2\pi} \int d\alpha e^{i\alpha x} Z^n\left(\frac{i\alpha}{n}\right) . \quad (1.7)$$

The law of large numbers [18] implies that $P_n(x)$ is, for large n , increasingly concentrated near the mean $\langle m \rangle = \lim_{n \rightarrow \infty} x$. The theory of large deviations [14] roughly states that when $x \neq \langle m \rangle$ its probability falls off exponentially with n .

To show this result, (1.7) has to be recast in the exponential form

$$P_n(x) = \frac{1}{2\pi} \int d\alpha e^{i\alpha x + n \ln Z(i\alpha/n)} = \frac{n}{2\pi} \int d\gamma e^{n[i\gamma x + \ln Z(i\gamma)]}, \quad (1.8)$$

with the simple substitution $\gamma = \alpha/n$.

This is a generalized Laplace integral of the form

$$I(n) = \int dy f(y) e^{n\phi(y)}, \quad (1.9)$$

for which the asymptotic (large n) behaviour can be extracted by means of saddle-point approximation. More specifically, when the integral is performed in the complex plane and involves complex analytic functions f and ϕ , if there exists a saddle point y_* (i.e. a point at which $\phi'(y_*) = 0$), then one can exploit the analyticity in order to deform the integration contour into a ϕ -constant-phase line passing through y_* . In this way, one can restrict the integration range to a small portion of the new path, from which the dominant contribution to the integral arises when n is large, after identifying correctly the steepest-descent curve passing through y_* . In particular, if both the integration path and the functions f and ϕ are real, then the presence of a saddle is guaranteed if the function $\phi(y)$ is upconvex in the whole integration range and has a maximum at an interior point y_* .

The leading behaviour of the integral for large n is [19]

$$I(n) = \sqrt{\frac{2\pi}{-n\phi''(y_*)}} e^{n\phi(y_*)} f(y_*) \left[1 + O\left(\frac{1}{n}\right) \right], \quad (1.10)$$

provided that neither $f(y)$ nor $\phi''(y)$ vanishes at y_* .

Passing to logarithms and dividing by n , one obtains

$$\frac{\ln I(n)}{n} = \phi(y_*) - \frac{\ln n}{2n} + \frac{\ln \left[f(y_*) \sqrt{-2\pi\phi''(y_*)} \right]}{n} + O\left(\frac{1}{n^2}\right). \quad (1.11)$$

The latter formulation is very common in thermodynamics [17], where it is customary to deal with the logarithm of the (very large) number of states.

10 Is the inertial-range scaling a genuine property of turbulence?

Applying (1.11) to expression (1.8), one has

$$\frac{\ln P_n(x)}{n} = s(x) + \frac{\ln n}{2n} + \frac{\ln(-Q/2\pi)}{2n} + O\left(\frac{1}{n^2}\right), \quad (1.12)$$

where Q is the second derivative of

$$q(\gamma) = i\gamma x + \ln Z(i\gamma) \quad (1.13)$$

evaluated at the unique stationary point γ_* that satisfies $q'(\gamma_*) = 0$ (see equation (1.8)). As n does not appear in Q , which is only a function of x , the right-hand side of expression (1.12) is thus structured as an inverse power series in n , except for the first subleading term which contains a logarithm. The (n -independent) dominant contribution,

$$s(x) \equiv \lim_{n \rightarrow \infty} \frac{\ln P_n(x)}{n},$$

usually called *Cramér* (or *rate*) *function* [20], vanishes at $x = \langle m \rangle$ together with its first derivative and turns out to be upconvex, being related to $\ln Z(\alpha)$ through a Legendre transform:

$$s(x) = \inf_{\alpha} [\alpha x + \ln Z(\alpha)].$$

Back to the thermodynamic context, $s(x)$ can be identified with the entropy, thus clarifying the meaning of (1.12).

It is important to note that the quantity which goes to a finite limit for large n is $n^{-1} \ln P_n(x)$ (1.12) and that for this quantity the corrections are additive subleading terms.

1.3.1 Classical multifractal results

It will now be shown that the classical multifractal results are obtained by applying the saddle-point technique only through its dominant behaviour, i.e. taking into account the sole n -independent term in (1.11), which corresponds to the exponential appearing in (1.10).

Indeed, for the multiplicative models, keeping only the leading-order contribution for large n in (1.12), one obtains a purely exponential behaviour for the PDF of the partial average x :

$$P_n(x) = e^{ns(x)}. \quad (1.14)$$

Equation (1.14) is strictly connected to the central-limit theorem [21], in the sense that small deviations from the mean value are well described by a Gaussian, which results from a second-order Taylor expansion of the exponent around the maximum located at $x_\star = \langle m \rangle$. However, larger deviations from the mean value do not follow a normal distribution [22, 23]. As (1.14) also applies to deviations $O(1)$, i.e. much larger than the standard deviation (which is $O(n^{-1/2})$), it is usually referred to as the large-deviation expression for the probability.

Assuming expression (1.14) for $P_n(x)$, (1.4) becomes

$$T_p(l) = \varepsilon^p \int dx e^{n[s(x) - xp \ln 2]} . \quad (1.15)$$

As (1.15) has the form of a Laplace integral (1.9), one can apply the saddle-point method again. Because of consistency, one has to consider only one term in expression (1.11), which amounts to say that, in the form (1.10), one only keeps the exponential. One thus obtains

$$T_p(l) = \varepsilon^p e^{n[s(x_\star) - x_\star p \ln 2]} \propto \left(\frac{\ell}{\ell_0} \right)^{x_\star p - s(x_\star) / \ln 2} ,$$

or, in the multifractal language (see equation (1.6)),

$$T_p(l) \propto \left(\frac{\ell}{\ell_0} \right)^{(3h_\star - 1)p + 3 - D(h_\star)} ,$$

where h_\star is the unique stationary point that satisfies $D'(h_\star) = 0$.

It is worth emphasizing that, in the multiplicative models, $P_n(x)$ can be obtained through a first use of the saddle-point approximation (starting from the single-variable probability distribution), which then imposes the number of terms to be considered in the second application of this technique to find T_p . On the contrary, in the general multifractal formulation [24], the former above-mentioned step is not possible, so one has to use other arguments to infer the dominant power-law scaling $(\ell/\ell_0)^{3-D(h)}$ for the probability in (1.6), thus having no indication on the number of terms to be retained in the second approximation.

In the following, it will be shown how an inconsistent application of the saddle-point method leads to the appearance of spurious logarithmic corrections.

12 Is the inertial-range scaling a genuine property of turbulence?

1.3.2 How spurious logarithmic corrections generate

Assuming the “sloppy” large-deviation expression (1.14) for the PDF, and consequently equation (1.15) for the moments of the local dissipation, one can now apply the saddle-point method in the form (1.10) and (at the leading order) obtain

$$T_p(l) = \varepsilon^p \sqrt{\frac{2\pi}{-ns''(x_*)}} e^{n[s(x_*) - x_* p \ln 2]} \propto \left(\frac{\ell}{\ell_0}\right)^{x_* p - s(x_*)/\ln 2} \left[-\ln \frac{\ell}{\ell_0}\right]^{-1/2}, \quad (1.16)$$

or, in the multifractal language (see equation (1.6)),

$$T_p(l) \propto \left(\frac{\ell}{\ell_0}\right)^{(3h_* - 1)p + 3 - D(h_*)} \left[-\ln \frac{\ell}{\ell_0}\right]^{-1/2}, \quad (1.17)$$

where h_* is the unique stationary point that satisfies $D'(h_*) = 0$.

As the velocity structure functions are proportional to the T_p 's according to (1.3), a logarithmic correction to the power law would then appear also for S_3 , thus violating the (exact) law of the four fifths.

1.3.3 The way to solve the paradox of logarithmic corrections

To solve the apparent paradox related to the presence of a logarithmic correction in the structure functions, it is necessary to refine the large-deviation expression (1.14) for the multiplicative models. In particular, one needs to take into account also the first (additive) subleading contribution in (1.12). This operation gives rise to the emergence of a (multiplicative) n -dependent prefactor (which accordingly should be regarded as subleading) to the exponential form (1.14), namely:

$$P_n(x) = \sqrt{n} e^{ns(x)}. \quad (1.18)$$

When applying equation (1.10) again to obtain the moments of the local dissipation by means of saddle-point approximation, the presence of \sqrt{n} at the numerator of (1.18) thus cancels the logarithmic correction in (1.16), which are spurious. This is simply due to the fact that equation (1.10) also incorporates the second term on the right-hand side of (1.11), so the

same “precision” must be used in (1.12) to have a cross cancellation of the corrections.

It is worth noticing that, if the PDF of the single variable m is continuously distributed, then the appearance of \sqrt{n} in the PDF of the partial average x follows from a theorem by Bahadur and Ranga Rao [25], which is reviewed in [26]. This constitutes the so-called theory of “refined large deviations”.

Back to the multifractal formalism, the logarithms in (1.17) thus disappear if the “probability” $(\ell/\ell_0)^{3-D(h)}$ is replaced by the more accurate expression

$$\left(\frac{\ell}{\ell_0}\right)^{3-D(h)} \left[-\ln \frac{\ell}{\ell_0}\right]^{1/2}.$$

As this represents the main result of this chapter, its implications will be discussed in the conclusion § 1.4.

1.3.4 Other ways to produce spurious logarithms and how to rule them out

One may wonder about the effect of the successive terms in (1.12) on the scaling behaviour of the structure functions for random multiplicative models. In particular, the $O(n^{-1})$ contribution in (1.12) simply leads to a n -independent correction in the PDF. Clearly, incorporating it and/or the $O(n^{-1})$ term in (1.11) while calculating T_p , does not change the scaling behaviour in n .

The situation is completely different for the fourth term on the right-hand side of (1.11), corresponding to the additive correction inside square brackets in (1.10). It has already been shown that a prefactor \sqrt{n} in $P_n(x)$ leads to the cancellation of any power-law dependence on n for the quantity T_p . One can easily understand that a term proportional to $\sqrt{n} \times 1/n = n^{-1/2}$ in $P_n(x)$, by virtue of its additive character, generates an additive contribution in T_p proportional to $n^{-1} \propto [-\ln(\ell/\ell_0)]^{-1}$.

Logarithms thus seem to appear again. But once again, to find T_p , consistency imposes to take into account the same number of terms in the two saddle points. There is thus the possibility to have a cancellation, with the final result that, once again, logarithmic corrections disappear, since (1.3) is an exact expression and has no logarithms.

To show in general that these cancellations really take place at any orders appears a cumbersome task. For the sake of simplicity, in the appendix

14 Is the inertial-range scaling a genuine property of turbulence?

§ 1.5 attention will be focused on a specific multifractal model: the *Novikov–Stewart model* [27].

1.4 Conclusion: back to multifractal turbulence

In multifractal language, the result obtained within the framework of the random multiplicative model is that the probability $P(\ell, h)$ to be within a distance ℓ of the set carrying singularities of scaling exponent between h and $h + dh$ is not $(\ell/\ell_0)^{3-D(h)}d\mu(h)$ but is actually given, for small ℓ , by

$$P(\ell, h) \propto \left(\frac{\ell}{\ell_0}\right)^{3-D(h)} \left[-\ln \frac{\ell}{\ell_0}\right]^{1/2} d\mu(h), \quad (1.19)$$

which has a subleading logarithmic correction. It is important to recall that it must be qualified “subleading” because the correct statement of the large-deviation leading-order result involves the logarithm of the probability divided by the logarithm of the scale. The correction is then a subleading additive term.

It is worth mentioning that the presence of a square root of a logarithm correction in the multifractal probability density was proposed by Meneveau and Sreenivasan [28] on the basis of a normalization requirement; they observed that without such a correction the singularity spectrum $f(\alpha)$ comes out wrong. They also pointed out that a similar correction had been proposed by van de Water and Schram [29] in connection with the measurement of generalized Renyi dimensions. Related discussions about the presence of logarithms can be found in [30, 31, 32].

Returning to the multifractal formalism of turbulence, beyond the random multiplicative model, it must be observed that the usual multifractal ansatz as made in PF [8] is only about the leading term of the probability, which is easily reinterpreted in geometrical language. Hence, it does not allow one to determine logarithmic corrections in structure functions. However, using Kolmogorov’s four-fifths law, one has an additional piece of information which implies that the multifractal probability should have a subleading logarithmic correction with precisely the form it has in (1.19). This improved form then rules out subleading logarithmic corrections in any of the structure functions.

Finally, a comment is required on those physical effects which are known to be responsible of subleading corrections (logarithmic or not) to isotropic scaling. There is at least one known instance which has a genuine logarithm in its third-order structure function, namely the Burgers equation (in the limit of vanishing viscosity) with a Gaussian random force which is white in time and has a $1/k$ spatial spectrum, where k is the wavenumber. As shown in [33] and [34], the Burgers equivalent of the four-fifths law implies then the presence of a logarithmic correction. What was less obvious is that another frequently considered structure function, defined with the absolute value of the velocity increment, has also a logarithmic correction but accompanied by a subdominant term (proportional to the separation without a log factor) which conspires to make this structure function appear to have anomalous power-law scaling with a non-trivial exponent [34]. This is actually an artifact which would also be present in three-dimensional Navier–Stokes turbulence with $1/k$ forcing. Particularly noteworthy are the contaminations by subdominant terms stemming from anisotropy [35].

1.5 Appendix: the Novikov–Stewart model

In the Novikov–Stewart model [27], the random variable W can only assume two distinct values, 0 and $1/\beta$, with probability $1 - \beta$ and β respectively ($0 < \beta < 1$). In order to avoid singularities for $m = -\log_2 W$, it is convenient to slightly modify the above statement, defining

$$P(W) = (1 - \beta)\delta(W - \chi) + \beta\delta(W - \xi), \quad (1.20)$$

where $\xi = [1 - \chi(1 - \beta)]/\beta$, and eventually taking the limit $\chi \rightarrow 0^+$ (which implies $\xi \rightarrow 1/\beta$).

From (1.20), a straightforward calculation gives

$$P(m) = P(W(m)) \left| \frac{dW}{dm} \right|$$

and then $Z(\alpha) = (1 - \alpha)e^{\alpha \log_2 \chi} + \beta e^{\alpha \log_2 \xi}$.

Now one has to perform the first saddle-point approximation, coherently with equation (1.8). According to (1.13), one gets

$$\gamma_* = \frac{i}{\log_2 \xi - \log_2 \chi} \ln \frac{\beta(x + \log_2 \xi)}{(1 - \beta)(-x - \log_2 \chi)},$$

16 Is the inertial-range scaling a genuine property of turbulence?

and the steepest-descent contour is parallel to the real axis at γ_* .

Upon substitution in (1.12), taking into account the correct coefficient of $O(n^{-2})$ which results in a $O(n^{-1})$ term in the expression for $P_n(x)$, the latter can be written more easily in terms of the variable $k = (-x - \log_2 \chi) / (\log_2 \xi - \log_2 \chi)$ as

$$\begin{aligned} P_n(k) &= P_n(x(k)) \left| \frac{dx}{dk} \right| \\ &= \sqrt{\frac{n}{2\pi k(1-k)}} \left(\frac{\beta}{k} \right)^{nk} \left(\frac{1-\beta}{1-k} \right)^{n(1-k)} \left[1 + g(k) \frac{1}{n} + O\left(\frac{1}{n^2}\right) \right], \end{aligned} \quad (1.21)$$

where $g(k) = (1 - k + k^2) / 12k(1 - k)$ and k ranges from 0 to 1. Expression (1.21) is associated to a Cramér function

$$s(k) = \lim_{n \rightarrow \infty} \frac{\ln P_n(k)}{n} = k \ln \frac{\beta}{k} + (1 - k) \ln \frac{1 - \beta}{1 - k}.$$

In order to calculate the moments of the local dissipation, from (1.4) one has

$$T_p(l) = \varepsilon^p \sqrt{\frac{n}{2\pi}} \int dk e^{n\phi(k)} \left[F(k) + G(k) \frac{1}{n} + O\left(\frac{1}{n^2}\right) \right]. \quad (1.22)$$

The integral of each addend has the same form of (1.9) with the relationship $\phi(k) = s(k) - xp \ln 2$. The functions $F(k) = [k(1 - k)]^{-1/2}$ and $G(k) = F(k)g(k)$ play the role of $f(y)$ in the zeroth- and first-order integrals, respectively. An explicit application of the saddle-point technique for the generalized Laplace integrals gives

$$\phi'(k_*) = 0 \Leftrightarrow k_* = \frac{\beta \xi^p}{(1 - \beta) \chi^p + \beta \xi^p}.$$

Thus,

$$\int dk F(k) e^{n\phi(k)} = \sqrt{\frac{2\pi}{n}} e^{n\phi(k_*)} \left[1 - H \frac{1}{n} + O\left(\frac{1}{n^2}\right) \right],$$

taking into account the first-order correction (the explicit form of H is not reported here for the sake of simplicity), and

$$\int dk G(k) e^{n\phi(k)} = \sqrt{\frac{2\pi}{n}} e^{n\phi(k_*)} \left[H + O\left(\frac{1}{n}\right) \right],$$

stopping at the leading-order contribution, with $\phi(k_*) = \ln[(1-\beta)\chi^p + \beta\xi^p]$. Summing the two integrals to get (1.22) and performing the limit $\chi \rightarrow 0^+$, one obtains

$$T_p(l) = \varepsilon^p e^{n \ln[(1-\beta)\chi^p + \beta\xi^p]} \left[1 + \mathcal{O}\left(\frac{1}{n^2}\right) \right] \\ \xrightarrow{\chi \rightarrow 0} \varepsilon^p \left(\frac{\ell}{\ell_0}\right)^{(p-1)\log_2 \beta} \left[1 + \mathcal{O}\left(-\ln \frac{\ell}{\ell_0}\right)^{-2} \right].$$

Apart from an error pushed to $\mathcal{O}(n^{-2})$, which would vanish if one proceeded to the following orders in the approximation, this coincides with the exact result that can be obtained performing the calculation in the discrete formalism.

In the latter case, the probability distribution for the (discrete) partial average x is exactly given by a binomial distribution, which can be written more easily in terms of another auxiliary variable $K = kn$ assuming only integer values between 0 and n . Namely,

$$P_n(K) = \binom{n}{K} \beta^K (1-\beta)^{n-K}. \quad (1.23)$$

From (1.4), without introducing any continuum approximation, i.e. performing a sum instead of an integral, one exactly finds a power-law behaviour for the moments of the local dissipation:

$$T_p(l) = \varepsilon^p \sum_{K=0}^n 2^{-n\chi p} P_n(K) = \varepsilon^p \left(\frac{\ell}{\ell_0}\right)^{-\log_2[(1-\beta)\chi^p + \beta\xi^p]} \xrightarrow{\chi \rightarrow 0} \varepsilon^p \left(\frac{\ell}{\ell_0}\right)^{(p-1)\log_2 \beta}.$$

Consequently, also for the velocity structure functions one has pure power laws with exponents $\zeta_p = p/3 + (p/3 - 1)\log_2 \beta$.

Logarithms are definitely absent: the same result must then hold also for the analysis performed in the continuum formalism taking into account every order in the approximation. It is worth noticing that, alternatively to the saddle-point technique, expression (1.21) can be obtained directly from (1.23) by means of Stirling's expansion for the factorial.

Chapter 2

Exact results for nonideal turbulence

I investigate the behaviour of the two-point equal-time correlation function, in the context of passive scalars, for forcing ensembles which are allowed to be, generally speaking, neither homogeneous nor isotropic. Exact analytical computations can be carried out in the framework of the Kraichnan model for each anisotropic sector. I will focus my attention on the isotropic sector with isotropic forcing in order to obtain a description of the influence of purely inhomogeneous contributions. It is shown how the homogeneous solution is recovered at separations smaller than an intrinsic typical lengthscale induced by inhomogeneities, and how the different Fourier modes in the centre-of-mass variable recombine themselves to give a “beating” (superposition of power laws) described by Bessel functions. The pure power-law behaviour is restored even if the inhomogeneous excitation takes place at very small scales, but is spoiled in the presence of intermediate-scale inhomogeneities. I will later focus on the point-source problem, carrying out exact analytical computations for a random-in-time forcing and showing numerical results for a constant emission.

The chapter is organized as follows: in the introduction § 2.1 I recall the importance of passive scalar turbulence and, in this context, the relevance of inhomogeneities and anisotropies. In section § 2.2 I formulate the general problem of two-point equal-time scalar correlations, which will be studied analytically for the Kraichnan ensembles, at first in the homogeneous isotropic case and then in the absence of invariance under translations and rotations; the statistical description of the isotropic sector is later provided,

with particular emphasis on some kinds of physically meaningful inhomogeneous forcings. In section § 2.3 I focus on the point-source problem, in particular on random emission. Conclusions follow in section § 2.4, hinting the exportability to Navier–Stokes (NS) turbulence. Appendices § 2.5 and § 2.6 are devoted to explain some calculation details and to a numerical study of the constant point-source emission, respectively.

2.1 Introduction

Since its origin, the turbulence theory has been faced prevalingly in the context of a homogeneous and isotropic model, i.e. in an idealized framework: the paradigm is the passive scalar model introduced by Kraichnan in 1968 [36, 37]. However, starting from the fundamental work by Kolmogorov in 1941 [1, 2], one of the key points for many theoretical achievements in turbulence research is the (statistical) restoration of homogeneity and isotropy of fluctuations at small scales [38, 39]. It is clearly impossible to provide a proper and consistent description of a great variety of systems where “non idealized” fluctuations are still alive. The characterization of the emission of a tracer from point-like sources, the study of scalar concentrations along channels with inhomogeneous boundaries, or in those systems whose large scales are driven by strong shears, are remarkable examples in which strong anisotropies [40, 41] and inhomogeneities [42] must be taken into account in order to obtain a correct picture of the statistical properties of those systems.

In the last decade a consistent progress in the development of a systematic analysis to separate isotropic fluctuations from the anisotropic ones in real turbulent flows and turbulent transport [35, 43, 44] has been carried out. It has been understood how to treat and face systems whose rotational symmetries are broken by the presence of an external forcing inducing anisotropic contributions. In particular, the study of a simplified model for passive scalar advection in stochastic flows, the Kraichnan model, has provided a clear understanding of the statistical properties in all anisotropic sectors of the scalar fluctuations. Indeed, closed equations for the equal-time correlation functions can be obtained: these are linear partial differential equations whose unforced solutions (also called zero modes [45]) generally exhibit anomalous scaling. This is in contrast with the forced solutions that possess (non-anomalous) dimensional scaling. This has given the insight to explain the universality in the statistical framework. Indeed, the anomalous properties of small scale statistics result from a decoupling between the zero mode scaling and dimensional scaling, and the universality of these properties naturally emerges because the zero-mode scaling properties are independent of the forcing mechanism (see [46] for an exhaustive review).

In the present chapter I formulate the concept of the possible small-scale homogeneity restoration by focusing on the two-point equal-time scalar correlation function for the Kraichnan advection model. The advecting velocity

is still homogeneous and isotropic but this is not for the scalar injection mechanism, which will be allowed to be neither isotropic nor homogeneous. As I will show, the inhomogeneous forcing induces a new lengthscale ℓ_q into the scalar dynamics, in terms of which quantitative conclusions on the persistence of small-scale inhomogeneity will be given. The aim of this investigation is twofold. Firstly, I want to show how the correct homogeneous limit can be restored going at separations (in the two-point scalar correlation function) smaller than ℓ_q . Secondly, I want to give some analytical insights about the opposite physical situation represented by the presence of inhomogeneous fluctuations on scales of the same order of the separation. In the latter regime the pure power-law behaviour (homogeneous limit) is replaced by the “beating” in superposition of different power laws originating from the scalar inhomogeneities.

The superposition can be carried out analytically inside a special context, provided by the scalar emission from a point source. Very recently, it has been shown [47, 48] that a new type of zero mode is responsible for the scale-invariance breakdown in the equilibrium domain, i.e. on scales exceeding the forcing integral scale. The important remark is that in the point-source problem this scale is formally put to zero: all dynamical scales thus belong to this regime. The specific issues that I investigate are the dispersion dynamics and the study of the stationary regime, related to two different kinds of point source: constant or random-in-time emission/absorption.

2.2 The two-point equal-time scalar correlation function

2.2.1 Homogeneous isotropic case

The basic equation governing the dynamics of a passive scalar field $\theta(\mathbf{x}, t)$ in a turbulent d -dimensional flow ($d > 1$) is the well-known advection-diffusion forced equation:

$$\partial_t \theta(\mathbf{x}, t) + \mathbf{v}(\mathbf{x}, t) \cdot \boldsymbol{\partial} \theta(\mathbf{x}, t) = \kappa_0 \partial^2 \theta(\mathbf{x}, t) + f(\mathbf{x}, t) . \quad (2.1)$$

The advecting velocity field $\mathbf{v}(\mathbf{x}, t)$ is assumed incompressible: $\boldsymbol{\partial} \cdot \mathbf{v} = 0$. Scalar fluctuations are injected into the system by the forcing term $f(\mathbf{x}, t)$, acting as an external source, and are dissipated at small scales via the molecular diffusivity κ_0 .

The passive character of the scalar field allows one to consider both velocity and forcing as given fields. Unfortunately, no general analytical solution is known for a turbulent velocity field, satisfying the (vectorial and nonlinear) NS equation

$$\partial_t \mathbf{v}(\mathbf{x}, t) + \mathbf{v}(\mathbf{x}, t) \cdot \partial \mathbf{v}(\mathbf{x}, t) = \nu \partial^2 \mathbf{v}(\mathbf{x}, t) + \mathbf{g}(\mathbf{x}, t) - \rho^{-1}(\mathbf{x}, t) \partial p(\mathbf{x}, t) ,$$

ν , \mathbf{g} , ρ and p being the kinematic viscosity, the total force acting per unit mass, the density and the pressure, respectively. It is thus necessary to pass to a statistical description of the problem, in spite of the linearity of (2.1). In particular, it is customary to assume \mathbf{v} and f as stochastic fields, i.e. with assigned statistical properties. The most common way to mimic real flows with stochastic ensembles is by far constituted by the *Kraichnan advection model* [36, 37], in which one specializes to Gaussian, zero-average, white-in-time velocity and forcing. The field \mathbf{v} will be assumed statistically homogeneous and isotropic throughout this chapter, whereas this condition is imposed only momentarily for f , which will be later allowed not to be invariant under translations. The statistics of \mathbf{v} is thus fully determined by its two-point correlation function,

$$\langle v_\mu(\mathbf{x}, t) v_\nu(\mathbf{x}', t') \rangle = \delta(t - t') D_{\mu\nu}^{(v)}(\mathbf{x} - \mathbf{x}') ,$$

whose spatial behaviour is described by

$$D_{\mu\nu}^{(v)}(\mathbf{r}) = D_0 \delta_{\mu\nu} - d_{\mu\nu}^{(v)}(\mathbf{r}) .$$

The coefficient D_0 represents the fuse-point value, while the second-order increments follow a power law,

$$d_{\mu\nu}^{(v)}(\mathbf{r}) = D_1 r^\xi \left[(d + \xi - 1) \delta_{\mu\nu} - \xi \frac{r_\mu r_\nu}{r^2} \right] ,$$

in the so-called *inertial range* of scales, i.e. for separations $r = |\mathbf{r}|$ smaller than the integral scale of the velocity field (L_v), above which $d_{\mu\nu}^{(v)}(\mathbf{r})$ saturates to an almost constant value whose order of magnitude is $D_1 L_v^\xi$. Consequently, since the correlation $D_{\mu\nu}^{(v)}(\mathbf{r})$ has to vanish for $r \rightarrow \infty$, the relation $D_0 \sim D_1 L_v^\xi$ holds. In what follows, I will always consider $r < L_v$. The parameter ξ , lying in the open interval $(0, 2)$, governs the roughness of the velocity field, whose Hölder exponent is $\xi/2$. Due to the lack of temporal memory of the flow, the Kolmogorov value [15] is $\xi = 4/3$; the limit cases $\xi = 0$ and $\xi = 2$

will be studied apart. The diffusive scale η , at which diffusive and advective effects are comparable (the former is expected to prevail below it, and vice versa), is defined by the relation:

$$\eta \equiv \left(\frac{2\kappa_0}{(d-1)D_1} \right)^{1/\xi}. \quad (2.2)$$

A convenient choice for f is to momentarily assume a spatial step-like form for its two-point correlation function

$$\langle f(\mathbf{x}, t) f(\mathbf{x}', t') \rangle = \delta(t - t') F(|\mathbf{x} - \mathbf{x}'|), \quad (2.3)$$

i.e.

$$F(r) = F_0 \Theta(L - r). \quad (2.4)$$

Indeed, the details of its behaviour around the forcing (usually large) scale L are not relevant (see, e.g., [49, 50, 51]), but in the following this choice will make it possible to perform exact matchings in $r = L$ by defining a precise upper limit L to the so-called *convective range* of scales, whose lower bound is roughly represented by η .

The assumption of δ -correlation in time is of course far from reality, but it has the remarkable advantage of leading to closed equations for the equal-time correlation functions $C_n^{(\theta)} \equiv \langle \theta(\mathbf{x}, t) \cdots \theta(\mathbf{x}^{(n)}, t) \rangle$ of any order n (see, e.g., [46]). On the contrary, the condition of Gaussianity is not a limiting factor. One of the most important features in turbulence is indeed provided by *intermittency* or *anomalous scaling*, i.e. the impossibility to deduce the behaviour of higher-order moments of physical quantities from the knowledge of lower-order ones. In this sense, “intermittent” can be interpreted as opposed to “Gaussian”, as in the latter situation the statistical distribution is completely determined by its mean and its variance. Both velocity and passive scalars are known to be intermittent in real turbulent flows, however it has also been proved that, even assuming a Gaussian advecting velocity, the advected passive scalar turns out to be nevertheless intermittent.

In this framework the mean value $\langle \theta \rangle$ shows trivial dynamics (being uniform because of homogeneity). The equation for the two-point equal-time scalar correlation function $C \equiv C_2^{(\theta)} = \langle \theta(\mathbf{x}, t) \theta(\mathbf{x}', t) \rangle$ can be derived analytically, multiplying (2.1) by $\theta(\mathbf{x}', t)$, symmetrizing the resulting expression, averaging over the stochastic fields \mathbf{v} and f , and finally exploiting

Furutsu–Novikov–Donsker’s (FND) rule for Gaussian integration by parts [52, 53, 54, 1]:

$$\partial_t C = d_{\mu\nu}^{(v)} \frac{\partial^2 C}{\partial r_\mu \partial r_\nu} + 2\kappa_0 \frac{\partial^2 C}{\partial r_\mu \partial r_\mu} + F. \quad (2.5)$$

The stationary version of (2.5), in which the left-hand side vanishes and C is only a function of the distance r between the two points ($\mathbf{r} = \mathbf{x} - \mathbf{x}'$), reads

$$r^{-(d-1)} \partial_r \{ r^{d-1} [2\kappa_0 + (d-1)D_1 r^\xi] \partial_r C(r) \} + F(r) = 0$$

and can be simply solved by splitting the integration interval [55]:

$$C(r) \simeq \begin{cases} c' - k' r^2 & \text{for } r \ll \eta \\ c - k r^{2-\xi} & \text{for } \eta \ll r < L \\ k'' r^{-(d+\xi-2)} & \text{for } r > L \end{cases},$$

where

$$c = \frac{F_0 L^{2-\xi}}{(d-1)(2-\xi)(d+\xi-2)D_1}, \quad c' = c - \frac{\xi F_0 \eta^{2-\xi}}{2d(d-1)(2-\xi)D_1},$$

$$k = \frac{F_0}{d(d-1)(2-\xi)D_1}, \quad k' = \frac{2-\xi}{2\eta^\xi} k, \quad k'' = \frac{(2-\xi)L^d}{d+\xi-2} k.$$

In the limit of small diffusivity, which will be assumed throughout the chapter, the steady-state merged-point value of the correlation is a constant (because of homogeneity) given by $\langle \theta^2 \rangle \simeq c$ and the stationary second-order structure function turns out to be a pure power law in the convective range:

$$S_2^{(\theta)}(r) \equiv \langle [\theta(\mathbf{x}, t) - \theta(\mathbf{x}', t)]^2 \rangle = \langle \theta^2(\mathbf{x}, t) \rangle + \langle \theta^2(\mathbf{x}', t) \rangle - 2\langle \theta(\mathbf{x}, t)\theta(\mathbf{x}', t) \rangle \\ = 2\langle \theta^2 \rangle - 2C(r) = 2kr^{2-\xi}. \quad (2.6)$$

The exponent $2 - \xi$ coincides with the predictions based on dimensional arguments and becomes $2/3$ for $\xi = 4/3$, according to the Kolmogorov–Obukhov–Corrsin (KOC) scaling [56].

Exact solutions, i.e. far from the perturbative limits $\xi \rightarrow 0$ [45], $\xi \rightarrow 2$ [57] and $d \rightarrow \infty$ [58], are not available for higher-order correlations.

2.2.2 Extension to the inhomogeneous anisotropic case

Inside the Kraichnan model, the hypotheses of homogeneity and isotropy will still be kept for the velocity, but will now be relaxed for the forcing,

i.e. expression (2.3) is replaced by

$$\langle f(\mathbf{x}, t) f(\mathbf{x}', t') \rangle = \delta(t - t') F(\mathbf{x}, \mathbf{x}') . \quad (2.7)$$

A dependence not only on the relative separation \mathbf{r} but also on the centre of mass $\mathbf{z} = (\mathbf{x} + \mathbf{x}')/2$ is thus introduced for the forcing, and the same is to be expected for the scalar correlation. In the (\mathbf{r}, \mathbf{z}) frame of reference, the equation for the two-point equal-time scalar correlation function reads:

$$\partial_t C = [2\kappa_0 \delta_{\mu\nu} + d_{\mu\nu}^{(v)}] \frac{\partial^2 C}{\partial r_\mu \partial r_\nu} + \frac{(D_0 + 2\kappa_0) \delta_{\mu\nu} + D_{\mu\nu}^{(v)}}{4} \frac{\partial^2 C}{\partial z_\mu \partial z_\nu} + F . \quad (2.8)$$

It is worth noticing that equation (2.8) can be rewritten in a more compact form introducing a $2d$ -dimensional variable

$$\vec{y} = \begin{pmatrix} \mathbf{r} \\ \mathbf{z} \end{pmatrix} .$$

Thus,

$$\partial_t C = \frac{\partial}{\partial y_i} J_i + F , \quad (2.9)$$

where $\vec{J}(\vec{y}, t)$ can be interpreted as a current expressed by

$$J_i = K_{ij} \frac{\partial}{\partial y_j} C .$$

The $2d \times 2d$ matrix $K(\vec{y})$ is made up of two non-zero $d \times d$ blocks:

$$K_{ij} = \begin{pmatrix} 2\kappa_0 \delta_{\mu\nu} + d_{\mu\nu}^{(v)}(\mathbf{r}) & 0 \\ 0 & \frac{(D_0 + 2\kappa_0) \delta_{\mu\nu} + D_{\mu\nu}^{(v)}(\mathbf{r})}{4} \end{pmatrix} . \quad (2.10)$$

A complete decoupling between the cross dependence of each of the two blocks on the other coordinate takes place at “small” (or, better, “not too large”) scales $r \ll L_v$, since here the order of magnitude of $d_{\mu\nu}(\mathbf{r}) \approx D_1 r^\xi$ is negligible with respect to $D_0 \sim D_1 L_v^\xi$. Therefore, $D_{\mu\nu}(\mathbf{r}) \simeq D_0 \delta_{\mu\nu}$ and the matrix becomes:

$$K_{ij} = \begin{pmatrix} 2\kappa_0 \delta_{\mu\nu} + d_{\mu\nu}^{(r)}(\mathbf{r}) & 0 \\ 0 & \frac{(D_0 + \kappa_0) \delta_{\mu\nu}}{2} \end{pmatrix} . \quad (2.11)$$

I shall later exploit this possible simplification and come back to this “ $2d$ -formalism” in section § 2.3.

Back to the (\mathbf{r}, \mathbf{z}) space, it is worth writing, *en passant*, the form assumed by (2.8) for merged points ($\mathbf{x} = \mathbf{x}' \Leftrightarrow r = 0$):

$$\partial_t \langle \theta^2 \rangle = -2\kappa_0 \left\langle \frac{\partial \theta}{\partial z_\mu} \frac{\partial \theta}{\partial z_\mu} \right\rangle + (D_0 + \kappa_0) \frac{\partial^2 \langle \theta^2 \rangle}{\partial z_\mu \partial z_\mu} + F(\mathbf{0}, \mathbf{z}) .$$

The presence of inhomogeneities and anisotropies makes it natural to work in the basis invariant under translations and rotations. The first step is performed by Fourier transforming in \mathbf{z} and defining

$$\begin{aligned} \hat{C} &\equiv \hat{C}(\mathbf{r}, \mathbf{q}) = \int d^d \mathbf{z} e^{-i\mathbf{q}\cdot\mathbf{z}} C(\mathbf{r}, \mathbf{z}) , \\ \hat{F} &\equiv \hat{F}(\mathbf{r}, \mathbf{q}) = \int d^d \mathbf{z} e^{-i\mathbf{q}\cdot\mathbf{z}} F(\mathbf{r}, \mathbf{z}) . \end{aligned}$$

The equation for \hat{C} corresponding to (2.8) reads:

$$\partial_t \hat{C} = [2\kappa_0 \delta_{\mu\nu} + d_{\mu\nu}^{(v)}(\mathbf{r})] \frac{\partial^2 \hat{C}}{\partial r_\mu \partial r_\nu} - \frac{(D_0 + 2\kappa_0) \delta_{\mu\nu} + D_{\mu\nu}^{(v)}(\mathbf{r})}{4} q_\mu q_\nu \hat{C} + \hat{F} . \quad (2.12)$$

This equation is differential only in \mathbf{r} and is algebraic in the centre-of-mass wavenumber \mathbf{q} . The second term on the right-hand side of (2.12) represents the inhomogeneous contribution and coherently vanishes for $q = 0$, which is equivalent to average all over the space. It is convenient to rewrite its \mathbf{r} -dependent coefficient in the following way:

$$\begin{aligned} -\frac{(D_0 + 2\kappa_0) \delta_{\mu\nu} + D_{\mu\nu}^{(v)}(\mathbf{r})}{4} = & - \left[\frac{D_0 + \kappa_0}{2} - \frac{(d-1)(d+\xi)D_1}{4d} r^\xi \right] \delta_{\mu\nu} \\ & + \frac{\xi D_1}{4d} r^\xi \left(\delta_{\mu\nu} - d \frac{r_\mu r_\nu}{r^2} \right) . \end{aligned} \quad (2.13)$$

Substituting it back, it is clear that the last term in (2.13) generates the only contribution (possibly apart from the forcing) in (2.12) not invariant under rotations of \mathbf{r} , because it gives rise to a scalar product between \mathbf{r} and \mathbf{q} that mixes different angular sectors. However, as already pointed out, at separations $r \ll L_v$ a simplification takes place, corresponding to the reduction of (2.10) into (2.11). It is worth noticing that, when r is of the order

of (or larger than) L_v , a coupling between anisotropy and inhomogeneity takes place: I shall later come back to this point. Here, I concentrate on the sole case $r \ll L_v$ in the stationary state with vanishing diffusivity and I can thus consider the simpler equation

$$d_{\mu\nu}(\mathbf{r}) \frac{\partial^2 \hat{C}}{\partial r_\mu \partial r_\nu} - \frac{D_0}{2} q^2 \hat{C} + \hat{F} = 0. \quad (2.14)$$

A dimensional-analysis balance between the first and the second term in (2.14) leads to the introduction of a new scale

$$\ell_q = \left[\frac{D_0}{2(d-1)D_1} q^2 \right]^{-1/(2-\xi)}, \quad (2.15)$$

associated to the strength of the scalar inhomogeneities and measuring the separation above which they become important.

The following aforementioned step consists in performing the decomposition in d -dimensional spherical harmonics [59]:

$$\begin{aligned} \hat{C}(\mathbf{r}, \mathbf{q}) &= \sqrt{\Omega} \sum_{l,m} \hat{C}_{l,m}(r, \mathbf{q}) Y_{l,m}(\Phi), \\ \hat{F}(\mathbf{r}, \mathbf{q}) &= \sqrt{\Omega} \sum_{l,m} \hat{F}_{l,m}(r, \mathbf{q}) Y_{l,m}(\Phi), \end{aligned}$$

with Φ denoting the solid angle associated with \mathbf{r} and Ω its overall value, and in studying the behaviour of the correlation function at separations r smaller than the forcing correlation length L , where \hat{F} (and consequently some $\hat{F}_{l,m} = \hat{F}_{l,m}(r, \mathbf{q})$) is different from zero.

Exploiting definition (2.15), the equation in each anisotropic sector (l, m) for the correlation function $\hat{C}_{l,m} = \hat{C}_{l,m}(r, \mathbf{q})$ reads

$$\begin{aligned} r^{-(d-1)} \partial_r \left(r^{d+\xi-1} \partial_r \hat{C}_l \right) - \frac{(d+\xi-1)l(d-2+l)}{d-1} r^{-2} \hat{C}_l - \ell_q^{-(2-\xi)} \hat{C}_l \\ + \frac{\hat{F}_l}{(d-1)D_1} = 0 \end{aligned} \quad (2.16)$$

where, because of degeneration, the dependence on the subscript m has been dropped.

The Fourier scale q^{-1} (mathematically ranging from 0 to ∞) at which physically relevant effects are expected can be larger or of the same order of L .

In the latter case one has $\ell_q/L \sim (L/L_v)^{\xi/(2-\xi)} \ll 1$ and the lengthscale ℓ_q lies inside the convective range. The homogeneous case is recovered when $q^{-1} \gg L$ so as to insure $\ell_q/L \gg 1$. An important exception is provided, in way of example, by the emission of a tracer from a point source, in which all q 's are excited with the same strength: this case will be investigated in section § 2.4.

It is easy to verify that the general solution of (2.16) is

$$\hat{C}_l(r, \mathbf{q}) = \hat{C}_{(\text{part})l}(r, \mathbf{q}) + r^{-(d+\xi-2)/2} [B_1 K_{\nu_l}(w) + B_2 I_{\nu_l}(w)] , \quad (2.17)$$

where

$$w = \frac{2}{2-\xi} \left(\frac{r}{\ell_q} \right)^{(2-\xi)/2} , \quad \nu_l = \frac{d+\xi-2}{2-\xi} \left[1 + \frac{4(d+\xi-1)l(d-2+l)}{(d-1)(d+\xi-2)^2} \right]^{1/2} .$$

The constants B_1, B_2 are fixed by the boundary conditions and K, I represent the Bessel functions [60] of complex argument. The particular solution $\hat{C}_{(\text{part})l}(r, \mathbf{q})$ of (2.16) can be found, for instance, exploiting the method of variation of constants [61], which leads to

$$\begin{aligned} \hat{C}_{(\text{part})l}(r, \mathbf{q}) = A r^{-(d+\xi-2)/2} & \left[K_{\nu_l}(w) \int_0^w d\omega \varphi_{l;\mathbf{q}}(\rho) \omega^{\nu_0+1} I_{\nu_l}(\omega) \right. \\ & \left. + I_{\nu_l}(w) \int_w^\infty d\omega \varphi_{l;\mathbf{q}}(\rho) \omega^{\nu_0+1} K_{\nu_l}(\omega) \right] , \end{aligned}$$

where

$$\begin{aligned} A &= \left(\frac{2-\xi}{2} \right)^{\nu_0} \ell_q^{(d-\xi+2)/2} , \quad \nu_0 = \nu_l|_{l=0} = \frac{d+\xi-2}{2-\xi} , \\ \omega \equiv w|_{r=\rho} &= \frac{2}{2-\xi} \left(\frac{\rho}{\ell_q} \right)^{(2-\xi)/2} , \quad \varphi_{l;\mathbf{q}}(r) = \frac{\hat{F}_l(r, \mathbf{q})}{(d-1)D_1} . \end{aligned}$$

Regularity at $r = 0$ imposes $B_1 = 0$ since $K_{\nu_l}(w) \stackrel{w \ll 1}{\sim} w^{-\nu_l}$, while the term with B_2 is regular as $r \rightarrow 0$ since $I_{\nu_l}(w) \stackrel{w \ll 1}{\sim} w^{\nu_l}$.

An exact solution can also be found for the values $r \gg L$. Indeed, in this case, one has $\hat{F}_l(r, \mathbf{q}) \simeq 0$, as the forcing correlation rapidly decreases for separations greater than L , and an unforced equation arises:

$$r^{-(d-1)} \partial_r \left(r^{d+\xi-1} \partial_r \hat{C}_l \right) - \frac{(d+\xi-1)l(d-2+l)}{d-1} r^{-2} \hat{C}_l - \ell_q^{-(2-\xi)} \hat{C}_l = 0 . \quad (2.18)$$

The solution of (2.18) reduces to the zero mode,

$$\hat{C}_l(r, \mathbf{q}) = r^{-(d+\xi-2)/2} [B_3 K_{\nu_l}(w) + B_4 I_{\nu_l}(w)] , \quad (2.19)$$

where regularity for $r \rightarrow \infty$ imposes $B_4 = 0$ as $I_{\nu_l}(w) \stackrel{w \gg 1}{\sim} w^{-1/2} e^w$, while the term with B_3 is regular because $K_{\nu_l}(w) \stackrel{w \gg 1}{\sim} w^{-1/2} e^{-w}$.

The correlation of a passive scalar field in the presence of inhomogeneous fluctuations, whose characteristic length is ℓ_q , can be thus computed in the limits of small ($r \ll L$) and large ($r \gg L$) separations with respect to the scalar integral scale L . One finds a dependence on some unknown constants (B_2, B_3) that can be fixed by the boundary conditions upon matching the behaviour of the solution at small and large scales. Under the assumption of an analytical forcing correlation function, $\hat{F}_l(r, \mathbf{q})$ (and consequently $\varphi_{l;\mathbf{q}}(r)$) is a smooth function of r whose asymptotic behaviour as $r \rightarrow 0$ is r^l . This clearly makes the determination of B_2, B_3 dependent on the functional form of $\hat{F}_l(r, \mathbf{q})$. To provide a simple example of how the boundary-condition constants can be fixed, I propose an illustrative calculation assuming a forcing whose correlation function is a step function in r in each sector, i.e.:

$$\hat{F}_l(r, \mathbf{q}) = \hat{F}_l(\mathbf{q}) \Theta(L - r) . \quad (2.20)$$

The analyticity of the forcing correlation function is obviously lost (only momentarily) but, neglecting all the unphysical properties of this statement, the complete solution can be easily written down, showing how the two constants can be explicitly calculated. Indeed, in this case, an exact matching can be performed in $r = L$ comparing the limits ($r \rightarrow L^-$, $r \rightarrow L^+$) of both \hat{C}_l and \hat{C}'_l (prime means derivative with respect to the variable r) deriving from the two expressions (2.17) and (2.19) (see appendix § 2.6). The final result is

$$\hat{C}_l(r; \ell_q) = \begin{cases} \varphi_{l;\mathbf{q}} \ell_q^{2-\xi} w^{-\nu_0} \left[I_{\nu_l}(w) \int_w^W d\omega \omega^{\nu_0+1} K_{\nu_l}(\omega) \right. \\ \quad \left. + K_{\nu_l}(w) \int_0^w d\omega \omega^{\nu_0+1} I_{\nu_l}(\omega) \right] & \text{for } 0 < r < L \\ \varphi_{l;\mathbf{q}} \ell_q^{2-\xi} w^{-\nu_0} K_{\nu_l}(w) \int_0^W d\omega \omega^{\nu_0+1} I_{\nu_l}(\omega) & \text{for } L < r < \infty . \end{cases} \quad (2.21)$$

where

$$W \equiv w|_{r=L} = \frac{2}{2-\xi} \left(\frac{L}{\ell_q} \right)^{(2-\xi)/2} , \quad \phi_{l;\mathbf{q}} = \varphi_{l;\mathbf{q}}(0)$$

(the forcing only appears in the latter r -independent prefactor).

Once one assumes a small-scale description with respect to the velocity integral scale (i.e. $L_v \rightarrow \infty$), the general solution thus depends on three fundamental scales r , L and ℓ_q . These scales represent the separation, the forcing correlation scale and the characteristic length of the inhomogeneities, respectively. From the general solution it is important to note (see appendix § 2.5) that taking the limit $\ell_q \rightarrow \infty$ for fixed L and r , (2.21) reduces to the well-known solution for the homogeneous case. Indeed, the latter solution satisfies the equation:

$$r^{-(d-1)} \partial_r \left(r^{d+\xi-1} \partial_r \hat{C}_l \right) - \frac{(d+\xi-1)l(d-2+l)}{d-1} r^{-2} \hat{C}_l + \varphi_{l;\mathbf{q}} = 0. \quad (2.22)$$

Anyway, in a small scale description with respect to the forcing correlation ($r \ll L$), the presence of a finite ℓ_q can reduce the range of pure power-law behaviour because of the presence of the Bessel functions in the solution. This scenario is clearly opposite to the one considered in the homogeneous limit where a pure power-law behaviour is found.

In order to get a deeper insight about these two different regimes, in the next section I concentrate on a purely isotropic situation where the forcing correlation function depends only on $q = |\mathbf{q}|$ and the correlation of the scalar field coincides with its isotropic sector. The previous unphysical assumption of step-like forcing correlation function is now completely justified in the isotropic ($l = 0$) sector, and an immediate comparison can be made with the homogeneous case forced by (2.4). Moreover, the final results for each \mathbf{q} thus depend on the forcing only through its correlation length L , except for a prefactor. So, this is the simplest, physically relevant assumption with a physical meaning that one can consider to obtain a clear and systematic description of the influence of inhomogeneous contributions.

2.2.3 Analysis of the inhomogeneous isotropic case

I focus here on the isotropic sector ($l = 0$) for the two-point equal-time scalar correlation function, \hat{C}_0 . The technical advantage is now that, alternatively to the method of variation of constants, the particular solution of (2.16) can be chosen as a constant, since the second term in (2.16) vanishes for $l = 0$ and the coefficient of the function $\hat{C}_0(r; \ell_q)$ reduces to a constant. The same

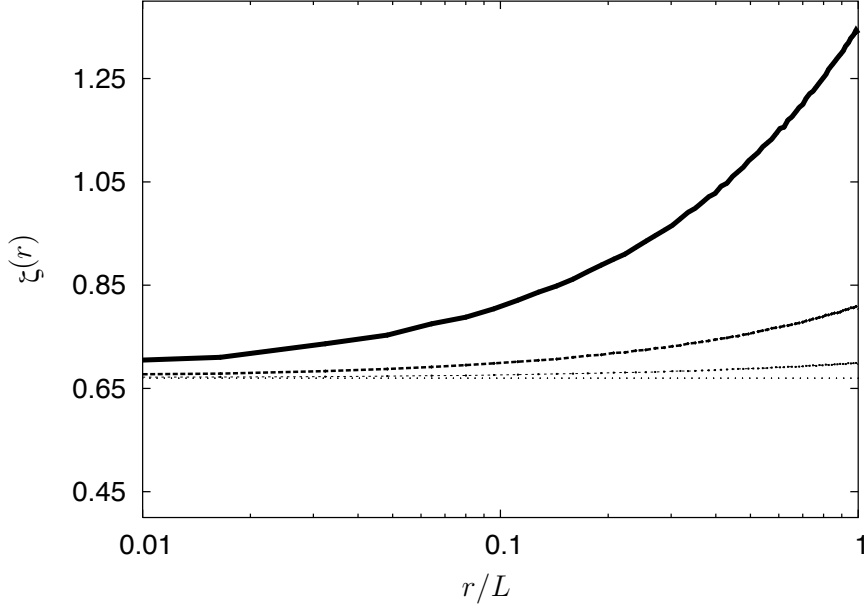


Figure 2.1: Local slopes of $\hat{S}(r; \ell_q) = \hat{C}_0(0; \ell_q) - \hat{C}_0(r; \ell_q)$ in the convective range. Plotted is $\zeta(r) = \frac{d \ln \hat{S}(r; \ell_q)}{d \ln r}$ as a function of r/L for different values of the length-scale ℓ_q . From top to bottom, the cases $\ell_q/L = 0.1, = 1, = 10$ are plotted, respectively. For comparison, the homogeneous case is also plotted (lowest plot).

arguments given for the general case can be repeated to obtain

$$\hat{C}_0(r; \ell_q) = \begin{cases} \phi_{0;q} \ell_q^{2-\xi} + A_2 r^{-(d+\xi-2)/2} I_{\nu_0}(w) & \text{for } 0 < r < L \\ A_3 r^{-(d+\xi-2)/2} K_{\nu_0}(w) & \text{for } L < r < \infty, \end{cases} \quad (2.23)$$

where A_2, A_3 are known functions of L and ℓ_q (see appendix § 2.6). As discussed in the previous section, the presence of the Bessel functions (the fingerprint of the scalar inhomogeneities) makes it impossible to see a clear power-law behaviour in the convective range when $\ell_q/L \sim 1$. This is clearly seen (figure 2.1) by calculating local-slopes (i.e. the logarithmic derivative, which would exactly represent the exponent in the presence of pure power laws) of the difference $\hat{S}(r; \ell_q) \equiv \hat{C}_0(0; \ell_q) - \hat{C}_0(r; \ell_q)$, strictly related to the second-order structure function, where $\hat{C}_0(r; \ell_q)$ is the general solution (2.23). For a fixed L and ξ (say, $\xi = 4/3$, corresponding to the KOC scaling [56]), I can change the ratio ℓ_q/L and examine the local slope behaviours as a function of r/L : the homogeneous case (single power-law behaviour in the convective range) is recovered only when $\ell_q \gg L$, while for ℓ_q of the

same order of L a coexistence of power laws spoils the pure scaling of the homogeneous case.

To be more precise, I focus on the asymptotic properties of (2.23). First of all, one can perform the limit $r/\ell_q \rightarrow 0$ to obtain

$$\hat{C}_0(r; \ell_q) \stackrel{r \ll \ell_q}{\approx} \hat{C}_{(\text{hom})0}(r; \ell_q) \equiv \begin{cases} a(\ell_q) + b_2(\ell_q)r^{2-\xi} & \text{for } 0 < r < L \\ b_3(\ell_q)r^{-(d+\xi-2)} & \text{for } L < r < \infty, \end{cases} \quad (2.24)$$

where $a(\ell_q)$, $b_2(\ell_q)$ and $b_3(\ell_q)$ can be obtained from the expansion of Bessel functions. In the limit $L \ll \ell_q$, a , b_2 and b_3 reduce to the well-known coefficients of the homogeneous isotropic case α , β_2 , and β_3 (see appendix § 2.6). If one also takes into account the successive terms of the expansion in (2.23),

$$I_{\nu_0}(w) = \left(\frac{1}{2}w\right)^{\nu_0} \sum_{k=0}^{\infty} [k! \Gamma(k + \nu_0 + 1)]^{-1} \left(\frac{1}{2}w\right)^{2k}, \quad (2.25)$$

no unique scaling exponent is clearly determined. To quantify how quickly the effect of inhomogeneity is lost as r/ℓ_q decreases, one can thus proceed in the following way. I fix $r = \text{golden section of } L$ as a representative point of the convective range and determine ℓ_q such that the sum of the terms with $k \geq 2$ in (2.25) is equal to a fixed fraction of the $k = 1$ term, from which the $r^{2-\xi}$ contribution in (2.24) originates (I neglect the $k = 0$ term, giving rise to a constant contribution). Percentages of 1%, 2%, 5%, 10% are obtained respectively for $\ell_q/L \simeq 58, 21, 5.3, 1.96$ (with $\xi = 4/3$ and $d = 3$).

In the opposite situation ($\ell_q \ll L$) the function $\hat{C}_0(r; \ell_q)$ approximates the step function $\mathcal{C}\Theta(L - r)$, where $\mathcal{C} \simeq \phi_{0;q}\ell_q^{2-\xi}$. Thus, if $\phi_{0;q} = F_0/(d-1)D_1$ is a constant (I shall call it ‘‘forcing of the first kind’’), the plot of $\hat{C}_0(r; \ell_q)$ collapses on the axis of the abscissas when $\ell_q \rightarrow 0$. On the contrary, if one wanted to keep \mathcal{C} finite, a scaling $\phi_{0;q} = F_0\ell_q^{-(2-\xi)}/(d-1)D_1 \propto q^2$ could be assumed: the collapse would now take place for $\ell_q \rightarrow \infty$; but this simply suggests that some kinds of forcing are not allowed (e.g. I also rule out $\phi_{0;q}$ ’s giving unbounded \mathcal{C} ’s or a ’s, as for example $\phi_{0;q} \propto \ell_q^\gamma$ with $\gamma > 0$ or $< -(2-\xi)$). The finiteness of both a and \mathcal{C} may thus be guaranteed assuming e.g. $\phi_{0;q} = (F_\ell\ell_q^{-(2-\xi)} + F_LL^{-(2-\xi)})/(d-1)D_1$ (‘‘forcing of the second kind’’), with F_ℓ, F_L constants. Of course there would be infinite kinds of allowed forcing, but I will focus on these two because of their physical relevance (the random-point-source problem investigated in section § 2.4 may roughly be seen as a limit of the forcing-of-the-first-kind for vanishing L). The value

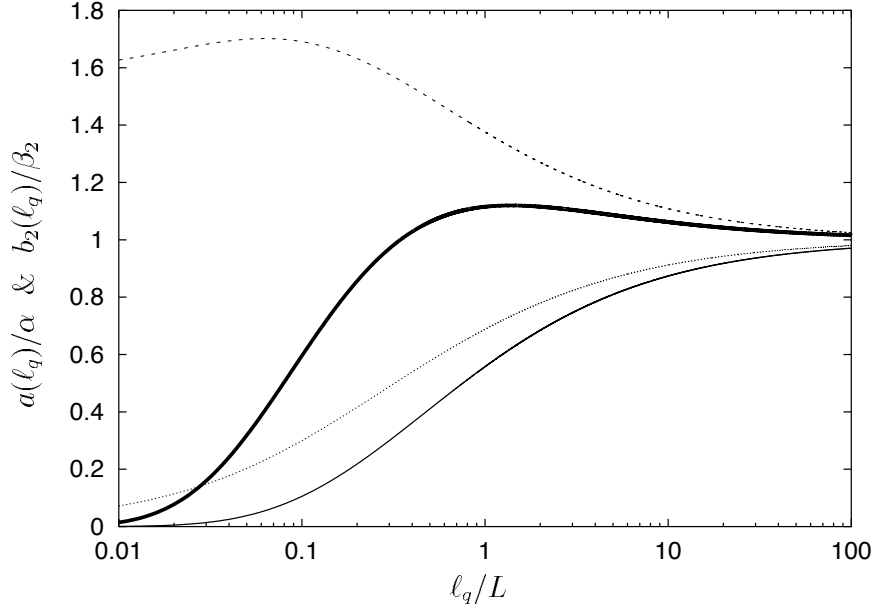


Figure 2.2: Ratios between “actual” (functions of ℓ_q) and “homogeneous” (limit values for $\ell_q \rightarrow \infty$) coefficients: dashed lines represent $a(\ell_q)/\alpha$, solid ones $b_2(\ell_q)/\beta_2$. Thin\thick lines are related to the forcing of the first\second kind, respectively.

chosen for ξ is its Kolmogorov value $4/3$ and I will focus on $d = 3$.

Figure 2.2 represents the ratios of the additive and multiplicative coefficients given by $a(\ell_q)$ and $b_2(\ell_q)$ to the corresponding homogeneous ones α and β_2 , as functions of ℓ_q/L , for both kinds of forcing. The “actual” values attain the “homogeneous” ones only for large ℓ_q 's.

In figure 2.3 I show the plots of the difference $\hat{C}_0(0; \ell_q) - \hat{C}_0(r; \ell_q)$, together with the respective power-law approximations, for two different values of ℓ_q/L , 10^2 and 10^{-2} : in the former case the two kinds of forcing substantially give the same result (only the first kind is thus represented) and the agreement is perfect all over the convective range, while in the latter the separation takes place for $r < \ell_q$ for both kinds of forcing. One should also notice that by decreasing ℓ_q , besides the slower convergence to the power-law behaviour (as remarked in figure 2.1), the value $\hat{C}_0(L; \ell_q)$ tends to decrease with the first kind of forcing and to increase with the second kind.

Figure 2.4 shows

$$\delta\hat{C}(r_L; \ell_q) \equiv \hat{C}_{(\text{hom})0}(r_L; \ell_q) - \hat{C}_0(r_L; \ell_q) ,$$

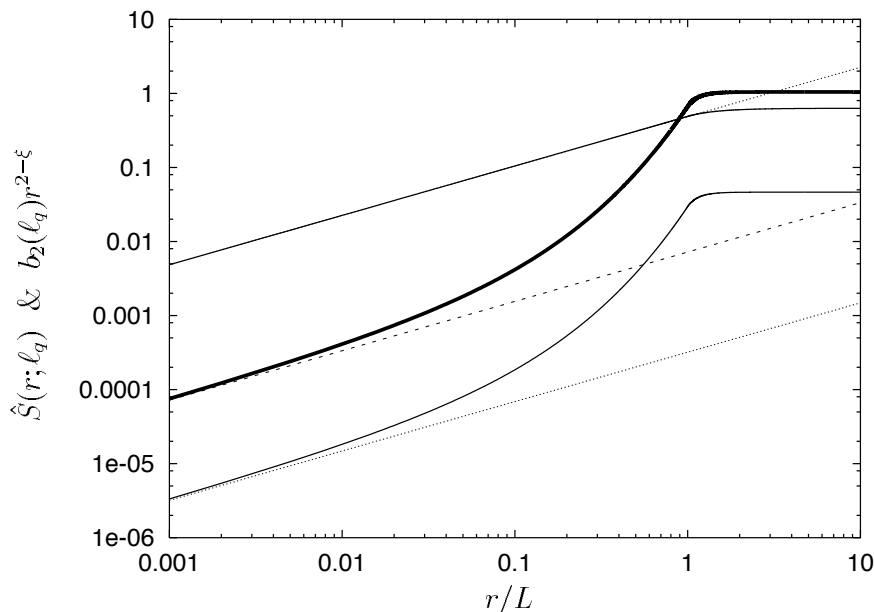


Figure 2.3: Plots of $\hat{S}(r; \ell_q) = \hat{C}_0(0; \ell_q) - \hat{C}_0(r; \ell_q)$ and of the respective power-law approximations (dashed lines) for $\ell_q/L = 10^2$ and forcing of the first kind (upper plot) and $= 10^{-2}$ and both kind of forcings (lower plots). Thin lines are related to the forcing of the first kind and thick lines are related to the forcing of the second kind.

i.e. the difference between the approximated and the actual expressions of $\hat{C}_0(r; \ell_q)$ as functions of ℓ_q/L , calculated for $r = r_L$ lying in the convective range (in this case r_L has been chosen as the golden section of L , but similar plots exist $\forall r < L$). The presence of a maximum is quite intuitive for the first kind of forcing, as both expressions vanish for infinitesimal ℓ_q , but is remarkable for the second kind, which means that the “error” of the approximation becomes negligible not only for large but also for small ℓ_q ’s.

The previous discussion has been carried out in the pseudo-Fourier space (\mathbf{r}, \mathbf{q}) , but the final results must be expressed in the physical space (\mathbf{r}, \mathbf{z}) and a superposition is then needed. It is thus useful to analyse some instructive cases of superpositions.

Figure 2.5 represents the simplest case of superposition, i.e. the excitation of two q ’s, e.g. q_1 and q_2 , with constant or ℓ_q -dependent amplitude. In particular the upper two plots are the (weighted) sum of the modes $\ell_{q_1}/L = 10^3$ and $\ell_{q_2}/L = 1$ and show very similar behaviours between each other (departure

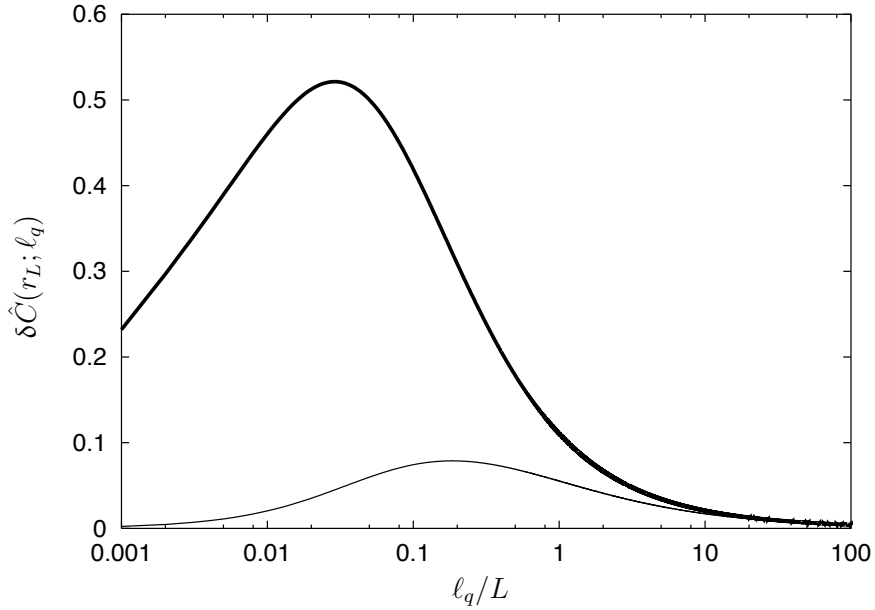


Figure 2.4: Difference between approximated (power-law behaviour with “actual” coefficients $a(\ell_q)$ and $b_2(\ell_q)$) and actual expressions of $\hat{C}_0(r)$ for $r =$ golden section of L . The thin line is related to the forcing of the first kind while the thick one to the forcing of the second kind.

from the $r^{2-\xi}$ straight line at r 's about one order of magnitude smaller than the smaller ℓ_q), while in the lower two ℓ_{q_1} is kept fixed but ℓ_{q_2} is reduced to $10^{-3}L$. In the former case, since the correlation function collapses towards the step function in the limit $\ell_q \rightarrow 0$, the structure function does not “feel” the smallest ℓ_q in the convective range. Obviously the restoration of the correct power-law behaviour depends on the degree of convergence of $\hat{C}_0(r; \ell_q)$ toward the step function (in this case the first kind of forcing converges more rapidly than the second one).

More realistic cases are connected to the excitation of a finite set of discrete modes: in this case the correctness of the power-law approximation is guaranteed (at least) for r 's sufficiently smaller than the minimum ℓ_q , but plots similar to the previous one, with three or more excited q 's, show the same behaviour (smaller and smaller ℓ_q 's cause at first an increase and then a decrease of the separation).

On the contrary, if the forcing has a continuum spectrum, one has to compute the the continuum Fourier antitransformed, which is well defined for

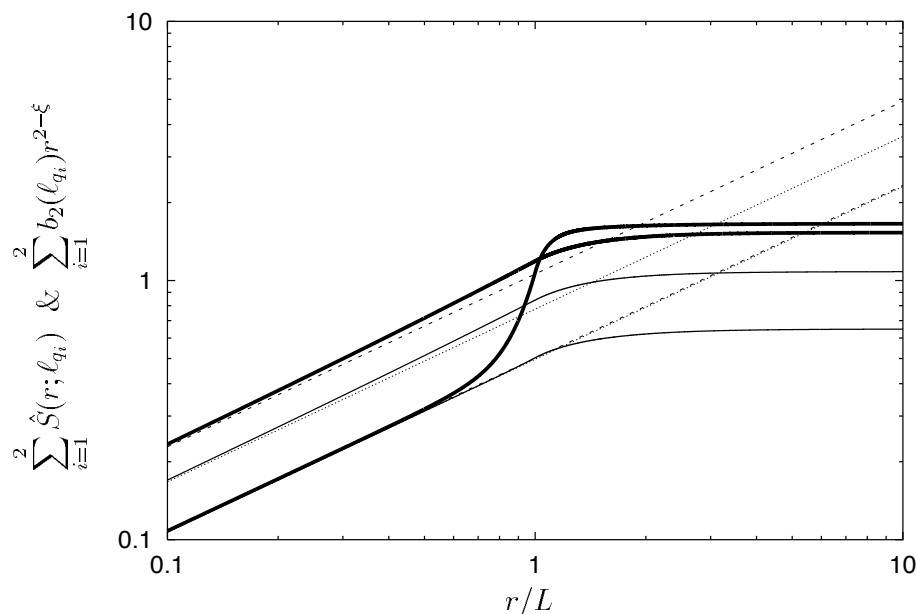


Figure 2.5: Plots of the superpositions of two $\hat{C}_0(0; \ell_q) - \hat{C}_0(r; \ell_q)$ and of the respective power-law approximations (dashed lines) for $\ell_{q_1}/L = 10^3$ and $\ell_{q_2}/L = 1$ (upper two plots) or $= 10^{-3}$ (lower two plots). Thin lines are related to the forcing of the first kind and thick lines are related to the forcing of the second kind.

the forcings I have considered. The result is that an inhomogeneous forcing which takes place at intermediate scales tends to deviate the correlation, from its homogeneous behaviour, more sensibly than if it was concentrated at large scales (which is quite obvious) or at small scales.

2.3 Random point-source emission

I shall now focus on the point-source problem, i.e. on the study of the scalar dispersion in turbulent flows following an emission (or absorption) from a very concentrated source, located e.g. in the origin of the coordinate system. Important examples of this problem are very common in everyday life: for instance, understanding the dispersion in the atmospheric boundary layer of pollutants released by a chimney is a crucial need for industrial societies.

Two relevant cases can be investigated: constant or random-in-time point-source emission. The former case will be studied separately in appendix

§ 2.6, because it requires an approach partially different from the one used up to now (which, on the contrary, can be applied to the random situation) and does not allow to carry out computations completely analytical, thus invoking some numerical shortcut.

Here, I concentrate myself on a Gaussian, zero-average, white-in-time forcing; namely,

$$f(\mathbf{x}, t) = f_0(t)\delta(\mathbf{x}) \quad (2.26)$$

with $\langle f(\mathbf{x}, t)f(\mathbf{x}', t') \rangle = \mathcal{F}_0\delta(t-t')\delta(\mathbf{x})\delta(\mathbf{x}')$, so that (from (2.7)) $F(\mathbf{r}, \mathbf{z}) = \mathcal{F}_0\delta(\mathbf{r})\delta(\mathbf{z})$. In the present case, the forcing-correlation transformed appearing in (2.12), $\hat{F}(\mathbf{r}, \mathbf{q}) = \mathcal{F}_0\delta(\mathbf{r})$, is independent of the centre-of-mass wavenumber. The simplifications performed in order to obtain the stationary equation (2.14) can be reproduced also in this case, and (at the end of the present section) it will be possible to quantify the effect of the approximation $r \ll L_v$, i.e. the relevance of the coupling between inhomogeneity and anisotropy; attention should, in principle, be paid to the limit of vanishing diffusivity, but for the rough flows ($\xi \neq 2$) considered here no commutation problem arises with the limit of vanishing forcing correlation length L . Upon introduction of the typical inhomogeneous lengthscale ℓ_q (2.15) and decomposition on the spherical harmonics, one obtains equation (2.16), whose solution, for $r \neq 0$ (in view of the δ character of the forcing) reduces to the zero mode given by (2.19). To determine the coefficients B_3 and B_4 in each sector, one can appropriately simulate the Dirac δ through a Heaviside Θ , exploiting the vanishing of the rescaled forcing $\varphi_l(r)$ (where the subscript \mathbf{q} has been dropped for obvious reasons) in all the anisotropic sectors $l \neq 0$:

$$\begin{aligned} \delta(\mathbf{r}) &= \frac{r^{-(d-1)}}{\Omega}\delta(r) = \lim_{L \rightarrow 0} \frac{r^{-(d-1)}}{\Omega L}\Theta(L-r) \\ &\Rightarrow \varphi_0(r) = \lim_{L \rightarrow 0} \frac{\mathcal{F}_0 r^{-(d-1)}}{(d-1)D_1\Omega L}\Theta(L-r). \end{aligned}$$

One can thus exploit the results obtained for finite L and consider also the solution for $r < L$, given by (2.17). Matching the solution \hat{C}_l and its first derivative in $r = L$, imposing regularity for small r and vanishing for large r , and eventually taking the limit $L \rightarrow 0$, one finds $B_4 = 0 \forall l$ and

$$B_3 = A \lim_{L \rightarrow 0} \int_0^W d\omega \varphi_l(\rho)\omega^{\nu_0+1} I_{\nu_l}(\omega) = \delta_{l,0} k_{\dagger} \frac{\mathcal{F}_0}{D_1} \ell_q^{-(d+\xi-2)},$$

where $k_{\dagger} = 2(2-\xi)^{-d/(2-\xi)}/(d-1)\Omega\Gamma(\nu_0+1)$ (Γ being Euler's function).

In the pseudospectral space (\mathbf{r}, \mathbf{q}) the scalar-correlation transformed thus

coincides with its isotropic projection and depends only on the moduli r and q (i.e. ℓ_q) as

$$\hat{C}(r; \ell_q) = k_{\dagger} \frac{\mathcal{F}_0}{D_1} \ell_q^{-(d+\xi-2)/2} r^{-(d+\xi-2)/2} K_{\nu_0}(w) .$$

Back to the physical space, the correlation is thus independent of the angle between \mathbf{r} and \mathbf{z} and is a function of r and z only:

$$C(r, z) = k_{\dagger} \frac{\mathcal{F}_0}{D_1} \left(\frac{D_1}{D_0} \right)^{d/2} r^{d\xi/2-2d-\xi+2} \left[1 + \frac{\Omega(2-\xi)^2 D_1}{4\pi D_0} z^2 r^{-(2-\xi)} \right]^{-\frac{d(4-\xi)}{2(2-\xi)}+1} . \quad (2.27)$$

For $d = 2$,

$$k_{\dagger} = k_{\dagger} 2^{-2} \pi^{-1} (2-\xi)^{(4-\xi)/(2-\xi)} \Gamma\left(\frac{2}{2-\xi}\right) ;$$

for $d = 3$,

$$k_{\dagger} = k_{\dagger} 2^{-1} \pi^{-3/2} (2-\xi)^{(7-2\xi)/(2-\xi)} \Gamma\left(\frac{3}{2} + \frac{1+\xi}{2-\xi}\right) .$$

Recalling that the ratio D_1/D_0 appearing in (2.27) is of the order of $L_v^{-\xi}$, two opposite developments are meaningful, corresponding to small or large values of the quantity

$$s = \left(\frac{z}{r}\right)^2 \left(\frac{r}{L_v}\right)^{\xi} . \quad (2.28)$$

For small s (i.e. small z or large r) the correlation is approximated by a power law in r ,

$$C \sim L_v^{-d\xi/2} r^{-d(4-\xi)/2+2-\xi} .$$

On the contrary, for large s , a power law in z is found, and r appears only in subleading terms:

$$C \sim L_v^{\xi(d+\xi-2)/(2-\xi)} z^{2-d(4-\xi)/(2-\xi)} [1 + \text{const.} \times L_v^{\xi} z^{-2} r^{2-\xi}] , \quad (2.29)$$

Expression (2.29) proves that, for r sufficiently smaller than z , the two-point equal-time structure function has a behaviour similar to the homogeneous case (power law in r with exponent $2-\xi$), thus a cascade-like mechanism is expected to take place. In the absence of a large-scale forcing (remember that $L \rightarrow 0$) like the one assumed in (2.4), this can be explained in the following

way. The velocity field sweeps the scalar, initially concentrated where it was released, and generates structures which, $\forall \mathbf{x}$, are correlated on the scale \mathbf{x} ; in other words, correlations between each point \mathbf{x} and the origin $\mathbf{x}' = \mathbf{0}$ are created. In the centre-of-mass frame of reference, this means that in every point \mathbf{z} ($= \mathbf{x}/2$) a local cascade can then take place, starting from separations \mathbf{r} of the order of \mathbf{z} , which thus plays the role of a local forcing correlation length. This can be easily shown in the “ $2d$ -formalism” introduced in section § 2.2: away from the origin, in the steady state, equation (2.9) takes the form

$$\frac{\partial J_i}{\partial y_i} = 0 \iff \boldsymbol{\partial}_r \cdot \mathbf{J}_r = -\boldsymbol{\partial}_z \cdot \mathbf{J}_z, \quad (2.30)$$

where the $2d$ vector \vec{J} is made up of two parts, \mathbf{J}_r and \mathbf{J}_z , parallel to the unit vectors \mathbf{r}/r and \mathbf{z}/z respectively. Only the former survived in the homogeneous case, giving rise to the convective-range balance

$$d_{\mu\nu}^{(v)}(\mathbf{r}) \frac{\partial^2 C}{\partial r_\mu \partial r_\nu} = -F(r), \quad (2.31)$$

which is the analytical expression of the aforementioned constant-flux argument: the derivative respect to r of the left-hand side of (2.31) vanishes, in view of the constance of the corresponding right-hand side. In the point-source case, the right-hand side of (2.30) suggests that the balance is to be written as

$$d_{\mu\nu}^{(v)}(\mathbf{r}) \frac{\partial^2 C}{\partial r_\mu \partial r_\nu} = -\frac{D_0}{2} \frac{\partial^2 C}{\partial z_\mu \partial z_\mu}, \quad (2.32)$$

but the vanishing of the derivative of the left-hand side of (2.32) still takes place for r sufficiently smaller than z . This is proved by figure 2.6, which moreover shows how this interpretation has its validity limit affected by a change in the ratio r/L_v appearing in the adimensional parameter s (2.28). One should indeed remember that the three scales r , z and L_v appear in a nontrivial way in s , whose smallness is the key point for approximation (2.29) and its consequences.

It is also worth noticing that the $r^{-(d+\xi-2)}$ behaviour, which is typical of the homogeneous situation for $r \gg L$, is never followed in this case (even if $L = 0$), unless one integrates the correlation on the whole space, thus averaging out the inhomogeneity; this is equivalent to consider $q = 0$ ($\ell_q \rightarrow \infty$) in the pseudo-spectral space.

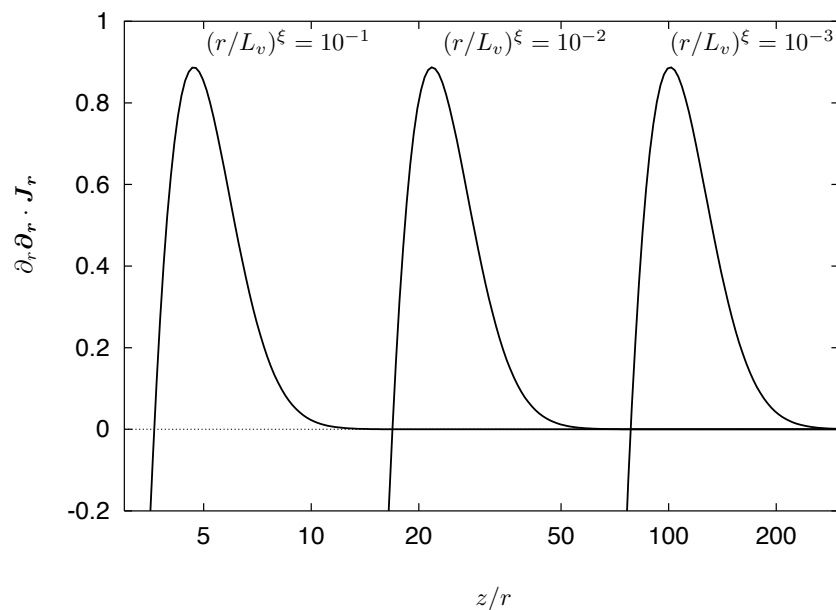


Figure 2.6: Derivative of the left-hand side of equation (2.32) respect to r , plotted vs z/r for $\xi = 4/3$ and $d = 3$. It is evident how the ratio r/L_v , labelling the three curves, affects the limits of the range in which approximation (2.29) is valid and a constant flux holds.

A last comment is required about the relevance of the so-called *finite-size effects*. In other words, one would like to quantify the error deriving from the approximation $r \ll L_v$, which was used to simplify (2.10) into (2.11), and thus to uncouple inhomogeneity from anisotropy. This quantification is now possible, if one proceeds in the following way. First of all, one should notice that, after the decomposition into spherical harmonics, no more foliation takes place. Namely, the equation for the isotropic sector is still a closed one (with the appearance of a new term),

$$r^{-(d-1)} \partial_r \left(r^{d+\xi-1} \partial_r \hat{C}_0 \right) - \ell_q^{-(2-\xi)} \left[1 - \frac{(d+\xi)D_1}{2d(d-1)D_0} r^\xi \right] \hat{C}_0 + \varphi_0(r) = 0 ,$$

and gives

$$\hat{C}_0 \propto r^{-(d+\xi-2)/2} K_{\nu_0}(w) \left[1 + \mathcal{O} \left(\frac{r}{L_v} \right)^\xi \right] , \quad (2.33)$$

but \hat{C}_0 now enters the equation for $l = 2$ as a forcing term (the $l = 1$ sector remains unforced because this procedure only couples even sectors, as can

be deduced by decomposition (2.13)). A simple power-counting operation is possible in Fourier space for $r \ll \ell_q$, where (exploiting the development of $K_{\nu_0}(w)$ for small arguments)

$$\hat{C}_0 \propto r^{-(d+\xi-2)} \left[1 + O\left(\frac{r}{\ell_q}\right)^{2-\xi} \right], \quad (2.34)$$

because in this regime one easily obtains

$$\hat{C}_2 \sim L_v^{-\xi} \ell_q^{-(2-\xi)} r^{-(d+\xi-4)} \sim \left(\frac{r}{L_v}\right)^\xi \left(\frac{r}{\ell_q}\right)^{2-\xi} \hat{C}_0. \quad (2.35)$$

Equation (2.35) shows that the first excited anisotropic sector carries a factor, with respect to the isotropic solution, given by the product between the corrections in (2.33) and in (2.34). Its interpretation is thus very simple and meaningful: at the lowest order, the anisotropic correction derives from the coupling of finite-size effects ($O(r/L_v)^\xi$) and of inhomogeneities ($O(r/\ell_q)^{2-\xi}$). Back to the physical space, such anisotropic corrections are expected to play an important role only when the scales r and z are comparable, but not when either is much greater than the other. An example is provided, for $z = r/2$, by the comparison between the cases $\mathbf{z} \parallel \mathbf{r}$ (where one of the two points in which the correlation is calculated lies on the source) and $\mathbf{z} \perp \mathbf{r}$ (where both points are $\sqrt{2}z$ away from the origin): a difference must clearly exist, but cannot be caught by the isotropic function $C_0(r, z)$ and turns out to be subdominant.

2.4 Conclusions

The properties of the two-point equal-time scalar correlation function for the Kraichnan model of advection have been studied in presence of anisotropies and inhomogeneities. The system can be described by the following three different scales: the separation (r), the forcing correlation length (L , vanishing in the point-source case) and, finally, the lengthscale of the inhomogeneities (ℓ_q). The model can be treated analytically and the properties of both small and large scales can be related to the typical lengthscale ℓ_q . This offers the possibility to analyse the breaking of translationally invariant properties by means of an external forcing term and to check if the small scale statistics

can be regarded as universal in the sense that it does not depend on the details of the inhomogeneous contribution. This somehow universal property is strictly connected to the restoration of a homogeneous limit for scales smaller than the typical inhomogeneous one. This limit ($r \ll \ell_q, L \ll \ell_q$) has been studied and it has been shown how the solution reproduces exactly the one that can be obtained starting from homogeneous equations. On the other side, the homogeneous power-law behaviour is completely spoiled when ℓ_q is of the order of the separation r and it can be seen as a “beating” of different power laws originating from the scalar inhomogeneities.

Summarizing, a pure power-law behaviour exists $\forall \ell_q$ going at sufficiently small r 's and this is a clear indication of the fact that the statistical description can be seen as the same of the homogeneous case but with a reduced range of pure scaling law behaviour. When one passes to the physical space, and if more inhomogeneous modes are excited, the restoration of a convective range is guaranteed if the excitation takes place only at large scales or at large scales together with very small scales ($\ell_q \rightarrow 0$).

The analysis of the superposition can be carried out analytically in the framework of the random-in-time point-source problem, where two different regimes can be identified. In particular, for $r \ll z$, a local cascade process takes place, even in the absence of large-scale forcing. Moreover, it has been possible to analyse the interplay between inhomogeneity, anisotropy and finite-size effects, which take into account the finiteness of the velocity integral scale.

The Kraichnan model has always been used in the past to stimulate the study of small-scale physics in the NS dynamics. In the inhomogeneous situation, it is likely that a typical lengthscale, ℓ_q , should exist also in that case and, even if it should depend on new and more physical quantities (with respect to the Kraichnan case), one expects a similar phenomenological behaviour concerning recovery of homogeneity in the small-scale statistics.

2.5 Appendix on calculation details

Starting from the equation for the projection of two-point equal-time correlation function in the anisotropic sector l , (2.16), and assuming a forcing whose correlation function is a step function in r , (2.20), one can perform an exact matching in $r = L$ by comparing the limits of $\hat{C}_l(r, \mathbf{q})$ and of $\hat{C}'_l(r, \mathbf{q})$ (prime means derivative respect to the variable r) deriving from (2.17) and

(2.19):

$$\left\{ \begin{array}{l} \lim_{r \rightarrow L^-} \hat{C}_l(r, \mathbf{q}) = \hat{C}_{(\text{part})l}(L, \mathbf{q}) + B_2 L^{-(d+\xi-2)/2} I_{\nu_l}(W) \\ \lim_{r \rightarrow L^+} \hat{C}_l(r, \mathbf{q}) = B_3 L^{-(d+\xi-2)/2} K_{\nu_l}(W) \end{array} \right. ,$$

$$\left\{ \begin{array}{l} \lim_{r \rightarrow L^-} \hat{C}'_l(r, \mathbf{q}) = \hat{C}'_{(\text{part})l}(L, \mathbf{q}) + B_2 \left[-\frac{d+\xi-2}{2} L^{-(d+\xi)/2} I_{\nu_l}(W) \right. \\ \left. + \ell_q^{-(2-\xi)/2} L^{-(d+2\xi-2)/2} I'_{\nu_l}(W) \right] \\ \lim_{r \rightarrow L^+} \hat{C}'_l(r, \mathbf{q}) = B_3 \left[-\frac{d+\xi-2}{2} L^{-(d+\xi)/2} K_{\nu_l}(W) \right. \\ \left. + \ell_q^{-(2-\xi)/2} L^{-(d+2\xi-2)/2} K'_{\nu_l}(W) \right] \end{array} \right. .$$

The correlation function must be continuous in $r = L$, and the same is true for its first derivative. One can thus write the complete solution (for all ℓ_q) as

$$\hat{C}_l(r, \mathbf{q}) = \begin{cases} \hat{C}_{(\text{part})l}(r, \mathbf{q}) + B_2 r^{-(d+\xi-2)/2} I_{\nu_l}(w) & \text{for } 0 < r < L \\ B_3 r^{-(d+\xi-2)/2} K_{\nu_l}(w) & \text{for } L < r < \infty, \end{cases} \quad (2.36)$$

where the two constants are

$$B_2 = -A\phi_{l;\mathbf{q}} \int_W^\infty d\omega \omega^{\nu_0+1} K_{\nu_l}(\omega), \quad B_3 = A\phi_{l;\mathbf{q}} \int_0^W d\omega \omega^{\nu_0+1} I_{\nu_l}(\omega).$$

Plugging the values of B_2 and B_3 in (2.36) one can obtain the exact solution written in terms of w and W :

$$\hat{C}_l(r, \mathbf{q}) = \begin{cases} \phi_{l;\mathbf{q}} \ell_q^{2-\xi} w^{-\nu_0} \left[I_{\nu_l}(w) \int_w^W d\omega \omega^{\nu_0+1} K_{\nu_l}(\omega) \right. \\ \left. + K_{\nu_l}(w) \int_0^w d\omega \omega^{\nu_0+1} I_{\nu_l}(\omega) \right] & \text{for } 0 < r < L \\ \phi_{l;\mathbf{q}} \ell_q^{2-\xi} w^{-\nu_0} K_{\nu_l}(w) \int_0^W d\omega \omega^{\nu_0+1} I_{\nu_l}(\omega) & \text{for } L < r < \infty. \end{cases}$$

In the limit $\ell_q \rightarrow \infty$ for fixed L and r , one finds the well-known solution for the homogeneous case. Indeed, in this limit, for $r < L$ one has

$$\begin{aligned} \phi_{l;\mathbf{q}} \ell_q^{2-\xi} w^{-\nu_0} I_{\nu_l}(w) \int_w^W d\omega \omega^{\nu_0+1} K_{\nu_l}(\omega) &\xrightarrow{\ell_q \rightarrow \infty} \frac{2\phi_{l;\mathbf{q}} \left(L^{2-\xi-\zeta_l^+} r^{\zeta_l^+} - r^{2-\xi} \right)}{(2-\xi)^2(\nu_0 - \nu_l + 2)\nu_l} \\ \phi_{l;\mathbf{q}} \ell_q^{2-\xi} w^{-\nu_0} K_{\nu_l}(w) \int_0^w d\omega \omega^{\nu_0+1} I_{\nu_l}(\omega) &\xrightarrow{\ell_q \rightarrow \infty} \frac{2\phi_{l;\mathbf{q}} r^{2-\xi}}{(2-\xi)^2(\nu_0 + \nu_l + 2)\nu_l}, \end{aligned}$$

and, for $r > L$,

$$\phi_{l;\mathbf{q}} \ell_q^{2-\xi} w^{-\nu_0} K_{\nu_l}(w) \int_0^W d\omega \omega^{\nu_0+1} I_{\nu_l}(\omega) \xrightarrow{\ell_q \rightarrow \infty} \frac{2\phi_{l;\mathbf{q}} L^{2-\xi-\zeta_l^-} r^{\zeta_l^-}}{(2-\xi)^2(\nu_0 + \nu_l + 2)\nu_l},$$

where $\zeta_l^\pm = (-\nu_0 \pm \nu_l)(2-\xi)/2$. One finally obtains

$$\hat{C}_l(r) = \begin{cases} \frac{2\phi_{l;\mathbf{q}}}{(2-\xi)^2(\nu_0 - \nu_l + 2)\nu_l} L^{2-\xi-\zeta_l^+} r^{\zeta_l^+} \\ \quad - \frac{4\phi_{l;\mathbf{q}}}{(2-\xi)^2((\nu_0 + 2)^2 - \nu_l^2)} r^{2-\xi} & \text{for } 0 < r < L \\ \frac{2\phi_{l;\mathbf{q}}}{(2-\xi)^2(\nu_0 + \nu_l + 2)\nu_l} L^{2-\xi-\zeta_l^-} r^{\zeta_l^-} & \text{for } L < r < \infty, \end{cases}$$

which is the solution that can be exactly obtained from the homogeneous equation projected along the anisotropic sector l , (2.22).

In the isotropic case the particular solution of the forced equation can be chosen as a constant, since the second term in (2.16) vanishes for $l = 0$ and the coefficient of the function $\hat{C}_0(r; \ell_q)$ reduces to a constant. The complete solution can thus be written in the form (2.23), where the two constants are

$$A_2 = -\frac{2\phi_{0;\mathbf{q}}}{2-\xi} L^{d/2} \rho_q^{(2-\xi)/2} K_{\nu_0+1}(W), \quad A_3 = -A_2 \frac{I_{\nu_0+1}(W)}{K_{\nu_0+1}(W)}.$$

Performing the limit $r, L \ll \ell_q$ and exploiting the expansion of Bessel functions, one easily obtains

$$\hat{C}_0(r; \ell_q) \stackrel{r \ll \ell_q}{\approx} \hat{C}_{(\text{hom})0}(r; \ell_q) \equiv \begin{cases} a(\ell_q) + b_2(\ell_q) r^{2-\xi} & \text{for } 0 < r < L \\ b_3(\ell_q) r^{-(d+\xi-2)} & \text{for } L < r < \infty, \end{cases}$$

where the coefficients can be found after simple but lengthy algebra:

$$\begin{aligned} a(\ell_q) &= \phi_{0;q} \ell_q^{2-\xi} + A_2 \frac{(2-\xi)^{-(d+\xi-2)/(2-\xi)}}{\Gamma(\nu_0+1)} \ell_q^{-(d+\xi-2)/2}, \\ b_2(\ell_q) &= A_2 \frac{(2-\xi)^{-(d-\xi+2)/(2-\xi)}}{\Gamma(\nu_0+2)} \ell_q^{-(d-\xi+2)/2}, \\ b_3(\ell_q) &= A_3 \frac{(2-\xi)^{(d+\xi-2)/2} \Gamma(\nu_0)}{2} \ell_q^{(d+\xi-2)/2}, \end{aligned}$$

with

$$\begin{aligned} a(\ell_q) \xrightarrow{\ell_q \rightarrow \infty} \alpha &= \frac{\hat{F}(0, \mathbf{0}) L^{2-\xi}}{(d-1)(2-\xi)(d+\xi-2)D_1}, \\ b_2(\ell_q) \xrightarrow{\ell_q \rightarrow \infty} \beta_2 &= -\frac{\hat{F}(0, \mathbf{0})}{d(d-1)(2-\xi)D_1}, \\ b_3(\ell_q) \xrightarrow{\ell_q \rightarrow \infty} \beta_3 &= \frac{\hat{F}(0, \mathbf{0}) L^d}{d(d-1)(d+\xi-2)D_1}, \end{aligned}$$

that correspond to the well-known homogeneous isotropic case.

2.6 Appendix on constant point-source emission

In this section I will show some results about the constant-point-source problem, i.e. a time-independent scalar emission from the origin: equation (2.26) of section § 2.3 should thus be replaced by $f(\mathbf{x}, t) = f_0 \delta(\mathbf{x})$. An immediate consequence is that the mean value $\langle \theta \rangle(\mathbf{x}, t)$ has now a nontrivial dynamics, ruled by

$$\partial_t \langle \theta \rangle = D_\kappa \partial^2 \langle \theta \rangle + f, \quad (2.37)$$

where $D_\kappa = D_0/2 + \kappa_0$. Equation (2.37) can be solved by a spatial Fourier transform ($\mathbf{x} \mapsto \mathbf{k}$) yielding

$$\langle \hat{\theta} \rangle(\mathbf{k}, t) = f_0 \int_0^t ds e^{-D_\kappa k^2 (t-s)} = f_0 \frac{1 - e^{-D_\kappa k^2 t}}{D_\kappa k^2}. \quad (2.38)$$

Back to the physical space, in three dimensions one obtains the asymptotic mean scalar profile

$$\langle \theta \rangle(\mathbf{x}, t) \xrightarrow{t \rightarrow \infty} \frac{f_0}{4\pi D_\kappa x}. \quad (2.39)$$

When writing the equation for the two-point equal-time scalar correlation function (the analogous of (2.8)), one must take into account the nonrandom character of forcing, therefore F should now be interpreted as the correlator $\langle \theta(\mathbf{x}, t)f(\mathbf{x}', t) + \theta(\mathbf{x}', t)f(\mathbf{x}, t) \rangle$. Specifically, one has:

$$\begin{aligned} \partial_t C = & \left[2\kappa_0 \delta_{\mu\nu} + d_{\mu\nu}^{(v)} \right] \frac{\partial^2 C}{\partial r_\mu \partial r_\nu} + \frac{(D_0 + 2\kappa_0) \delta_{\mu\nu} + D_{\mu\nu}^{(v)}}{4} \frac{\partial^2 C}{\partial z_\mu \partial z_\nu} \\ & + f_0 \left[\delta \left(\mathbf{z} + \frac{\mathbf{r}}{2} \right) \langle \theta \rangle \left(\mathbf{z} - \frac{\mathbf{r}}{2}, t \right) + \delta \left(\mathbf{z} - \frac{\mathbf{r}}{2} \right) \langle \theta \rangle \left(\mathbf{z} + \frac{\mathbf{r}}{2}, t \right) \right], \end{aligned}$$

which, after Fourier transforming ($\mathbf{z} \mapsto \mathbf{q}$), reads (compare with (2.12)):

$$\begin{aligned} \partial_t \hat{C} = & \left[2\kappa_0 \delta_{\mu\nu} + d_{\mu\nu}^{(v)} \right] (\mathbf{r}) \frac{\partial^2 \hat{C}}{\partial r_\mu \partial r_\nu} - \frac{(D_0 + 2\kappa_0) \delta_{\mu\nu} + D_{\mu\nu}^{(v)}(\mathbf{r})}{4} q_\mu q_\nu \hat{C} \\ & + f_0 \left[e^{i\mathbf{q} \cdot \mathbf{r}/2} \langle \theta \rangle(-\mathbf{r}, t) + e^{-i\mathbf{q} \cdot \mathbf{r}/2} \langle \theta \rangle(\mathbf{r}, t) \right]. \end{aligned}$$

In the limit of vanishing diffusivity and for separations much smaller than the velocity integral scale, the steady-state equation corresponding to (2.14) is:

$$d_{\mu\nu}(\mathbf{r}) \frac{\partial^2 \hat{C}}{\partial r_\mu \partial r_\nu} - \frac{D_0}{2} q^2 \hat{C} + \frac{f_0^2 \cos(\mathbf{q} \cdot \mathbf{r}/2)}{\pi D_0 r} = 0. \quad (2.40)$$

The correlation \hat{C} is thus a function of the moduli r , q and of the angle γ between \mathbf{q} and \mathbf{r} . Therefore, (2.40) can be rewritten as:

$$\begin{aligned} \partial_r \left(r^{2+\xi} \partial_r \hat{C} \right) + \frac{2+\xi}{2} r^\xi \partial_{\cos \gamma} \left[(1 - \cos^2 \gamma) \partial_{\cos \gamma} \hat{C} \right] - \frac{D_0}{4D_1} q^2 r^2 \hat{C} \\ + \frac{f_0^2}{2\pi D_0 D_1} r \cos \left(\frac{qr \cos \gamma}{2} \right) = 0. \end{aligned} \quad (2.41)$$

The decomposition onto spherical harmonics now coincides with a projection on the Legendre polynomials $p_l(\cos \gamma)$. Indeed, writing

$$\hat{C}(\mathbf{r}, \mathbf{q}) = \sum_{l=0}^{\infty} \hat{c}_l(r, q) p_l(\cos \gamma)$$

and exploiting the plane wave expansion, (2.41) becomes

$$\begin{aligned} \partial_r \left(r^{2+\xi} \partial_r \hat{c}_l \right) - \frac{(2+\xi)l(l+1)}{2} r^\xi \hat{c}_l - \frac{D_0}{4D_1} q^2 r^2 \hat{c}_l \\ + \frac{(-1)^{l/2} (2l+1) f_0^2}{2\pi D_0 D_1} r j_l \left(\frac{qr}{2} \right) = 0, \end{aligned} \quad (2.42)$$

j_l being the spherical Bessel function. Focusing on the isotropic sector $l = 0$, (2.42) simplifies in

$$\partial_r (r^{2+\xi} \partial_r \hat{c}_0) - \frac{D_0 q^2}{4D_1} r^2 \hat{c}_0 + \frac{f_0^2}{\pi D_0 D_1 q} \sin\left(\frac{qr}{2}\right) = 0,$$

which, for $0 < \xi < 2$, clearly possesses the same zero modes of the general inhomogeneous case studied in section § 2.2, involving modified Bessel functions. Unfortunately, no exact complete solution can be found analytically for every q , which is then needed to perform the Fourier antitransformed. One can thus focus on the limit case $\xi = 2$, representing smooth flows, where the zero modes consist in power laws, and finds:

$$\begin{aligned} \hat{c}_0(r, q) = & \frac{f_0^2 \mathcal{Q}^{-1} R^{-1}}{\pi D_0^{3/2} D_1^{1/2}} \left\{ -\frac{Q^{(\mathcal{Q}-1)/2} R^{(\mathcal{Q}-1)/2}}{2^{(\mathcal{Q}+1)/2}} \cos\left[\frac{\pi}{4}(\mathcal{Q}-1)\right] \Gamma\left[-\frac{1}{2}(\mathcal{Q}+1)\right] \right. \\ & + \frac{1}{\mathcal{Q}-1} {}_1F_2\left(-\frac{1}{4}(\mathcal{Q}-1); \frac{3}{2}, -\frac{1}{4}(\mathcal{Q}-1)+1; -\frac{Q^2 R^2}{16}\right) \\ & \left. + \frac{1}{\mathcal{Q}+1} {}_1F_2\left(\frac{1}{4}(\mathcal{Q}+1); \frac{3}{2}, \frac{1}{4}(\mathcal{Q}+1)+1; -\frac{Q^2 R^2}{16}\right) \right\}, \end{aligned}$$

F being the hypergeometric function. The adimensional variables are defined as $R = r(D_0/D_1)^{-1/\xi}$ and $Q = q(D_0/D_1)^{1/\xi}$, with $\mathcal{Q} = (9 + Q^2)^{1/2}$. This expression can then be antitransformed numerically to find the isotropic behaviour of the correlation function:

$$C_{(\text{is})}(r, z) = \frac{1}{2\pi^2 z} \int dq q \sin(qz) \hat{c}_0(r, q).$$

An alternative subject of investigation may be represented by the fluctuation field $\vartheta \equiv \theta - \langle \theta \rangle$, satisfying

$$\partial_t \vartheta + \mathbf{v} \cdot \boldsymbol{\partial} \vartheta = \kappa_0 \partial^2 \vartheta - \mathbf{v} \cdot \boldsymbol{\partial} \langle \theta \rangle - \frac{D_0}{2} \partial^2 \langle \theta \rangle.$$

The resulting equation for the two-point, equal-time, scalar-fluctuation correlation function $C_2^{(\vartheta)} \equiv \langle \vartheta(\mathbf{x}, t) \vartheta(\mathbf{x}', t) \rangle$ reads:

$$\begin{aligned} \partial_t C_2^{(\vartheta)} = & [2\kappa_0 \delta_{\mu\nu} + d_{\mu\nu}^{(v)}] \frac{\partial^2 C_2^{(\vartheta)}}{\partial r_\mu \partial r_\nu} + \frac{(D_0 + 2\kappa_0) \delta_{\mu\nu} + D_{\mu\nu}^{(v)}}{4} \frac{\partial^2 C_2^{(\vartheta)}}{\partial z_\mu \partial z_\nu} \\ & + \frac{f_0^2}{16\pi^2 D_\kappa^2} D_{\mu\nu}^{(v)} \frac{(z_\mu + r_\mu/2)(z_\nu - r_\nu/2)}{|\mathbf{z} + \mathbf{r}/2|^3 |\mathbf{z} - \mathbf{r}/2|^3}. \end{aligned}$$

It is worth noticing that equation (2.38) does not yield a stationary state in two dimensions: in simple words, this is due to the fact the scalar, continuously pumped by the source, does not have “room enough” to spread, and therefore continues to accumulate in every point. One could thus modify the starting equation (2.1) by introducing, on its right-hand side, an additive linear term simulating deposition:

$$\partial_t \theta(\mathbf{x}, t) + \mathbf{v}(\mathbf{x}, t) \cdot \boldsymbol{\partial} \theta(\mathbf{x}, t) = \kappa_0 \partial^2 \theta(\mathbf{x}, t) + f(\mathbf{x}, t) - \tau^{-1} \theta(\mathbf{x}, t) .$$

It can be shown that equation (2.38) now takes the form

$$\langle \hat{\theta} \rangle(\mathbf{k}, t) = f_0 \frac{1 - e^{-(D_\kappa k^2 + 1/\tau)t}}{D_\kappa k^2 + 1/\tau} ,$$

which leads to the steady state

$$\langle \theta \rangle(\mathbf{x}, t) \xrightarrow{t \rightarrow \infty} \frac{f_0}{D_\kappa} K_0 \left(\frac{x}{\sqrt{D_\kappa \tau}} \right) .$$

Part II

Turbulence at macroscopic scales

Chapter 3

Analytical models for closures

The issue of the parameterization of small scale (“subgrid”) turbulence is addressed in the context of passive scalar transport. I focus on the Kraichnan advection model which lends itself to the analytical investigation of the closure problem. I derive systematically the dynamical equations which rule the evolution of the coarse-grained scalar field. At the lowest-order approximation in l/r , l being the characteristic scale of the filter defining the coarse-grained scalar field and r the inertial-convective-range separation, the classical eddy-diffusivity parameterization of small scales is recovered. At the next-leading order a dynamical closure is obtained. The latter outperforms the classical model and is therefore a natural candidate for subgrid modelling of scalar transport in generic turbulent flows.

The chapter is organized as follows: in the introduction § 3.1 I underline the necessity of coarse-graining processes in turbulence, in particular for the study of passive scalars. In section § 3.2 I recall the basic equations and I introduce the filtering process. In section § 3.3 I show an application to a particular situation which provides an example of exact closure. In section § 3.4 I focus again on the Kraichnan advection model and I list some exact expressions for the coarse-grained fields. Section § 3.5 provides a series of possible closures, emerging with different degrees of approximation or in different contexts. Conclusions and perspectives follow in section § 3.6. The three appendices § 3.7, § 3.8 and § 3.9 are devoted respectively to: provide some exact analytical expressions, study the limit cases of purely diffusive or smooth flows, quote some results on small-scale quantities.

3.1 Introduction

One of the most striking characteristics of hydrodynamic turbulence is the presence of a wide range of active length and time scales. If, on the one hand, this huge number of active scales is the ideal framework to investigate “classical” problems in the realm of basic turbulent research (e.g. in relation to global scale invariance and its violation in the form of intermittency and anomalous scaling, which was the object of investigation in the previous part), on the other hand the proliferation of degrees of freedom leaves severe limitations to the deterministic description of turbulent fields. Moreover, these scales are strongly and nonlinearly coupled, a fact that makes analytical approaches, at best, impractical. The situation does not look better for direct numerical simulations of turbulent systems: to fully resolve a turbulent flow requires at least L/η grid points in each spatial direction [1], L and η being the integral scale and the dissipation scale respectively (see also [62] for a possible reformulation accounting for the temporal degrees of freedom, which leads to a further increase in the required computational work). In the atmosphere, for instance, the ratio L/η may become of the order of 10^9 ($\eta \sim 10^{-3}$ m and $L \sim 10^6$ m), thus requiring the dynamical description of 10^{27} spatial degrees of freedom. This remains, up to now and probably also in the near future, a prohibitive task.

To overcome the problem, “coarse-grained” versions of the original hydrodynamic equations are often considered in order to describe large-scale features of the original full system. As a matter of fact, in many situations of practical interest (e.g. the description of the evolution of a pollutant emitted by sources in the atmospheric boundary layer) one is not interested in describing the details (i.e. small-scale dynamics) of turbulent fields but, rather, in focusing on their large-scale behaviour. In other words, one passes from a detailed description of *mesoscopic* scales, as in the previous part of this manuscript, to a study of the sole *macroscopic* scales, which represent the subject of the present part. The large-eddy simulation (LES) technique is probably the most popular example [63] of this viewpoint. The success of such a strategy is however strongly dependent on the realism of the description of small scales in terms of the large, explicitly resolved, scales. The problem of representing small unresolved scales in the absence of scale separation — the long-known *closure problem* — attracts a great deal of attention in many domains, ranging from geophysics to engineering [64], and is one among the many challenges of turbulence theory.

My goal here is to shed some light on this aspect within the context of scalar turbulence, where considerable progresses have been achieved in the last few years [65, 46]. For this purpose I will consider a particular model of passive scalar transport [36, 37] where the LES strategy can be formulated and the problem of relating unresolved scales to resolved ones can be successfully attacked analytically.

In this respect, the Kraichnan model has some characteristics of paramount importance. First, exact expressions for relevant statistical observables can be derived from first principles, that is from equation (3.1): this amounts to saying that the observables for the “fully resolved case” are known. An example is expression (3.17) for the two-point equal-time scalar correlation function, an observable tightly related to the Fourier spectrum of the scalar field. Moreover, closures for the large-scale dynamics can be derived in a systematical way (see section § 3.5) and their predictions can be analytically checked against the exact solution. These features make the Kraichnan model an ideal playground for studying LES closures.

3.2 Large-eddy simulation for passive scalar turbulence

3.2.1 Basic equation and phenomenology

According to what stated at the beginning of section § 2.2, the basic equation governing the dynamics of a passive scalar field $\theta(\mathbf{x}, t)$ is the well-known advection-diffusion forced equation

$$\partial_t \theta(\mathbf{x}, t) + \mathbf{v}(\mathbf{x}, t) \cdot \partial \theta(\mathbf{x}, t) = \kappa_0 \partial^2 \theta(\mathbf{x}, t) + f(\mathbf{x}, t). \quad (3.1)$$

The advecting velocity field $\mathbf{v}(\mathbf{x}, t)$ is assumed incompressible: $\partial \cdot \mathbf{v} = 0$. Scalar fluctuations are injected into the system at a large scale L by the forcing term $f(\mathbf{x}, t)$, acting as an external source. Scalar dissipation takes place at small scales, of order η , and is accounted for by the molecular diffusivity κ_0 .

A strong analogy with the NS turbulence holds: the number of active spatial degrees of freedom [66] rapidly increases with the Péclet number Pe (the analogous of the Reynolds number) and scales as $(L/\eta)^d \sim Pe^{3d/4}$, where d is the space dimension (≥ 2). The advantage of dealing with (3.1) instead of

NS consists both in the linearity of the equation and in the scalar character of the unknown field, and finally in the locality of the physical-space description (i.e. the analogous of the pressure field is absent). Nevertheless, the importance of scalar turbulence is underlined by the considerable progress that has been achieved in the last few years in this context [65].

3.2.2 Definition of the filtering process

Coarse-grained fields (denoted with a tilde) are obtained from the original, fully-resolved fields through a convolution with a low-pass isotropic filter P_l of characteristic length l , lying in the convective range of scales: $\eta \ll l \ll L$. In particular, one has

$$\tilde{\theta}(\mathbf{x}, t) \equiv \int d^d \mathbf{y} P_l(\mathbf{x} - \mathbf{y}) \theta(\mathbf{y}, t) = \int d^d \mathbf{s} P_l(\mathbf{s}) \theta(\mathbf{x} + \mathbf{s}, t) = (P_l \star \theta)(\mathbf{x}, t), \quad (3.2)$$

and similarly for $\tilde{\mathbf{v}} \equiv P_l \star \mathbf{v}$ and $\tilde{f} \equiv P_l \star f$. The filtering process thus defines a linear operator which commutates with any partial derivative, because of the structure of the convolution kernel, but which does not factorize when acting on products (the filtered of a product is not the product of the filtered).

Small-scale fluctuations, denoted with a star, are defined as:

$$\theta^* \equiv \theta - \tilde{\theta}, \quad \mathbf{v}^* \equiv \mathbf{v} - \tilde{\mathbf{v}}, \quad f^* \equiv f - \tilde{f}. \quad (3.3)$$

3.2.3 The problem of closure in the large scale

The large-eddy simulation (LES) strategy is carried out by convolving (3.1) with the filter P_l , in order to obtain an equation for the coarse-grained fields:

$$\partial_t \tilde{\theta} + \widetilde{\mathbf{v} \cdot \partial \theta} = \kappa_0 \partial^2 \tilde{\theta} + \tilde{f}. \quad (3.4)$$

Unfortunately, this is not a closed equation in the large scales, as the multiplicative (in the filtering operation) term still involves a product between fully-resolved fields. I thus rearrange it in the form

$$\partial_t \tilde{\theta} + \tilde{\mathbf{v}} \cdot \partial \tilde{\theta} = \kappa_0 \partial^2 \tilde{\theta} + \tilde{f} - \partial \cdot \boldsymbol{\tau}^{(\theta)}, \quad (3.5)$$

where the subgrid scalar flux $\boldsymbol{\tau}^{(\theta)}$ is given by:

$$\boldsymbol{\tau}^{(\theta)} \equiv \widetilde{\mathbf{v} \theta} - \tilde{\mathbf{v}} \tilde{\theta}. \quad (3.6)$$

The aim of LES closures [63] is to express $\partial \cdot \tau^{(\theta)}$ in terms of coarse-grained fields, in order to get a closed equation describing the large-scale dynamics autonomously. Once this purpose is accomplished, (3.5) can be integrated numerically on a mesh of spacing l instead of η , as it would be necessary for the original equation (3.1). This less-demanding integration means a huge gain in memory and CPU time requirements and represents the essential advantage of the LES strategy.

From a general point of view, the perfect closure (i.e. having the “true” $\tau^{(\theta)}$) is able to correctly represent all the observables built by filtering the “true” field θ . On the contrary, only some observables, and some of them in principle better than others, can be correctly described by any empirical closure. It is worth noticing that, which observable is properly reproduced, can be assessed only *a posteriori* (e.g. by comparing LES predictions against experiments).

Unluckily, no general closed expression for $\partial \cdot \tau^{(\theta)}$ in terms of $\tilde{\theta}$ and $\tilde{\mathbf{v}}$ is available: this is a clear indication of the strong coupling between all scales which is typical in turbulence. A remarkable exception is provided by the case where there is a marked scale separation between velocity and scalar length and time scales. It is then possible to show [67, 68, 69] that the effect of unresolved scales is just the renormalization of the molecular diffusion coefficient κ_0 to an enhanced eddy diffusivity κ_{eff} (generally speaking, an eddy-diffusivity tensorial field). General expressions for the eddy diffusivity as a function of the flow properties do not exist, and in most cases κ_{eff} can be determined only numerically.

Here, my aim is to consider the challenging situation where there is no scale separation [64] between velocity and scalar and to explore, in such a context, the existence of effective equations for $\tilde{\theta}$.

3.2.4 Structure of small-scale contributions

An alternative expression of $\partial \cdot \tau^{(\theta)}$ can be obtained, for future purpose, plugging in (3.6) the decomposition (3.3). One has:

$$\partial \cdot \tau^{(\theta)} = \mathcal{L} + \tilde{\mathcal{C}} + \tilde{\mathcal{R}} , \quad (3.7)$$

where

$$\left\{ \begin{array}{ll} \mathcal{L} \equiv \widetilde{\tilde{\mathbf{v}} \cdot \partial \tilde{\theta}} - \tilde{\mathbf{v}} \cdot \partial \tilde{\theta} & \text{(Leonard-like term)} \\ \mathcal{C} \equiv \tilde{\mathbf{v}} \cdot \partial \theta^* + \mathbf{v}^* \cdot \partial \tilde{\theta} & \text{(cross term)} \\ \mathcal{R} \equiv \mathbf{v}^* \cdot \partial \theta^* & \text{(Reynolds-like term)} \end{array} \right. . \quad (3.8)$$

3.3 An example of exact closure

I now specialize to stochastic velocities and forcings, i.e. to the case in which both \mathbf{v} and f are fields with assigned statistical properties; I denote with brackets the average over their statistical distribution: it is then clear that this ensemble average commutes with the spatial average represented by the filtering process.

Also in this framework, a renowned example of exact closure exists. Indeed, for times t larger than the largest velocity time scale, the mean field $\langle \theta \rangle$ experiences the cumulative effect of velocity via an eddy-diffusivity coefficient (see equation (2.37), which however arose in another context):

$$\partial_t \langle \theta \rangle = \kappa_{\text{tot}} \partial^2 \langle \theta \rangle + \langle f \rangle . \quad (3.9)$$

The expression for κ_{tot} (here supposed to be isotropic, as actually is in the presence of isotropic velocity fields) follows from the well-known Taylor formula:

$$\kappa_{\text{tot}} = \kappa_0 + \frac{1}{2d} \int_0^\infty d\tau \langle \mathbf{v}(\tau) \cdot \mathbf{v}(0) \rangle . \quad (3.10)$$

Having accounted for the advective term through a linear diffusive one, in this particular case the nonlinearity problem faced while passing from equation (3.1) to (3.4) does not exist any more and the same eddy-diffusivity equation must then hold also for the averaged coarse-grained field $\langle \tilde{\theta} \rangle$. By virtue of linearity, from (3.9) one has:

$$\partial_t \langle \tilde{\theta} \rangle = \kappa_{\text{tot}} \partial^2 \langle \tilde{\theta} \rangle + \langle \tilde{f} \rangle . \quad (3.11)$$

I now look for an eddy-diffusivity-type closure in the equation for $\tilde{\theta}$ such that, starting from it, (3.11) is recovered. I ask, in other words, that the closure is able to reproduce the averaged, long-time behaviour of $\tilde{\theta}$. The searched equation is

$$\partial_t \tilde{\theta} + \tilde{\mathbf{v}} \cdot \partial \tilde{\theta} = \kappa_{\text{eff}} \partial^2 \tilde{\theta} + \tilde{f} , \quad (3.12)$$

where κ_{eff} has to be determined. I can use Taylor's formula again to obtain

$$\kappa_{\text{tot}} = \kappa_{\text{eff}} + \frac{1}{2d} \int_0^\infty d\tau \langle \tilde{\mathbf{v}}(\tau) \cdot \tilde{\mathbf{v}}(0) \rangle . \quad (3.13)$$

A simple comparison between equations (3.10) and (3.13) yields:

$$\kappa_{\text{eff}} = \kappa_0 + \frac{1}{2d} \int_0^\infty d\tau [\langle \mathbf{v}(\tau) \cdot \mathbf{v}(0) \rangle - \langle \tilde{\mathbf{v}}(\tau) \cdot \tilde{\mathbf{v}}(0) \rangle] . \quad (3.14)$$

3.4 Kraichnan advection model

3.4.1 Basic properties and known results

I further restrict my attention to the well-known Kraichnan advection model [36, 37], already described in section § 2.2, whose main features are summarized here. Both velocity and forcing are Gaussian, white-in-time and zero-mean random fields, statistically stationary, homogeneous and isotropic.

The spatial part of the velocity second-order increments follows an inertial-range power law:

$$d_{\mu\nu}^{(v)}(\mathbf{r}) = D_1 r^\xi \left[(d + \xi - 1) \delta_{\mu\nu} - \xi \frac{r_\mu r_\nu}{r^2} \right], \quad (3.15)$$

where ξ represents the roughness exponent and lies in the open interval $(0, 2)$; the limit cases $\xi = 0$ and $\xi = 2$ will be studied in the appendix § 3.8.

A convenient choice for f is to assume a step-function form for its two-point spatial correlation: $F_L(r) = F_0 \Theta(L - r)$.

The equation for the two-point equal-time correlation function $C_2^{(\theta)}$ reads

$$\partial_t C_2^{(\theta)} = d_{\mu\nu}^{(v)} \partial_\mu \partial_\nu C_2^{(\theta)} + 2\kappa_0 \partial^2 C_2^{(\theta)} + F_L \quad (3.16)$$

and its stationary version has the following convective-range ($\eta \ll r < L$) solution:

$$C_2^{(\theta)}(r) = c - k r^{2-\xi}, \quad (3.17)$$

with

$$c = \frac{F_0 L^{2-\xi}}{(d-1)(2-\xi)(d+\xi-2)D_1}, \quad k = \frac{F_0}{d(d-1)(2-\xi)D_1}.$$

I recall that in the limit of small viscosity, which will be assumed throughout the chapter, the merged-point value of the correlation is given by $\langle \theta^2 \rangle \simeq c$ and the stationary second-order structure function turns out to be a pure power law in the convective range: $S_2^{(\theta)}(r) = 2k r^{2-\xi}$.

The equation for the steady-state dissipation, which I write for future purpose, arises from (3.16) evaluated at merged points:

$$2\kappa_0 \langle (\boldsymbol{\partial}\theta)^2 \rangle = F_0. \quad (3.18)$$

Equation (3.18) is the analytical expression of the so-called *dissipative anomaly*, according to which the scalar average dissipation $\kappa_0 \langle (\boldsymbol{\partial}\theta)^2 \rangle$ keeps finite

also for vanishing diffusivity, as it is only determined by the large-scale scalar input F_0 . The latter conservatively cascades through the convective range (unaffected by the advective term, which has a flux-like structure) toward smaller and smaller scales, until diffusivity becomes efficient and stops the cascade process.

3.4.2 Second-order correlation function of the coarse-grained passive scalar

To provide a benchmark for the various closures, I first evaluate the stationary coarse-grained correlation function by its definition:

$$\begin{aligned} C_2^{(\tilde{\theta})}(r) &\equiv \langle \tilde{\theta}(\mathbf{x}, t) \tilde{\theta}(\mathbf{x}', t) \rangle \\ &= \int d^d \mathbf{y} \int d^d \mathbf{y}' P_l(\mathbf{x} - \mathbf{y}) P_l(\mathbf{x}' - \mathbf{y}') \langle \theta(\mathbf{y}, t) \theta(\mathbf{y}', t) \rangle \quad (3.19) \\ &= \int d^d \mathbf{s} \int d^d \mathbf{s}' P_l(\mathbf{s}) P_l(\mathbf{s}') C_2^{(\theta)}(|\mathbf{r} + \mathbf{s} + \mathbf{s}'|). \end{aligned}$$

Its exact value is reported in the appendix for $d = 3$ and a top-hat spherical filter, $P_l(s) = 3\Theta(l - s)/4\pi l^3$ (from now on, unless explicitly stated, I will confine myself to this situation). Here I only need to express its Taylor's expansion in the parameter l/r , with r lying in the convective range:

$$\begin{aligned} C_2^{(\tilde{\theta})}(r) = c - kr^{2-\xi} &\left[1 + \frac{1}{5}(2 - \xi)(3 - \xi) \left(\frac{l}{r}\right)^2 \right. \\ &\left. + \frac{3}{175}\xi(\xi - 1)(2 - \xi)(3 - \xi) \left(\frac{l}{r}\right)^4 + \mathcal{O}\left(\frac{l}{r}\right)^6 \right]. \quad (3.20) \end{aligned}$$

Clearly, as the separation r increases and becomes much greater than the filter scale l , the unfiltered result is recovered. On the other side, a lower limit for the physical consistence of the latter expansion can be intuitively identified in $r \geq 2l$, because for smaller separations the two integration domains in (3.19) would partially overlap. Expression (3.20) represents, therefore, the best result that can be achieved by means of a closure.

For a 3-D Gaussian filter, $P_l(s) = (2\pi l^2)^{-3/2} e^{-s^2/2l^2}$, the coefficient of the $(l/r)^2$ term in (3.20) is $(2 - \xi)(3 - \xi)$. For a 2-D top-hat filter, $P_l(s) = \Theta(l - s)/\pi l^2$, it becomes $(2 - \xi)^2/4$.

3.4.3 Properties of the filtered velocity and forcing

At this stage, it is also convenient to analyse the behaviour of the filtered velocity and forcing. By definition, both $\tilde{\mathbf{v}}$ and $\tilde{\mathbf{f}}$ are Gaussian, white-in-time and zero-mean random fields, statistically stationary, homogeneous and isotropic. The large-scale character of the forcing reflects in the fact that its two-point correlation $\langle \tilde{\mathbf{f}}(\mathbf{r}, t) \tilde{\mathbf{f}}(\mathbf{0}, 0) \rangle = \delta(t) \mathcal{F}_L(r)$ keeps the same spatial step-like form

$$\mathcal{F}_L(r) = \int d^d \mathbf{s} \int d^d \mathbf{s}' P_l(\mathbf{s}) P_l(\mathbf{s}') F_L(|\mathbf{r} + \mathbf{s} + \mathbf{s}'|) = F_L(r) \quad \text{for } r \notin \mathcal{L} ,$$

where the interval $\mathcal{L} \equiv [L - 2l, L + 2l]$ becomes negligible for $l \ll L$.

Second-order increments of the coarse-grained velocity,

$$\langle [\tilde{v}_\mu(\mathbf{r}, t) - \tilde{v}_\mu(\mathbf{0}, 0)] [\tilde{v}_\nu(\mathbf{r}, t) - \tilde{v}_\nu(\mathbf{0}, 0)] \rangle = 2\delta(t) d_{\mu\nu}^{(\tilde{v})}(\mathbf{r}) ,$$

are given by

$$d_{\mu\nu}^{(\tilde{v})}(\mathbf{r}) = \int d^d \mathbf{s} \int d^d \mathbf{s}' P_l(\mathbf{s}) P_l(\mathbf{s}') [d_{\mu\nu}^{(v)}(\mathbf{r} + \mathbf{s} + \mathbf{s}') - d_{\mu\nu}^{(v)}(\mathbf{s} + \mathbf{s}')] \quad (3.21)$$

$$= A(r) \delta_{\mu\nu} + B(r) \frac{r_\mu r_\nu}{r^2} . \quad (3.22)$$

The exact expressions of the coefficients $A(r)$ and $B(r)$ are quite cumbersome (see appendix); a much more useful and meaningful quantity is provided by the following power-series expansion in l/r :

$$\begin{aligned} d_{\mu\nu}^{(\tilde{v})}(\mathbf{r}) &= D_1 r^\xi \left\{ \left[(2 + \xi) \delta_{\mu\nu} - \xi \frac{r_\mu r_\nu}{r^2} \right] - \frac{2^\xi 48 \delta_{\mu\nu}}{(4 + \xi)(6 + \xi)} \left(\frac{l}{r} \right)^\xi + \mathcal{O} \left(\frac{l}{r} \right)^2 \right\} \\ &= d_{\mu\nu}^{(v)}(\mathbf{r}) \left[1 + \mathcal{O} \left(\frac{l}{r} \right)^2 \right] - \frac{2^\xi 48 D_1 l^\xi}{(4 + \xi)(6 + \xi)} \delta_{\mu\nu} . \end{aligned} \quad (3.23)$$

The latter will be extensively used in the following.

Similar results also hold for both the 3-D Gaussian and the 2-D top-hat filter, but with different numerical coefficients.

3.4.4 Analysis of the filtered equation

The first step, in order to find closed equations for the large scales, consists in deriving the exact equations for the two-point correlation function of the

filtered field. With the same procedure used when passing from (3.1) to (3.16), starting from equation (3.5) one can write:

$$\begin{aligned} & \partial_t \langle \tilde{\theta}(\mathbf{x}, t) \tilde{\theta}(\mathbf{x}', t) \rangle + 2 \langle \tilde{\theta}(\mathbf{x}, t) (\tilde{\mathbf{v}} \cdot \partial \tilde{\theta})(\mathbf{x}', t) \rangle = \\ & = 2\kappa_0 \partial^2 \langle \tilde{\theta}(\mathbf{x}, t) \tilde{\theta}(\mathbf{x}', t) \rangle + \mathcal{F}_L(|\mathbf{x} - \mathbf{x}'|) - 2 \langle \tilde{\theta}(\mathbf{x}, t) \partial \cdot \boldsymbol{\tau}^{(\theta)}(\mathbf{x}', t) \rangle. \end{aligned} \quad (3.24)$$

This is the starting point for my systematic procedure to construct closure approximations. The second term on the left-hand side depends on $\tilde{\mathbf{v}}$ and $\tilde{\theta}$ only, but I cannot transform it (yet) into a contribution with the structure of the first term on the right-hand side of (3.16) because, at this stage, I am not able to apply FND's rule on it, as I do not know the functional derivative of $\tilde{\theta}$ with respect to $\tilde{\mathbf{v}}$ explicitly. The last term on the right-hand side of (3.24), which is not expressed as a function of coarse-grained fields, is the ‘‘disturbing’’ quantity: my purpose is therefore to find its perturbative expansion in l/r .

It is not difficult (although quite lengthy) to prove that:

$$\langle \tilde{\theta}(\mathbf{x}, t) \partial \cdot \boldsymbol{\tau}^{(\theta)}(\mathbf{x}', t) \rangle = \frac{2^\xi 4(3 - \xi) F_0}{(4 + \xi)(6 + \xi)} \left(\frac{l}{r}\right)^\xi - \frac{\xi^2 F_0}{30} \left(\frac{l}{r}\right)^2 + \mathcal{O}\left(\frac{l}{r}\right)^{2+\xi}. \quad (3.25)$$

More specifically, exploiting decomposition (3.7) and definitions (3.8), one can show that (3.25) consists of:

$$\left\{ \begin{array}{l} \langle \mathcal{L}(\mathbf{x}, t) \tilde{\theta}(\mathbf{x}', t) \rangle = \mathcal{O}\left(\frac{l}{r}\right)^{2+\xi} \\ \langle \mathcal{C}(\mathbf{x}, t) \tilde{\theta}(\mathbf{x}', t) \rangle = -\frac{(3 - \xi)(\xi^2 + 10\xi + 24 - 2^\xi 24) F_0}{3(4 + \xi)(6 + \xi)} \left(\frac{l}{r}\right)^\xi \\ \quad - \frac{\xi^2 F_0}{30} \left(\frac{l}{r}\right)^2 + \mathcal{O}\left(\frac{l}{r}\right)^{2+\xi} \\ \langle \mathcal{R}(\mathbf{x}, t) \tilde{\theta}(\mathbf{x}', t) \rangle = \frac{(3 - \xi)(\xi^2 + 10\xi + 24 - 2^\xi 12) F_0}{3(4 + \xi)(6 + \xi)} \left(\frac{l}{r}\right)^\xi + \mathcal{O}\left(\frac{l}{r}\right)^{2+\xi}. \end{array} \right. \quad (3.26)$$

The first line of (3.26) suggests that the Leonard-type term does not contribute, at the lowest two orders, to the equation for the two-point correlation of the coarse-grained scalar. Since my closures are derived from this equation up to the second order, it follows that the Leonard-type term will not contribute to small-scale parameterizations. This fact is not a consequence of the Kraichnan advection model but rather seems to hold for general advection

models. For standard closure models based on single-point quantities, the contribution from the Leonard stress in the parameterizations is, generally speaking, non-zero.

Moreover, it is easy to see that the sum of the last two equations in (3.26) exactly coincides with (3.25), in spite of the further convolution required in (3.7) on the cross and Reynolds-like terms. This is in accordance with the following result, that can be obtained after simple algebra:

$$\langle \mathcal{C}(\mathbf{x}, t)\theta(\mathbf{x}', t) \rangle + \mathcal{O}\left(\frac{l}{r}\right)^{2+\xi} = \langle \mathcal{C}(\mathbf{x}, t)\tilde{\theta}(\mathbf{x}', t) \rangle = \langle \tilde{\mathcal{C}}(\mathbf{x}, t)\tilde{\theta}(\mathbf{x}', t) \rangle + \mathcal{O}\left(\frac{l}{r}\right)^{2+\xi}.$$

The same result holds replacing \mathcal{C} with \mathcal{R} and has been obtained exploiting a further identity, holding for any couple of fields \mathbf{f}_1 and \mathbf{f}_2 in the presence of statistical homogeneity: $\langle \tilde{\mathbf{f}}_1(\mathbf{r}, t)\mathbf{f}_2(\mathbf{0}, 0) \rangle = \langle \mathbf{f}_1(\mathbf{r}, t)\tilde{\mathbf{f}}_2(\mathbf{0}, 0) \rangle$.

It is also interesting to study when the cross term and the Reynolds-like one dominate over each other. At the lowest order, $(l/r)^\xi$, one should thus compare the absolute values of the two numerical coefficients (functions of ξ) appearing on the second and on the last line of (3.26): the result is that the former prevails for $\xi > \xi_0$, with $\xi_0 \simeq 0.92$, and the latter is dominant when ξ does not exceed this critical value ξ_0 . Furthermore, one can easily prove that the two terms composing \mathcal{C} (3.8) give the same contribution to the parameterization at the lowest order, each being half of the numerical coefficient appearing on the second line of (3.26).

Once again, expressions with the same structure of (3.25) and (3.26) also hold for the 3-D Gaussian filter, with different numerical coefficients. On the contrary, for the 2-D top-hat filter, it turns out that the second-order coefficient in (3.25) vanishes.

3.5 Examples of analytical closures

3.5.1 Importance of small-scale contributions

I shall now focus on consequences of relation (3.25): it is immediate to realize that neglecting small-scales effects completely, i.e. assuming $\partial \cdot \boldsymbol{\tau}^{(\theta)} = 0$, makes equation (3.24) unbalanced at order $(l/r)^\xi$. In other words, if one assumes a closure of the kind

$$\partial_t \tilde{\theta} + \tilde{\mathbf{v}} \cdot \partial \tilde{\theta} = \kappa_0 \partial^2 \tilde{\theta} + \tilde{f},$$

starting from it one would obtain a non-analytical expansion for the coarse-grained scalar correlation, $C_2^{(\tilde{\theta})}(r) = c - kr^{2-\xi}[1 + O(l/r)^\xi]$, clearly in contrast with the exact result (3.20).

3.5.2 Constant-eddy-diffusivity closure

The first issue thus consists in finding a way to take order $(l/r)^\xi$ into account properly. For this purpose it is sufficient to notice that the diffusive contribution in (3.24), or equivalently (at this order of approximation) in (3.16), turns out to be proportional to $r^{-\xi}$, precisely

$$\kappa_0 \partial^2 C_2^{(\theta)} = -\frac{(3-\xi)F_0\kappa_0}{6D_1 r^\xi}. \quad (3.27)$$

It is then clear that an effective-diffusivity term, like the one proposed in (3.12), must be able to correctly reproduce the lowest-order contribution of (3.25). More specifically, writing $\kappa_{\text{eff}} = \kappa_0 + \kappa_1$, the equation

$$\partial_t \tilde{\theta} + \tilde{\mathbf{v}} \cdot \boldsymbol{\partial} \tilde{\theta} = \kappa_{\text{eff}} \partial^2 \tilde{\theta} + \tilde{f} \quad (3.28)$$

is balanced at order $(l/r)^\xi$ if

$$\kappa_1 = \frac{2^\xi 24}{(4+\xi)(6+\xi)} D_1 l^\xi \quad (3.29)$$

(to prove this, it is sufficient to replace κ_0 with κ_1 in (3.27) and to compare the result with (3.25)). It is worth noticing that expression (3.29) also follows from the integral in (3.14), which substantially amounts to compute the difference between total and large-scale kinetic energies in the presence of δ -correlated flows. This is in accordance with equation (3.23), from which one deduces

$$\kappa_1 \delta_{\mu\nu} = \lim_{r \rightarrow \infty} \frac{d_{\mu\nu}^{(\mathbf{v})}(\mathbf{r}) - d_{\mu\nu}^{(\tilde{\mathbf{v}})}(\mathbf{r})}{2}. \quad (3.30)$$

Two more remarks about this kind of closure, which I will call ‘‘constant eddy diffusivity’’ (CED), emerge from the consideration that the fraction (function of ξ) in (3.29) always stands between 1 and 2. First, reminding that from (2.2) one has $\kappa_0 = D_1 \eta^\xi$, a remarkable increase in the transport coefficient is found ($l \gg \eta \Rightarrow \kappa_{\text{eff}} \simeq \kappa_1 \gg \kappa_0$): this is a typical effect in turbulence. Second, an effective dissipative scale comparable to the filtering

length l arises for $\tilde{\theta}$: the analogy is evident between the roles played by l for $\tilde{\theta}$ and by the molecular dissipative scale η for the original field θ .

The equation for the coarse-grained scalar correlation arising from (3.28) has exactly the same structure of the fully-resolved corresponding (3.16):

$$\partial_t C_2^{(\tilde{\theta})} = d_{\mu\nu}^{(\tilde{v})} \partial_\mu \partial_\nu C_2^{(\tilde{\theta})} + 2\kappa_{\text{eff}} \partial^2 C_2^{(\tilde{\theta})} + \mathcal{F}_L . \quad (3.31)$$

The stationary solution of (3.31) in the convective range is:

$$C_2^{(\tilde{\theta})}(r) = c - kr^{2-\xi} \left[1 + \frac{1}{5}(2-\xi)(3+\xi) \left(\frac{l}{r}\right)^2 + \text{O}\left(\frac{l}{r}\right)^4 \right] . \quad (3.32)$$

A comparison with the exact result (3.20) shows that the CED closure is able to capture the correct order of the deviation from the fully-resolved scalar correlation (3.17), i.e. $(l/r)^2$, but with a wrong coefficient. It can be proved that the maximum error takes place at $\xi = 1$.

From (3.31) one derives the following equation for the steady-state dissipation:

$$2\kappa_{\text{eff}} \langle (\partial \tilde{\theta})^2 \rangle = F_0 . \quad (3.33)$$

Owing to the fact that $\kappa_{\text{eff}} \gg \kappa_0$, the comparison of (3.18) with (3.33) proves that the average of the square gradient of the scalar is much smaller for the filtered field than for the original one, as one would intuitively expect.

For the 3-D Gaussian filter or the 2-D top-hat filter, expression (3.29) becomes

$$\kappa_1 = \frac{2^{1+\xi}}{3\sqrt{\pi}} (3+\xi) \Gamma\left(\frac{3+\xi}{2}\right) D_1 l^\xi$$

or

$$\kappa_1 = \frac{2+\xi}{2} \frac{\Gamma(2+\xi)}{\Gamma(2+\xi/2)\Gamma(3+\xi/2)} D_1 l^\xi$$

respectively. Consequently, the ratio $\kappa_1/D_1 l^\xi$ stands between 1 and 10 in the former case and between 1/2 and 1 in the latter. Plugging these values of κ_1 in equation (3.28) or (3.31) and computing the coarse-grained correlation, for the 3-D Gaussian filter one obtains a result similar to (3.32), without the 1/5 factor in the $(l/r)^2$ term. However, for the 2-D top-hat filter, the second-order coefficient is $(2-\xi)^2/4$ and exactly coincides with its “true” value, i.e. one gets the remarkable result that the error in the approximation is automatically pushed at higher orders.

3.5.3 Improved closure

My aim is now to improve the constant-eddy-diffusivity closure, exact at order $(l/r)^\xi$, by introducing a new closure which is accurate up to order $(l/r)^2$. At this stage, one has no hint of how to implement this closure, differently from what happens with the intuitive emergence of the eddy diffusivity; a trivial Taylor expansion on the turbulent fields would actually prove wrong [70, 71].

However, one knows that a term proportional to l^2 , in the equation for the coarse-grained scalar correlation, has to be reproduced: it is then reasonable to add, on the right-hand side of the equation for $\tilde{\theta}$, a new contribution proportional to some power of l . The minimal guess could be represented by the addition of a term linear in l , which would be able to generate a quadratic correction in the equation for the correlation when applying FND's rule. This guess is however ruled out by symmetry considerations, because one would need to introduce some additional field (with the dimensions of the vorticity) which cannot appear in the equation for $\tilde{\theta}$ for parity conservation.

The next possibility is thus to add a term quadratic in l , in which the coarse-grained fields must appear in the tensorial form $\tilde{\mathbf{v}}\partial\tilde{\theta}$. Dimensional considerations then require the presence of a square length at denominator, but no scales other than the filter width can appear, because I am dealing with a single-point equation and neither L nor η are relevant. A second derivative is thus required. If one completely neglects higher orders in l (it is important to underline that this ansatz is not trivial at all, because they would give rise to spurious contributions at lower orders), then the searched equation must have the following form:

$$\partial_t\tilde{\theta} + \tilde{\mathbf{v}} \cdot \partial\tilde{\theta} = \kappa_{\text{eff}}\partial^2\tilde{\theta} + \tilde{f} + l^2 \left(\alpha\partial^2\tilde{\mathbf{v}} \cdot \partial\tilde{\theta} + \beta\partial\tilde{\mathbf{v}} : \partial\partial\tilde{\theta} + \gamma\tilde{\mathbf{v}} \cdot \partial\partial^2\tilde{\theta} \right). \quad (3.34)$$

The coefficients α , β and γ can be uniquely found by imposing the correct description of order $(l/r)^2$ and, at the same time, the vanishing of any spurious modification to order $(l/r)^\xi$, which has already been captured by the CED closure. In other words, one asks that the value of κ_{eff} previously found remains unchanged in (3.34) (alternative conditions will be shown later in this section). With these hypotheses, one has $\alpha = 0$ and $\beta = \gamma = -\xi/15$, so that (3.34) can be written as:

$$\partial_t\tilde{\theta} + \tilde{\mathbf{v}} \cdot \partial\tilde{\theta} = \kappa_{\text{eff}}\partial^2\tilde{\theta} + \tilde{f} - \frac{\xi}{15}l^2\partial_\mu\partial_\nu(\tilde{v}_\mu\partial_\nu\tilde{\theta}) \quad (3.35)$$

(for a comparison with the corresponding nonlinear closure in NS turbulence see, e.g., [72, 73]).

It is worth noticing that this closure, which has been obtained through Eulerian considerations, has no Lagrangian counterpart, differently from CED. Indeed, an expansion in the spirit of Kramers–Moyal would yield a term with the same structure of the one introduced on the right-hand side of (3.34), but it turns out that my triplet of coefficients α , β , γ appearing in (3.35) does not satisfy the constraints imposed by Pawula’s theorem [74, 75]. This fact is also related to the breaking of Galilean invariance in (3.35), which has been obtained in the frame of reference where the velocity is zero-mean and is not exportable. Moreover, the universality of κ_{eff} is no more present in the triplet, whose value has been determined exploiting the explicit solution for $C_2^{(\tilde{\theta})}$.

The equation for the two-point equal-time correlation function arising from (3.35) has now a different structure:

$$\begin{aligned} \partial_t C_2^{(\tilde{\theta})} &= d_{\mu\nu}^{(\tilde{v})} \partial_\mu \partial_\nu C_2^{(\tilde{\theta})} + 2\kappa_{\text{eff}} \partial^2 C_2^{(\tilde{\theta})} + \mathcal{F}_L + \frac{2\xi}{15} l^2 \partial_\lambda \left[d_{\mu\nu}^{(\tilde{v})} \partial_\lambda \partial_\mu \partial_\nu C_2^{(\tilde{\theta})} \right] + \\ &+ \frac{\xi}{225} l^4 \left\{ \partial_\kappa \partial_\lambda \left[d_{\mu\nu}^{(\tilde{v})} \partial_\kappa \partial_\lambda \partial_\mu \partial_\nu C_2^{(\tilde{\theta})} \right] + V_{\kappa\lambda\mu\nu} \partial_\kappa \partial_\lambda \partial_\mu \partial_\nu C_2^{(\tilde{\theta})} \right\}, \quad (3.36) \end{aligned}$$

where $V_{\kappa\lambda\mu\nu}$ satisfies $\langle \tilde{v}_\mu(\mathbf{0}, t) \partial_\kappa \partial_\lambda \tilde{v}_\nu(\mathbf{0}, 0) \rangle = \delta(t) V_{\kappa\lambda\mu\nu}$.

The stationary solution of (3.36) in the convective range is:

$$C_2^{(\tilde{\theta})}(r) = c - kr^{2-\xi} \left[1 + \frac{1}{5} (2-\xi)(3-\xi) \left(\frac{l}{r} \right)^2 + \mathcal{O} \left(\frac{l}{r} \right)^{2+\xi} \right]. \quad (3.37)$$

Comparing (3.37) with (3.20), one concludes that this new kind of closure is able to reproduce the exact structure of the coarse-grained scalar correlation up to the second order with the correct value of the coefficient, differently from what happens in (3.32). One also notices that the error is now $\mathcal{O}(l/r)^{2+\xi}$ instead of $\mathcal{O}(l/r)^4$: in order to balance also this contribution in the proper way, one would have to add other terms on the right-hand side of (3.35), paying attention to take unmodified the lower orders which have already been captured.

A last comment on (3.35) is worthwhile. It turns out that the same dissipation equation (3.33) generated from CED still holds. This is in accordance with the flux-like structure of the last term on the right-hand side of (3.35),

which gives no contribution to the equation for the dissipation. Exploiting homogeneity (H) and incompressibility (I), one has indeed:

$$\begin{aligned} \langle \tilde{\theta} \partial_\mu \partial_\nu (\tilde{v}_\mu \partial_\nu \tilde{\theta}) \rangle &\stackrel{\text{I}}{=} \langle \tilde{\theta} \partial_\nu (\tilde{v}_\mu \partial_\mu \partial_\nu \tilde{\theta}) \rangle \stackrel{\text{H}}{=} -\langle (\partial_\nu \tilde{\theta}) \tilde{v}_\mu \partial_\mu \partial_\nu \tilde{\theta} \rangle \\ &\stackrel{\text{I}}{=} -\langle (\partial_\nu \tilde{\theta}) \partial_\mu (\tilde{v}_\mu \partial_\nu \tilde{\theta}) \rangle \stackrel{\text{H}}{=} \langle (\partial_\mu \partial_\nu \tilde{\theta}) \tilde{v}_\mu \partial_\nu \tilde{\theta} \rangle \quad . \end{aligned}$$

Comparing the third and the last member of this chain of equalities, I deduce that all terms must vanish; in particular, also the first one is thus zero, which proves my assertion.

For the 3-D Gaussian filter, the correct values of the triplet are $\alpha = 0$ and $\beta = \gamma = -\xi/3$. The closed equation for $\tilde{\theta}$ has thus the same structure of (3.35) and leads to a coarse-grained correlation expressed by (3.37) but without the $1/5$ factor near $(l/r)^2$, which is exact up to the second-order. The same accuracy is obtained for the 2-D top-hat filter with $\alpha = \beta = \gamma = 0$, coherently with what stated at the end of subsections § 3.4.4 and § 3.5.2.

Before proceeding, I would like to stress the conditions I specified when (uniquely) fixing the values of α , β and γ in equation (3.34) in order to obtain (3.35): 1) correct description of $O(l/r)^2$, 2) complete neglect of terms containing powers of l higher than 2, and 3) absence of any modification of $O(l/r)^\xi$ i.e. of κ_{eff} .

3.5.4 An alternative closure

I am now going to show an example of what happens if the possibility of taking filters of (slightly) different length between scalar and velocity is allowed. In particular, if one defines a new coarse-grained velocity as $\tilde{\mathbf{v}} \equiv P_{al} * \mathbf{v}$ (with $a = \sqrt{(3-\xi)/(3+\xi)}$, i.e. slightly less than unity), then I assert that an equation with the same structure as in (3.28),

$$\partial_t \tilde{\theta} + \tilde{\mathbf{v}} \cdot \partial \tilde{\theta} = \kappa_{\text{eff}} \partial^2 \tilde{\theta} + \tilde{f} \ ,$$

is able to reproduce for the correlation the same degree of approximation of (3.37), with an error pushed again at $O(l/r)^4$ and without any need of introducing additive terms like on the right-hand side of (3.34). The same expression (3.14) for the eddy diffusivity still holds, with $\tilde{\mathbf{v}}$ replaced by $\tilde{\mathbf{v}}$; this amounts to perform the same replacing in expression (3.30) for $\kappa_1 = \kappa_{\text{eff}} - \kappa_0$, whose numerical value is now a^ξ times the value given by (3.29), in accordance with the substitution $l \mapsto al$.

3.5.5 Absence of eddy diffusivity

I now present some other possible closures, which emerge if one pursues aims different from those specified previously.

From another point of view, the condition 3) fixed at the end of section § 3.5.3 could be modified into: 3bis) modification of $O(l/r)^\xi$ such that κ_{eff} is restored to its original value κ_0 . In other words, one would now like to pass from equation (3.5) directly to

$$\partial_t \tilde{\theta} + \tilde{\mathbf{v}} \cdot \partial \tilde{\theta} = \kappa_0 \partial^2 \tilde{\theta} + \tilde{f} + l^2 \left(\alpha' \partial^2 \tilde{\mathbf{v}} \cdot \partial \tilde{\theta} + \beta' \partial \tilde{\mathbf{v}} : \partial \partial \tilde{\theta} + \gamma' \tilde{\mathbf{v}} \cdot \partial \partial^2 \tilde{\theta} \right), \quad (3.38)$$

imposing that the contribution in parentheses on the right-hand side of (3.38) is able to correctly balance both $O(l/r)^\xi$ and $O(l/r)^2$. This goal can be accomplished for

$$\alpha' = \frac{\xi + 2}{\xi(3 + \xi)(6 + \xi)}, \quad \beta' = \frac{-\xi^4 - 9\xi^3 - 18\xi^2 + 120\xi + 240}{15\xi(3 + \xi)(6 + \xi)},$$

$$\gamma' = \frac{-\xi^4 - 9\xi^3 - 18\xi^2 + 60\xi + 120}{15\xi(3 + \xi)(6 + \xi)}.$$

It is worth noticing that, in this way, the term proportional to l^2 in (3.38) has no more an overall flux-like structure, differently from what happened in (3.35). Consequently, it gives rise to a non-zero contribution in the equation for the dissipation.

Conditions 3) and 3bis) represent two completely different points of view: in the first one the diffusive term captures $O(l/r)^\xi$ completely, in the second one it gives no contribution. Of course, there exists an infinite range of intermediate possibilities if one considers both the renormalized diffusivity and the triplet as unknowns.

3.5.6 Absence of second-order correction

Suppose now to be interested to measure “pure” convective-range scaling behaviour by means of a LES strategy. More specifically, referring to (3.17), my aim here is to reproduce the asymptotic behaviour $C_2^{(\theta)}(r) \sim r^{2-\xi}$ even in the presence of finite-size effects, i.e. induced by the filter cut-off l , which would imply the additive corrections in powers of l/r shown in (3.20). In plain words, one renounces to describe the actual coarse-grained correlation function (3.20), with the aim of isolating the scaling behaviour which would

be observed at higher-Reynolds-number (and thus higher-resolution) numerical simulations.

Assuming the conditions 2) and 3) mentioned at the end of section § 3.5.3, this amounts to modify condition 1) into: 1bis) absence of second-order correction in the coarse-grained correlation. This aim is accomplished simply assuming $\alpha = 0$ and $\beta = \gamma = -(3 + \xi)/30$.

It can be shown indeed that, starting from the equation

$$\partial_t \tilde{\theta} + \tilde{\mathbf{v}} \cdot \boldsymbol{\partial} \tilde{\theta} = \kappa_{\text{eff}} \partial^2 \tilde{\theta} + \tilde{f} - \frac{3 + \xi}{30} l^2 \partial_\mu \partial_\nu (\tilde{v}_\mu \partial_\nu \tilde{\theta}),$$

the coarse-grained correlation turns out to be:

$$C_2^{(\tilde{\theta})}(r) = c - kr^{2-\xi} \left[1 + \mathcal{O} \left(\frac{l}{r} \right)^{2+\xi} \right].$$

The deviation from the fully-resolved correlation is pushed at a higher order: I have thus obtained a better recovery of the original field in its two-point correlation function.

3.6 Conclusions

Summarizing, a systematic procedure to derive closed dynamical equations for a coarse-grained passive scalar field in the statistical steady-state has been obtained in the framework of the Kraichnan advection model.

The question that naturally arises, is whether those results are relevant to realistic advection models. The answer is given by the outcome of the procedure itself. Two well-known closures that are commonly used in applications are recovered from first principles: the constant eddy-diffusivity parameterization of small-scales, and the passive scalar version of the non-linear eddy-viscosity closure used in hydrodynamic turbulence. Of course, the values of the effective diffusivity and of the triplet of coefficients that appear in these closures can be analytically computed only in the Kraichnan model. However, it is believed that the form of the parameterization can be exported without modifications to real situations as well. Clearly, in this case the free parameters have to be determined *a posteriori* by some empirical procedure.

The validity of this approach has been checked by direct numerical simulations (DNS). In order to test my LES closures I focused on two dimensions

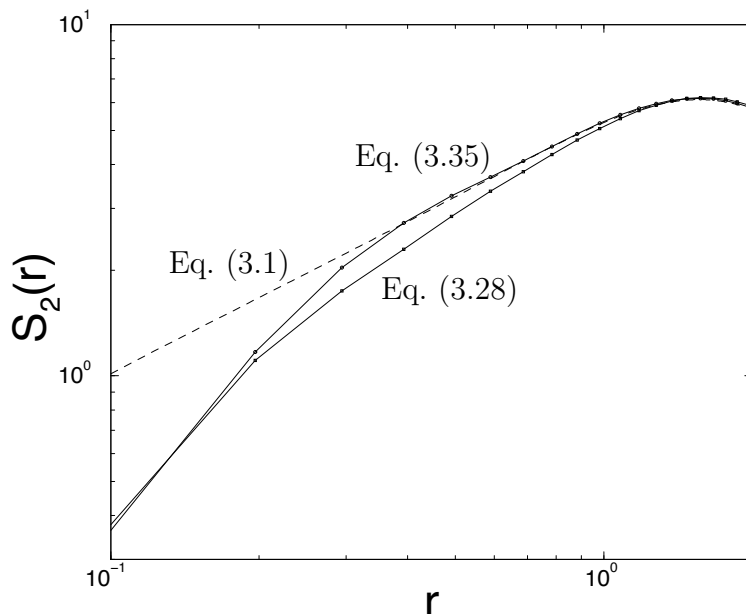


Figure 3.1: DNS vs LES for $S_2(r)$. Notice how accurately the improved closure (3.35) reproduces the DNS prediction (dashed curve) from (3.1). Constant-eddy-diffusivity closure given by (3.28) is clearly insufficient to capture the correct convective-range scaling.

and I simultaneously integrated (on a biperiodic lattice) the NS equation together with (3.1) for the “true” field θ , and both (3.28) and (3.35) for the coarse-grained field $\tilde{\theta}$. The lattice for the equation for \mathbf{v} and θ is formed by 1024×1024 grid points, while $\tilde{\theta}$ is solved with solely 64×64 grid points. The field $\tilde{\mathbf{v}}$ appearing in the LES equation has been obtained by filtering the actual DNS field \mathbf{v} with a Gaussian filter. In figure 3.1, the actual second-order structure function (dashed line) $S_2(r) = \langle [\theta(\mathbf{r}) - \theta(\mathbf{0})]^2 \rangle$ and the LES counterparts $\langle [\tilde{\theta}(\mathbf{r}) - \tilde{\theta}(\mathbf{0})]^2 \rangle$ (full lines) are shown for both the improved and the standard eddy-diffusivity closure. DNS simulation accurately reproduces the expected KOC scaling $r^{2/3}$. It is quite impressive as, despite the small resolution, the improved closure is able to accurately reproduce both the actual $2/3$ exponent and the relative prefactor. On the contrary, there is no signature of convective range for the constant-eddy-diffusivity closure. Details on the method to numerically integrate the system can be found, e.g., in [76].

I conclude by mentioning a possible generalization of this work. My

analysis has been carried for the second-order correlation function of the scalar field. There are two reasons for this choice. First, the second-order correlation function is the Fourier transform of the spectrum of scalar variance, a statistical indicator widely used to characterize most of the statistical properties of scalar turbulence. Second, for the Kraichnan model only the second-order correlation function has a simple, closed analytical expression. For higher-order correlation functions only perturbative expressions (for example in the limit of small ξ) are available [46]. However, should one focus on a higher-order correlation function, how would these results change? Although the analysis appears much more cumbersome than the one presented here, the procedure described in § 3.5 can be completed as well: it is still possible to obtain a closed equation for the coarse-grained correlation function at any order in l/r , from which one can identify the corresponding dynamical equations for the large-scale scalar field. The question is: will the latter dynamical equation have the same structure of the coarse-grained scalar equation derived from the second-order correlation? And if this is the case, will the coefficients be the same? Even if the functional form of the closure is preserved, a modification of the effective coefficients would mean that strong small-scale fluctuations — associated to higher-order correlation functions — must be described by parameters different from the ones used for less intense fluctuations. That would question the applicability of closure models to the description of the statistics of turbulent fields as temperature or concentration, which are characterized by a wide range of fluctuation intensities. This challenging issue is left for future research.

3.7 Appendix on exact analytical expressions

In this section I show the exact analytical expressions of some quantities, of which I have only reported perturbative expressions throughout the chapter.

3.7.1 Coarse-grained passive scalar

The correlation of the coarse-grained passive scalar mentioned in (3.20) is:

$$\begin{aligned}
C_2^{(\tilde{\theta})}(r) = & c - \frac{3F_0}{8(2-\xi)(4-\xi)(5-\xi)(6-\xi)D_1l^6} \left\{ -\frac{l}{7-\xi} \left[R_+^{7-\xi} - R|R_-|^{7-\xi} \right] \right. \\
& - \frac{l^2}{(7-\xi)r} \left[R_+^{7-\xi} + R|R_-|^{7-\xi} - 2r^{7-\xi} \right] + \frac{l}{(8-\xi)r} \left[R_+^{8-\xi} - |R_-|^{8-\xi} \right] \\
& + \frac{1}{(7-\xi)(8-\xi)} \left[R_+^{8-\xi} + |R_-|^{8-\xi} - 2r^{8-\xi} \right] + \frac{l}{(7-\xi)(8-\xi)r} \left[R_+^{8-\xi} \right. \\
& \left. - |R_-|^{8-\xi} \right] - \frac{1}{(7-\xi)(9-\xi)r} \left[R_+^{9-\xi} + R|R_-|^{9-\xi} - 2r^{9-\xi} \right] \left. \right\},
\end{aligned}$$

where $R_{\pm} = r \pm 2l$ and $R = \text{sgn}(R_-)$. The fuse-point value is given by

$$\langle \tilde{\theta}^2 \rangle = c - \frac{48F_0l^{2-\xi}}{2^\xi(2-\xi)(4-\xi)(5-\xi)(6-\xi)D_1},$$

i.e. $\langle \tilde{\theta}^2 \rangle < \langle \theta^2 \rangle = c$.

Keeping (2.6) and (3.20) into account, this leads to the following expression for the two-point coarse-grained scalar structure function in the convective range:

$$\begin{aligned}
S_2^{(\tilde{\theta})}(r) & \equiv \langle [\tilde{\theta}(\mathbf{r}, t) - \tilde{\theta}(\mathbf{0}, t)]^2 \rangle = 2\langle \tilde{\theta}^2 \rangle - 2C_2^{(\tilde{\theta})}(r) = \\
& = 2 \left[c - \frac{48F_0l^{2-\xi}}{2^\xi(2-\xi)(4-\xi)(5-\xi)(6-\xi)D_1} \right] \\
& \quad - 2 \left\{ c - kr^{2-\xi} \left[1 + \mathcal{O}\left(\frac{l}{r}\right)^2 \right] \right\} \\
& = S_2^{(\theta)}(r) \left[1 + \mathcal{O}\left(\frac{l}{r}\right)^{2-\xi} \right]. \tag{3.39}
\end{aligned}$$

Expression (3.39) shows that spurious corrections $\mathcal{O}(l/r)^{2-\xi}$, which are absent in the correlation, appear in the structure function when filtering. In other words, it is not true that the coarse-grained structure function is obtained by performing a double convolution on the fully-resolved corresponding quantity (this result is in accordance with the integral expression of the coarse-grained velocity structure function in (3.21)). Of course, this fact does not spoil my closures at all, but it makes it easier to deal with correlation functions.

3.7.2 Coarse-grained velocity

The coefficients $A(r)$ and $B(r)$ appearing in (3.22) are uniquely determined by the system

$$\begin{cases} 2rB'(r) - 6B(r) = -rG(r) \\ 3A(r) + B(r) = G(r) \end{cases},$$

with $B(0) = 0$ and

$$\begin{aligned} G(r) = & -\frac{2^\xi 144 D_1 l^\xi}{(4+\xi)(6+\xi)} + \frac{9D_1}{2(2+\xi)(4+\xi)l^6} \left\{ -\frac{l}{5+\xi} \left[R_+^{5+\xi} - R|R_-|^{4+\xi} \right] \right. \\ & - \frac{l^2}{(5+\xi)r} \left[R_+^{5+\xi} + R|R_-|^{5+\xi} - 2r^{5+\xi} \right] + \frac{l}{(6+\xi)r} \left[R_+^{6+\xi} - |R_-|^{6+\xi} \right] \\ & + \frac{1}{(5+\xi)(6+\xi)} \left[R_+^{6+\xi} + |R_-|^{6+\xi} - 2r^{6+\xi} \right] + \frac{l}{(5+\xi)(6+\xi)r} \times \\ & \left. \times \left[R_+^{6+\xi} - |R_-|^{6+\xi} \right] - \frac{1}{(5+\xi)(7+\xi)r} \left[R_+^{7+\xi} + R|R_-|^{7+\xi} - 2r^{7+\xi} \right] \right\}. \end{aligned}$$

A series expansion in l/r gives

$$A(r) = D_1 r^\xi \left[(2+\xi) - \frac{2^\xi 48}{(4+\xi)(6+\xi)} \left(\frac{l}{r}\right)^\xi + \frac{1}{5} \xi^2 (3+\xi) \left(\frac{l}{r}\right)^2 + O\left(\frac{l}{r}\right)^4 \right]$$

and

$$B(r) = D_1 r^\xi \left[-\xi + \frac{1}{5} \xi (3+\xi) (2-\xi) \left(\frac{l}{r}\right)^2 + O\left(\frac{l}{r}\right)^4 \right].$$

3.8 Appendix on limit cases

The values $\xi = 0$ and $\xi = 2$ have been excluded from my analysis up to now, because they represent two limit cases: a purely diffusive flow and a smooth flow, respectively. It is however interesting to analyse them, as in the former case an exact closure can be found, and in the latter a logarithmic law arises.

3.8.1 Purely diffusive flow

In the case $\xi = 0$ the definition of η (2.2) is meaningless, but physically it corresponds to a diffusive range extending to infinity. This can be understood

very simply noticing that the velocity field reduces to a white noise, as its second-order moment (3.15) takes a diagonal form completely independent from the separation: $d_{\mu\nu}^{(\mathbf{v})}(\mathbf{r}) = (d-1)D_1\delta_{\mu\nu}$.

Consequently, the overall effect of the advective term is barely of diffusive type and consists in an addition of the quantity $(d-1)D_1$ to the original contribution $2\kappa_0$ in (3.16). As there is no more need to split the integration interval in (3.17), the correlation is exactly expressed by

$$C_2^{(\theta)}(r) = c - kr^2 \quad \text{for } r < L ,$$

with

$$c = \frac{F_0 L^2}{2(d-2)[2\kappa_0 + (d-1)D_1]} = \langle \theta^2 \rangle \quad \text{for } d \neq 2$$

and

$$k = \frac{F_0}{2d[2\kappa_0 + (d-1)D_1]} .$$

By definition, an exact calculation in 3-D yields:

$$C_2^{(\tilde{\theta})}(r) = c - kr^2 \left[1 + \frac{6}{5} \left(\frac{l}{r} \right)^2 \right] = c' - kr^2 ,$$

with

$$c' = c - \frac{F_0 l^2}{10(\kappa_0 + D_1)} = \langle \tilde{\theta}^2 \rangle .$$

In this case, the structure functions of the coarse-grained field and of the original one turn out to be identical: $S_2^{(\tilde{\theta})}(r) = 2kr^2 = S_2^{(\theta)}(r)$.

The interesting point is that CED closure (3.28) is now exact also for the correlation function, as it happened in (3.12) only for the mean value. This is in accordance with the vanishing of the last term on the right-hand side of (3.35). From the analytical point of view, the exactness of the eddy-diffusivity closure is due to the vanishing of the second-order structure function of the coarse-grained velocity, $d_{\mu\nu}^{(\tilde{\mathbf{v}})}(\mathbf{r}) = 0$, which imposes an exact balancing between the forcing and the diffusive terms in (3.31).

3.8.2 Smooth flow

If $\xi = 2$, the second-order spatial increments of the velocity (3.15) scale with r^2 , so \mathbf{v} is a differentiable field. The passive-scalar correlation is exactly given

by

$$C_2^{(\theta)}(r) = c - k \ln \frac{r^2 + \eta^2}{L^2 + \eta^2} \quad \text{for } r < L, \quad (3.40)$$

where

$$k = \frac{F_0}{6(d-1)D_1}$$

and

$$c = -\frac{F_0}{d^2(d-1)D_1} {}_2F_1 \left(1, \frac{d}{2}; 1 + \frac{d}{2}; \frac{2\kappa_0}{(d-1)D_1 L^2} \right).$$

Exploiting its definition, for $d = 3$, the coarse-grained scalar correlation shows a second-order correction in l/r with respect to its fully-resolved corresponding value (3.40),

$$C_2^{(\tilde{\theta})}(r) = C_2^{(\theta)} - \frac{F_0}{30D_1} \left(\frac{l}{r} \right)^2 + \mathcal{O} \left(\frac{l}{r} \right)^4, \quad (3.41)$$

while no difference exists for the velocity structure function: $d_{\mu\nu}^{(\mathbf{v})} = d_{\mu\nu}^{(\tilde{\mathbf{v}})}$.

The key point is that $\mathcal{O}(l/r)^\xi$ and $\mathcal{O}(l/r)^2$ obviously coincide, so CED closure cannot be introduced by itself because it is intimately entangled with the improved closure (3.35). The latter captures the second-order correction in (3.41) correctly.

3.9 Appendix on small-scale correlations

The equation for the subgrid field θ^* is easily obtained by subtracting (3.4) from (3.1):

$$\partial_t \theta^* + \left(\mathbf{v} \cdot \partial \theta - \widetilde{\mathbf{v} \cdot \partial \theta} \right) = \kappa_0 \partial^2 \theta^* + f^*,$$

If one rewrites equation (3.24) in the form

$$\begin{aligned} \partial_t \langle \tilde{\theta}(\mathbf{x}, t) \tilde{\theta}(\mathbf{x}', t) \rangle &= 2\kappa_0 \partial^2 \langle \tilde{\theta}(\mathbf{x}, t) \tilde{\theta}(\mathbf{x}', t) \rangle + \mathcal{F}_L(|\mathbf{x} - \mathbf{x}'|) \\ &+ \int d^d \mathbf{y} \int d^d \mathbf{y}' P_l(\mathbf{x} - \mathbf{y}) P_l(\mathbf{y} - \mathbf{y}') d_{\mu\nu}^{(\mathbf{v})}(\mathbf{y} - \mathbf{y}') \partial_\mu \partial_\nu \langle \theta(\mathbf{y}, t) \theta(\mathbf{y}', t) \rangle, \end{aligned}$$

it can be shown that the two-point equal-time correlation of the subgrid field, $C_2^{(\theta^*)} \equiv \langle \theta^*(\mathbf{x}, t) \theta^*(\mathbf{x}', t) \rangle$, satisfies

$$\begin{aligned} \partial_t \langle \theta^*(\mathbf{x}, t) \theta^*(\mathbf{x}', t) \rangle &= 2\kappa_0 \partial^2 \langle \theta^*(\mathbf{x}, t) \theta^*(\mathbf{x}', t) \rangle \\ &+ \int d^d \mathbf{y} \int d^d \mathbf{y}' Q_l(\mathbf{x} - \mathbf{y}) Q_l(\mathbf{x}' - \mathbf{y}') d_{\mu\nu}^{(\mathbf{v})}(\mathbf{y} - \mathbf{y}') \partial_\mu \partial_\nu \langle \theta(\mathbf{y}, t) \theta(\mathbf{y}', t) \rangle, \end{aligned} \quad (3.42)$$

and that the cross-correlation between the coarse-grained and the subgrid scalar, $C_2^{(\tilde{\theta}, \theta^*)} \equiv \langle \tilde{\theta}(\mathbf{x}, t) \theta^*(\mathbf{x}', t) \rangle$, obeys to

$$\begin{aligned} \partial_t \langle \tilde{\theta}(\mathbf{x}, t) \theta^*(\mathbf{x}', t) \rangle &= 2\kappa_0 \partial^2 \langle \tilde{\theta}(\mathbf{x}, t) \theta^*(\mathbf{x}', t) \rangle \\ &+ \int d^d \mathbf{y} \int d^d \mathbf{y}' P_l(\mathbf{x} - \mathbf{y}) Q_l(\mathbf{x}' - \mathbf{y}') d_{\mu\nu}^{(\nu)}(\mathbf{y} - \mathbf{y}') \partial_\mu \partial_\nu \langle \theta(\mathbf{y}, t) \theta(\mathbf{y}', t) \rangle. \end{aligned} \quad (3.43)$$

Unfortunately, neither (3.42) nor (3.43) represents an equation closed in its unknown, because both involve the fully-resolved correlation (it is also worth noticing that the forcing term completely disappears in both of them). However, exploiting expressions (3.17) and (3.20), in the stationary state and for convective-range separations it can easily be proved that:

$$\begin{aligned} C_2^{(\tilde{\theta}, \theta^*)}(r) &= kr^{2-\xi} \left[\frac{1}{10} (2-\xi)(3-\xi) \left(\frac{l}{r}\right)^2 \right. \\ &\quad \left. + \frac{19}{1400} \xi(\xi-1)(2-\xi)(3-\xi) \left(\frac{l}{r}\right)^4 + \mathcal{O}\left(\frac{l}{r}\right)^6 \right], \\ C_2^{(\theta^*)}(r) &= -kr^{2-\xi} \left[\frac{1}{100} \xi(\xi-1)(2-\xi)(3-\xi) \left(\frac{l}{r}\right)^4 + \mathcal{O}\left(\frac{l}{r}\right)^6 \right]. \end{aligned}$$

Chapter 4

Numerical results for the statistics of large excursions

The large-eddy simulation technique is exploited to investigate statistics of temperature fluctuations, $\Delta_r\theta$, in atmospheric boundary layers (ABL) with different degrees of convection. Statistical characterizations were found for both strong and weak fluctuations. In terms of PDF's of $\Delta_r\theta$, weak and strong fluctuations reflect themselves in different rescaling properties of PDF cores and tails, respectively. For the cores, the observed rescaling is $P(\Delta_r\theta) = r^{-\alpha}\mathcal{P}(\Delta_r\theta/r^\alpha)$, while for the tails the data are compatible with $P(\Delta_r\theta) \propto r^{\zeta_\infty}$. Such two rescaling properties are equivalent to saying $\langle |\Delta_r\theta|^n \rangle \sim r^{\zeta_n}$, with $\zeta_n = \alpha n$ for small n 's and $\zeta_n = \zeta_\infty = \text{const.}$ for large n 's. Both α and ζ_∞ turn out to be z -independent within the mixed layer and, more importantly, they do not vary appreciably by changing the degree of convection in the ABL. Also addressed is the question related to the geometrical structure of temperature jumps contributing to large $|\Delta_r\theta|$. Finally, the possible relevance of these results to the long-standing problem of subgrid scale parameterizations is discussed.

The chapter is organized as follows: introductory section § 4.1 recalls the question about scale invariance in temperature fluctuations. In section § 4.2 I present the basic statistical tools I shall exploit in the present work to characterize, from a statistical point of view, both weak and strong temperature fluctuations. In sections § 4.3 and § 4.4, I introduce two statistical indicators through which information on the geometrical structure of both weak and strong temperature fluctuations can be easily extracted. In section § 4.5 I give a short presentation of the LES model used in the present study. The

three case studies here simulated are described in section § 4.6. Results and discussion are reported in section § 4.7. The results of two sensitivity tests at higher resolution are reported in section § 4.8. Finally, discussions and perspectives are reserved to the concluding section § 4.9.

4.1 Introduction

One of the key challenges in turbulence research is to find statistical features of turbulent systems that remain unchanged at different scales. This is also one of the main aim of the present chapter. The aforementioned property is known as *scale invariance* and attracts a great deal of attention both from theoretical points of view (see, e.g., [65]) and for applicative purposes related, e.g., to the well-known problem of parameterizing small-scale motion in large-eddy simulation models of turbulence (see, e.g., [63]). Indeed, the key point of the LES strategy is that turbulence fields at scales larger than the spatial resolution of the model, say l , are dynamically described during the simulation while smaller scales (subgrid scales, SGS) are filtered out and need to be parameterized in terms of large scales. It is now clear that the exploitation of scale invariance permits to “replicate” statistical properties of large (resolved) scales to the smallest (unresolved) scales, thus becoming an important tool for the problem of SGS parameterizations [63].

When following such an approach for SGS modelling, the accurate knowledge of the possible presence of scale-invariance in the system and, if any, the precise form through which it is manifest become crucial. To be more specific, classical theories of turbulence à la Kolmogorov (see [1] for a modern presentation) use (global) scale-invariance in the so-called inertial range of scales (i.e., scales of motion far from both the region where energy is injected into the system and the region where it is dissipated) as a central assumption. Focusing, from now on, on passive scalar turbulence, the result is that the scalar field, say the (virtual potential) temperature θ , is scale-invariant of exponent $1/3$. Namely,

$$\Delta_r \theta \sim \chi^{1/2} \epsilon^{-1/6} r^{1/3} , \quad (4.1)$$

ϵ and χ being the energy flux and the dissipation rate of temperature variance, respectively.

In terms of PDF of temperature differences, relation (4.1) means the simple rescaling

$$P(\Delta_r \theta) = r^{-1/3} \mathcal{P}(\Delta_r \theta / r^{1/3}) .$$

Following such a theory, the sole exponent $1/3$ is thus sufficient to collapse all PDF's for different separations r . Note that the rescaling property (4.1) is equivalent to saying that all moments $\langle |\Delta_r \theta|^n \rangle$ behave as a power law r^{ζ_n} with $\zeta_n = n/3$, a linear function of the order n .

Exploiting now scale-invariance as a tool for SGS parameterizations, features of the field θ at large scales, r , can be interpolated at the small unresolved scales following fractal interpolation techniques similar to that implemented by Scotti and Meneveau [77].

The open question here is related to the estimation of the possible departure from the scaling (4.1) for the temperature field in convective atmospheric boundary layers. There, the issue of SGS parameterizations is a central problem as far as either LES or ensemble-averaged models of turbulence are concerned. To be more specific, a very weak departure from (4.1) would suggest the success of fractal interpolation techniques (see again [77]) for SGS parameterizations of temperature fields. On the contrary, a strong departure from (4.1) would strongly motivate to adopt the recently proposed multifractal interpolation scheme [78], where the entire set of scaling exponents ζ_n , a nonlinear function of n , must be known to implement the SGS parameterization strategy. Answering the above question is one of the main goals of the present chapter.

Before proceeding along this line, I recall some recent results related to the issue of scale-invariance and its possible violation in scalar turbulence. If, on the one hand, results supporting the breakdown of the concept of global scale-invariance have been known for a long time (see e.g. [65] and references therein), on the other hand a precise characterization of its violation has been provided, at least in idealized models of scalar turbulence, just very recently. The key result is related to the evidence of the so-called *intermittency saturation*, that amounts to saying the saturation to a constant value, ζ_∞ , of the high-order moments of temperature differences: $\langle |\Delta_r \theta|^n \rangle \sim r^{\zeta_\infty}$ for n large enough. Large moments n being involved in such a behaviour, intermittency saturation represents the statistical characterization of strong events, i.e. large jumps $|\Delta_r \theta|$, with respect, e.g., to the root mean square (RMS), σ , of the temperature field, a typical fluctuation of the system. I shall denote such events as “fronts” (see section § 4.3 for a precise definition).

Intermittency saturation in passive scalar turbulence has been proved exploiting field theory methods (see [79]) by Balkovsky and Lebedev [80] for the problem of scalar advection by Gaussian, short-correlated-in-time velocity in the limit of high dimensions of the physical space. For this model, exploiting the Lagrangian method described in [49], strong evidences of intermittency saturation have been provided [50, 51, 76]. Numerical evidences in scalar turbulence in less idealized contexts (but still very far from reality) have been provided for the passive case [81] and for an active scalar model

mimicking convection [82]. There, the numerical results have been obtained exploiting DNS in two dimensions. The first, preliminary, numerical evidence of intermittency saturation in “realistic” situations has been given in [83] in a convective boundary layer simulated by a LES model. In such preliminary investigation, the authors reported results relative to the sole simulation B by Moeng and Sullivan [84] without addressing, e.g., the question on whether their conclusions change by varying the characteristics of the ABL.

Answering this question is important from both theoretical and practical viewpoints. On the theoretical side, it would permit both to assess the robustness of the new found statistical characterization and also to shed some light on the possible existence of ubiquitous properties shared by different types of ABL. This point is related to the long-standing problem of identifying “universal” properties of complex systems, an aim shared with many other research fields including, e.g., statistical mechanics and field theories. As far as applicative issues are concerned, the knowledge of the dependence of scaling exponents (and in particular of the saturation exponent ζ_∞) on the degree of convection is essential information that must be available to apply multifractal interpolation schemes (which use scaling exponents) in a LES. Such essential information was not available in [83].

Another important point left open in [83] is related to the geometrical characterization of the intense jumps which lead to the observed intermittency saturation. In particular on whether the leading contribution to saturation is given by jumps concentrated on the smallest resolved length scales or, on the contrary, by “large-scale” objects. Apart the *per se* interest, answering this question is important because it provides a quantitative justification for the use of LES strategies to investigate large fluctuations of temperature fields. The above issues, together with many other aspects left open in [83], will be addressed in the present chapter, which substantially represents an application of the technique analysed in chapter 3 (closures are assumed as already given, here) to practical situations, in order to answer — from the numerical point of view — to some of the questions issued in the first part of the manuscript.

4.2 Global scale invariance and its violation

In this section I define the concept of *scale invariance* and I also give the statistical characterization of its violation in scalar turbulence. The concept

of *intermittency saturation* will also be introduced both from the point of view of rescaling properties of the PDF of temperature differences and in terms of behaviour of the exponents of high-order moments.

By definition, scale invariance means reproducing itself on different time or space scales. More quantitatively, focusing on space scales, a statistical observable $S_n(r)$ (e.g., a moment of the temperature difference, $\Delta_r\theta$, at the scale r : $S_n(r) = \langle (\Delta_r\theta)^n \rangle$ where $\Delta_r\theta \equiv \theta(\mathbf{r}, t) - \theta(\mathbf{0}, t)$) is scale invariant under the transformation $r \mapsto \lambda r$ if there exists a number $\mu(\lambda, n)$ such that $S_n(\lambda r)/S_n(r) = \mu(\lambda, n)$, i.e. such ratio does not depend on the scale r . It is immediate to check that the class of functions satisfying such relation are the power laws:

$$S_n(r) = A_n r^{\zeta_n} ,$$

where A_n is some prefactor and $\mu = \lambda^{\zeta_n}$ (or, equivalently, $\zeta_n = \log \mu / \log \lambda$). If ζ_n is a linear function of the order n (e.g., $\zeta_n = \alpha n$), one speaks of *global scale invariance*. Physically speaking, the latter property means that scale invariance holds for each type of fluctuation, from the smallest to the largest ones. Indeed, defining the typical fluctuation as $[S_n(r)]^{1/n}$, the ratio $[S_n(\lambda r)]^{1/n}/[S_n(r)]^{1/n}$ does not depend either on the scale r or on the order n .

When ζ_n is a nonlinear function of n , a situation named *local scale invariance* (also known as *intermittency* or *anomalous scaling*) arises. One has $[S_n(\lambda r)]^{1/n}/[S_n(r)]^{1/n} = \lambda^{\zeta_n/n}$, i.e. the ratio does not depend on the scale r but it does depend on the order n . Fluctuations having the same strength (i.e., captured by the same exponent n) thus reproduce themselves at smaller scales in a self-similar fashion, but this is not for fluctuations with different intensity.

From general inequalities in probability theory (known as Hölder inequalities [1]) the function ζ_n must be a convex function of the order n . This means that, focusing on even orders (odd orders could vanish due to symmetries of the system), the ζ_n curve for $n > n_0$ must lie below the straight line joining ζ_{n_0-2} and ζ_{n_0} . A generalization of the argument presented in [1] indicates that a decreasing ζ_n would entail arbitrarily large temperature differences at very small scales, sometimes unlikely, given the maximum principle for the advection-diffusion equation. The curve ζ_n thus lies in between the linear behaviour and the constant, i.e. $\zeta_n = \zeta_\infty$ for n large enough. The latter possibility is known as *intermittency saturation*.

The concept of scale invariance and its violation can be easily character-

ized also in terms of PDF. Focusing on the global scale invariance, one can consider again $\Delta_r\theta$ and its PDF $P(\Delta_r\theta)$. It is immediate to verify that global scale invariance (a linear behaviour *vs* n for the exponent ζ_n) is equivalent to the following rescaling property of the PDF:

$$P(\Delta_r\theta) = r^{-\alpha}\mathcal{P}(\Delta_r\theta/r^\alpha). \quad (4.2)$$

This means that, for each scale r , all fluctuations $\Delta_r\theta$ are controlled by the same function $\mathcal{P}(\Delta_r\theta/r^\alpha)$. Scale information is factorized out in the power law with exponent α .

For the case of *local scale invariance*, the rescaling (4.2) does not hold and, more generally, it is impossible to find a global (i.e. valid for the whole PDF) rescaling.

In the presence of *intermittency saturation*, the PDF again admits a simple rescaling, which is however restricted on the tails. To be more specific, intermittency saturation is equivalent to the PDF taking the following form:

$$P(\Delta_r\theta) = \frac{r^{\zeta_\infty}}{\sigma} Q\left(\frac{\Delta_r\theta}{\sigma}\right) \quad \text{for } |\Delta_r\theta| > \lambda\sigma \quad (\lambda > 1), \quad (4.3)$$

where Q is some function which does not depend on the separation r and σ is the RMS of the temperature field.

The factorization in (4.3) has a simple physical interpretation in the convective boundary layer (CBL). It states that the probability of having a large temperature fluctuation can be thought of as due to the following two events: 1) the separation r must cross the plume interface; 2) the temperature jump across the plume interface must be larger than the typical fluctuation σ . The first event occurs with probability $\propto r^{\zeta_\infty}$, while the second with probability $\propto Q$.

In terms of cumulative probabilities, i.e. the sum (integral) of the PDF over the large temperature excursions (i.e. for $|\Delta_r\theta| > \lambda\sigma$, with $\lambda > 1$), defined as:

$$\text{Prob}[|\Delta_r\theta| > \lambda\sigma] \equiv \int_{-\infty}^{-\lambda\sigma} d(\Delta_r\theta) P(\Delta_r\theta) + \int_{\lambda\sigma}^{+\infty} d(\Delta_r\theta) P(\Delta_r\theta),$$

it is immediately checked from (4.3) that saturation is equivalent to the following power-law behaviour, holding for different values of $\lambda > 1$:

$$\text{Prob}[|\Delta_r\theta| > \lambda\sigma] \sim r^{\zeta_\infty}. \quad (4.4)$$

The scaling exponents, ζ_∞ , can be thus easily extracted by measuring the slope of $\log\{\text{Prob}[|\Delta_r\theta| > \lambda\sigma]\}$ *vs* $\log r$.

4.3 Fronts: mature vs nonmature objects

As shown in the preceding section, the concept of intermittency saturation involves large temperature fluctuations. Indeed, the condition $|\Delta_r\theta| > \lambda\sigma$ selects the sole fluctuations belonging to the tails of the PDF of temperature differences. The problem is now to understand the geometrical structure of such strong events, in particular focusing on the size on which they are concentrated. I shall start from a simple nontrivial example which provides a first clue that strong temperature jumps might be “large-scale” objects. Such first conclusion (that I shall corroborate in the following sections by several numerical evidences) suggests that large fluctuations of temperature can be properly described by coarse-grained models of turbulence, as is the LES strategy.

4.3.1 An example from passive scalar advection

The example I report here is relative to the passive transport of temperature field in the Kraichnan advection model [36, 37], which has already been introduced in the previous chapters. In such an idealized model of scalar transport, the phenomenon of intermittency saturation has been proved both analytically and by means of direct numerical simulations and Lagrangian methods [46]. The latter strategy also permitted to highlight the role of fronts in the observed intermittency saturation.

Simple physical considerations suggest that strong temperature gradients would occur along the direction of compression, while weak temperature gradients should preferentially occur along the stretching directions. More quantitatively, one should expect (averages are with respect to the velocity statistical ensemble)

$$\langle e_{\mu\nu}^{(v)} \partial_\mu \theta \partial_\nu \theta \rangle < 0 . \quad (4.5)$$

By virtue of the above considerations, the negative sign is apparent by transforming (4.5) to the principal coordinates which diagonalize the strain-rate tensor $e_{\mu\nu}^{(v)} \equiv (\partial_\mu v_\nu + \partial_\nu v_\mu)/2$.

The above heuristic arguments become rigorous within the Kraichnan model, where (4.5) can be analytically proved.

I shall now pass to the crucial point which is of interest here. If strong temperature gradients arose from temperature jumps concentrated on the dissipative lengthscale, the negative sign in (4.5) would disappear when the

coarse-grained fields (i.e. the LES fields) $\tilde{\theta}$ and $\tilde{\mathbf{v}}$ replace the fully-resolved fields θ and \mathbf{v} , because of the smoothing produced by the filtering operation defining the coarse-grained fields. On the contrary, if strong temperature gradients are large-scale objects, then one should have:

$$\langle e_{\mu\nu}^{(\tilde{\mathbf{v}})} \partial_\mu \tilde{\theta} \partial_\nu \tilde{\theta} \rangle < 0 ,$$

where $e_{\mu\nu}^{(\tilde{\mathbf{v}})} \equiv (\partial_\mu \tilde{v}_\nu + \partial_\nu \tilde{v}_\mu)/2$. Such inequality has been proved within the Kraichnan model, thus providing a first quantitative motivation to use LES to investigate large fluctuations of temperature fields. Also such a preliminary conclusion will be confirmed *a posteriori* from my data analysis of realistic ABL's.

4.3.2 A quantitative definition of mature and nonmature fronts

In figure 4.1 I sketched two possible situations, both of them leading, in principle, to intermittency saturation. The first option (figure 4.1 (a)) is that strong jumps are preferentially concentrated on the smallest scales. If one describes the full range of scales (e.g. exploiting a DNS), this amounts to stating the existence of large fluctuations concentrated on the dissipative length scale, η , of the system. Below η the dynamics is intimately diffusive and disturbances necessarily disappear. Within a LES scheme the smallest scale is larger than η , and the latter is thus replaced by an artificial small-scale cut-off (I shall continue to denote it by η), below which fluctuations are dissipated due to the action of SGS terms. I shall denote such strong fluctuations as *mature fronts*.

The second possibility (figure 4.1 (b)) is that, for a strong event occurring in the interval $[\mathbf{x}, \mathbf{x} + \mathbf{r}]$, one does not observe excursions concentrated on η . This means that the strong jump has the whole length r as a support. I shall denote such strong fluctuations as *nonmature fronts*.

More formally, I introduce the event “front” in the interval $[\mathbf{x}, \mathbf{x} + \mathbf{r}]$ as

$$\text{front} \equiv \{|\theta(\mathbf{x} + \mathbf{r}) - \theta(\mathbf{x})| > \sigma\}$$

and the probability of its occurrence

$$\text{Prob}(\{\text{front}\}) \equiv \text{Prob}\{|\theta(\mathbf{x} + \mathbf{r}) - \theta(\mathbf{x})| > \sigma\} ,$$

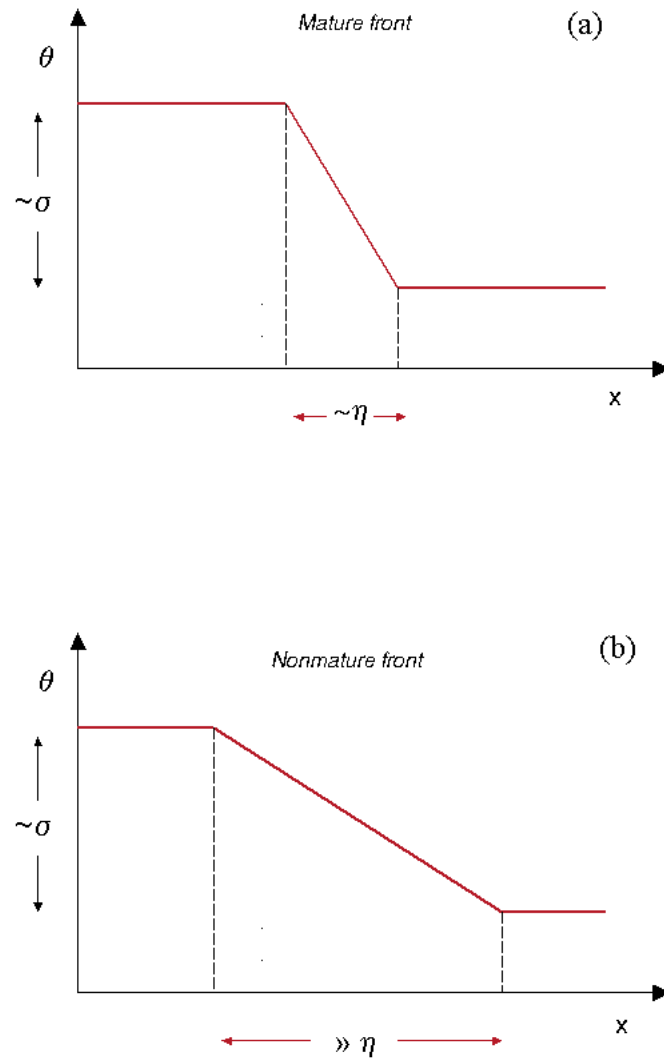


Figure 4.1: A schematic view of (a) a mature front; (b) a nonmature front.

where I fixed, in way of example, $\lambda = 1$.

Such a probability can be viewed as the sum of the probabilities associated

to the two events:

$$\begin{aligned} \{\text{front, mature}\} &\equiv \{|\theta(\mathbf{x} + \mathbf{r}) - \theta(\mathbf{x})| > \sigma\} \cap \\ &\{\exists \mathbf{x}' \in [\mathbf{x}, \mathbf{x} + \mathbf{r}] : |\theta(\mathbf{x}' + \boldsymbol{\eta}) - \theta(\mathbf{x}')| > \sigma\} , \end{aligned}$$

$$\begin{aligned} \{\text{front, nonmature}\} &\equiv \{|\theta(\mathbf{x} + \mathbf{r}) - \theta(\mathbf{x})| > \sigma\} \cap \\ &\{\forall \mathbf{x}' \in [\mathbf{x}, \mathbf{x} + \mathbf{r}] |\theta(\mathbf{x}' + \boldsymbol{\eta}) - \theta(\mathbf{x}')| < \sigma\} . \end{aligned}$$

Namely,

$$\text{Prob}(\{\text{front}\}) = \text{Prob}(\{\text{front, mature}\}) + \text{Prob}(\{\text{front, nonmature}\}) . \quad (4.6)$$

In section § 4.7.2 I shall exploit (4.6) to address the question on the geometrical shape associated to strong events.

4.4 Weak events: cancelled vs uncanceled objects

In the preceding section I introduced probabilistic tools which are used to investigate the relation between geometry and large temperature excursions. I proceed now in a similar way in order to characterize, from a geometrical point of view, weak temperature fluctuations.

Once a weak (e.g., less than σ) temperature excursion is identified between two points x_1 and x_2 , one of two possibilities may occur: 1) within the interval connecting x_1 to x_2 there exist successive front structures that cancel each other, in a way to reproduce a weak jump between points x_1 and x_2 (for a schematic view see figure 4.2 with A $\equiv x_1$ and B $\equiv x_2$); 2) there are no fronts in such interval (see figure 4.2, with C $\equiv x_1$ and D $\equiv x_2$).

I shall call such two options “weak event with cancellation” and “weak event without cancellation”, respectively.

To proceed more formally, I introduce the smooth event in the interval $[\mathbf{x}, \mathbf{x} + \mathbf{r}]$ as

$$\{\text{smooth event}\} \equiv \{|\theta(\mathbf{x} + \mathbf{r}) - \theta(\mathbf{x})| < \sigma\}$$

and the probability of its occurrence

$$\text{Prob}(\{\text{smooth event}\}) \equiv \text{Prob}\{|\theta(\mathbf{x} + \mathbf{r}) - \theta(\mathbf{x})| < \sigma\} ,$$

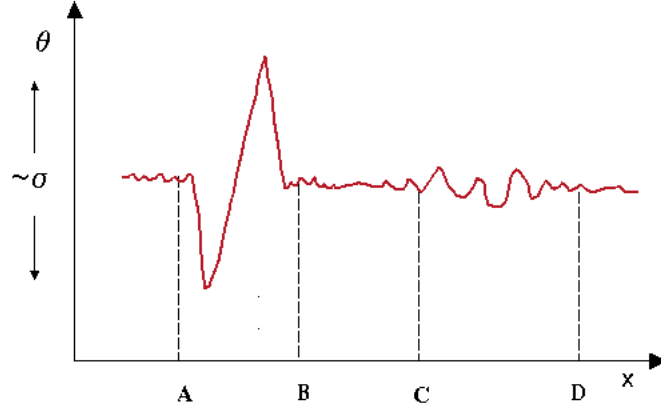


Figure 4.2: A schematic view on how a weak fluctuation can emerge. In between points A and B, one has a weak fluctuation originated from cancellation of two strong events; in between points C and D, the weak fluctuation arises because the temperature field is smooth within the interval.

where I fixed, as in section § 4.3, $\lambda = 1$.

Such a probability can be viewed as the sum of the probabilities associated to the two events:

$$\{\text{smooth event, with cancellations}\} \equiv \{|\theta(\mathbf{x} + \mathbf{r}) - \theta(\mathbf{x})| < \sigma\} \cap \{\exists \mathbf{x}' \in [\mathbf{x}, \mathbf{x} + \mathbf{r}] \exists \delta \in [\boldsymbol{\eta}, \mathbf{r}] : |\theta(\mathbf{x}' + \delta) - \theta(\mathbf{x}')| > \sigma\},$$

$$\{\text{smooth event, without cancellations}\} \equiv \{|\theta(\mathbf{x} + \mathbf{r}) - \theta(\mathbf{x})| < \sigma\} \cap \{\forall \mathbf{x}' \in [\mathbf{x}, \mathbf{x} + \mathbf{r}] \forall \delta \in [\boldsymbol{\eta}, \mathbf{r}] |\theta(\mathbf{x}' + \delta) - \theta(\mathbf{x}')| < \sigma\},$$

with the associated probability.

One thus has:

$$\text{Prob}(\{\text{weak event}\}) = \text{Prob}(\{\text{weak event, with cancellation}\}) + \text{Prob}(\{\text{weak event, without cancellation}\}).$$

In section § 4.7.4, I shall exploit the above indicators to have insights on the geometrical structure (e.g., the size) of thermal plumes in the CBL.

4.5 The large-eddy simulation model

In order to investigate the structure of temperature fluctuations in CBL's, I used the NCAR LES model described in [85] and [86]. Such a model has been widely used and tested to investigate basic research problems in the framework of boundary layer flows (see, e.g., [87, 88, 84], among the others). The LES strategy is an intermediate technique between the DNS, where all turbulent scales of motion are dynamically described, and the Reynolds-averaged Navier–Stokes equations (RANS) in which the flow variables are decomposed into a mean and a fluctuating part via some more-or-less complex turbulence models and only the mean part is described in a dynamical way. The LES consists in computing (according to the dynamical equations) the dynamics of the large eddies, while modelling the smallest, unresolved, ones. Such an approach is based on the well-known cascade scenario *à la* Kolmogorov [1], where small eddies originate from instabilities of the largest eddies. The intimate chaotic character of this process makes small eddies more universal, as well as more isotropic and homogeneous, than the largest ones. It thus turns out that the modelling of subgrid scales is considerably simpler and more accurate than that of the largest, nonuniversal, anisotropic and inhomogeneous scales.

The LES equations used here are obtained by filtering the governing (full-scale) equations with a Gaussian filter of variance equal to the grid mesh l , the role of which is to average out fluctuations on scales smaller than l . For the sake of clarity, I report hereafter the NS and the continuity equations for an incompressible flow, together with the advection-diffusion forced equation for the potential temperature θ :

$$\partial_t v_\mu + \mathbf{v} \cdot \boldsymbol{\partial} v_\mu = \nu \partial^2 v_\mu + \left(g \frac{\theta}{\theta_0} \delta_{\mu 3} - h \epsilon_{\mu\nu 3} v_\nu + f_\mu^{(\mathbf{v})} \right) - \frac{1}{\rho_0} \partial_\mu p \quad (4.7)$$

$$\boldsymbol{\partial} \cdot \mathbf{v} = 0 \quad (4.8)$$

$$\partial_t \theta + \mathbf{v} \cdot \boldsymbol{\partial} \theta = \kappa_0 \partial^2 \theta + f^{(\theta)} \quad (4.9)$$

where h is the Coriolis parameter, $f^{(\theta)}$ and $f_\mu^{(\mathbf{v})}$ represent the effect of external forcing mechanism and $g(\theta/\theta_0)\delta_{\mu 3}$ is the buoyancy term (in the Boussinesq approximation, which also accounts for the presence of ρ_0), because of which the temperature turns out to be an *active* scalar in this case.

Upon introduction of the coarse-grained fields (3.2) and of the respective sub-grid components (3.3), applying the three-dimensional Gaussian filter oper-

ator to equations (4.7), (4.8) and (4.9) gives the following filtered equations:

$$\begin{aligned} \partial_t \tilde{\mathbf{v}} + \tilde{\mathbf{v}} \cdot \boldsymbol{\partial} \tilde{v}_\mu &= \nu \partial^2 \tilde{v}_\mu + \left(g \frac{\tilde{\theta}}{\theta_0} \delta_{\mu 3} - h \epsilon_{\mu\nu 3} \tilde{v}_\nu + \tilde{f}_\mu^{(v)} \right) - \frac{1}{\rho_0} \partial_\mu \tilde{p} - \partial_\nu \tau_{\mu\nu}^{(v)} \\ \boldsymbol{\partial} \cdot \tilde{\mathbf{v}} &= 0 \\ \partial_t \tilde{\theta} + \tilde{\mathbf{v}} \cdot \boldsymbol{\partial} \tilde{\theta} &= \kappa_0 \partial^2 \tilde{\theta} + \tilde{f}^{(\theta)} - \boldsymbol{\partial} \cdot \boldsymbol{\tau}^{(\theta)}, \end{aligned}$$

where $\tau_{\mu\nu}^{(v)} = \widetilde{v_\mu v_\nu} - \tilde{v}_\mu \tilde{v}_\nu$ is the SGS flux of momentum (its correspondent for heat, $\boldsymbol{\tau}^{(\theta)}$, has already been defined in (3.6)).

SGS terms must be expressed in terms of resolved, large-scale, fields in order to have closed equations for $\tilde{\mathbf{v}}$ and $\tilde{\theta}$. In the present LES, SGS fluxes are related to the resolved fields via the *downgradient* diffusion assumption:

$$\begin{aligned} \tau_{\mu\nu}^{(v)} &= \widetilde{v_\mu v_\nu} - \tilde{v}_\mu \tilde{v}_\nu - 2K_M S_{\mu\nu} \\ \boldsymbol{\tau}^{(\theta)} &= \widetilde{\mathbf{v}\theta} - \tilde{\mathbf{v}}\tilde{\theta} - K_H \boldsymbol{\partial} \tilde{\theta}, \end{aligned}$$

where $S_{\mu\nu}$ is equal to $e_{\mu\nu}^{(\tilde{v})}$ plus the modification introduced in [86], leading to the so-called ‘‘two-part eddy viscosity’’. K_M and K_H are the eddy-diffusion coefficients of momentum and heat, respectively, which are related to dynamical quantities in empirical ways. The choice in the present LES model is:

$$K_M = 0.1l\sqrt{\tilde{e}^*}, \quad K_H = \left(1 + \frac{2l}{DS}\right) K_M,$$

where $\sqrt{\tilde{e}^*}$ is a typical velocity constructed from the SGS turbulence energy, \tilde{e}^* , whose equation is solved in the present LES model. For negative stratifications (the main concern of the present study), one has $l = DS \equiv (Dx Dy Dz)^{1/3}$, Dx , Dy and Dz being the grid spacing in x , y and z , respectively.

More details on the used LES model can be found in [85] and [86] and references therein.

4.6 The simulated convective boundary layers

In the next sections, I shall report results relative to the analysis of four different convective boundary layers simulated by a LES model with different

Sim.	L (km)	L_z (km)	Res.	τ_* (s)	T (τ_*)	Q_* (mK s^{-1})	U_g (m s^{-1})	$-z_i/L_{\text{MO}}$
B	5	2	128^3	510	36	0.24	10	18
1	5	2	128^3	500	8	0.29	5	200
SB1	3	1	128^3	530	24	0.05	15	1.6
B2	5	2	256^3	510	36	0.24	10	18

Table 4.1: The relevant parameters characterizing simulations Sim. B, Sim. 1, Sim. SB1 and Sim. B2. In this table, L and L_z are the domain extension along the horizontal and vertical directions, respectively; Res. is the number of grid points, τ_* is the turnover time, T is the duration of the quasi-steady state inside which statistical analysis has been performed, Q_* is the heat flux from the bottom boundary, U_g is the geostrophic wind and $-z_i/L_{\text{MO}}$ is the stability parameter (z_i and L_{MO} being the mixed-layer depth and the Monin-Obukhov length, respectively).

spatial resolutions (128^3 and 256^3 grid points). The simulations performed at the higher resolution 256^3 , and the relative results, will be discussed in section § 4.8. This high-resolution simulation serves as a sensitivity test on the model resolution and also permits to address the question on the possible effect of SGS parameterizations on the large-scale, resolved, dynamics and thus on the results I am going to show in the next sections.

Three of these analysed simulations are well-known in literature: I reproduced the simulations B (see also [83] for a preliminary investigation) and SB1 (hereafter referred to as Sim. B and Sim. SB1) by Moeng and Sullivan [84] and simulation 1 (Sim. 1) by Nieuwstadt and Brost [89]. At variance of [89] (which is a decaying simulation), I maintained a constant heat flux from the bottom boundary for the entire duration of the simulation. A quasi-steady state was thus reached in my Sim. 1.

Note that, with respect to Moeng–Sullivan’s and Nieuwstadt–Brost’s simulations, I increased the spatial resolution to 128^3 grid points. I performed one more simulation, Sim. B2, which is similar to Sim. B but with higher resolution.

All simulations reproduce a convective boundary layer but with different ratios between buoyancy production and shear production (see table 1 for a list of the relevant parameters of the simulations). As is well known, the stability parameter $-z_i/L_{\text{MO}}$ (where z_i is the mixed-layer height and L_{MO} is the Monin-Obukhov length) provides a measure of the atmospheric sta-

bility. This amounts to saying that in the turbulent-kinetic-energy equation the buoyancy production is larger than the contribution associated to the shear term [90] when $-z_i/L_{\text{MO}} \gtrsim 1$. According to Deardorff [91], a convective regime is encountered for $-z_i/L_{\text{MO}} > 4.5$. From the values of z_i/L_{MO} reported in table 4.1, Sim. 1 is relative to a pure buoyancy-dominated convective regime ($-z_i/L_{\text{MO}} = 200$); Sim. B is still relative to a convective regime ($-z_i/L_{\text{MO}} = 18$) but it is also affected by a relatively small shear. Finally, Sim. SB1 represents an intermediate case ($-z_i/L_{\text{MO}} = 1.5$) between a pure shear and a pure buoyancy-dominated boundary layer.

4.6.1 The quasi-steady state for the simulated boundary layers

My statistical analysis was carried out after the quasi-steady state had been reached. The latter corresponds to a linear behaviour of the potential-temperature flux with the elevation from the bottom boundary, or, equivalently, to the linear-in-time growth of potential temperature averaged in the mixed layer. In my simulations, the presence of quasi-steady states has been assessed in both ways.

Sim. B

The quasi-steady state has been reached, as in [84], after about six large-eddy turnover times, τ_* (defined as $\tau_* = z_i/w_*$, where w_* is the convective velocity scale). After that time, the simulation has been advanced in time for $36\tau_*$ more and the simulated potential-temperature field saved at $0.5\tau_*$ intervals for the analysis. My data set was thus formed by 72 (almost independent) potential temperature snapshots.

Sim. 1

The quasi-steady state has been reached after about $5\tau_*$. After that time, the simulation has been advanced in time for $8\tau_*$ more and the simulated potential-temperature field saved every $0.5\tau_*$, thus forming a data set of 16 independent snapshots.

I was unable to perform a longer integration because of the rapid growth of the mixed layer, progressively invading the whole boundary layer.

Sim. SB1

The quasi-steady state has been reached after about $10\tau_*$. After that time, the simulation has been advanced in time for $24\tau_*$ more and the simulated potential-temperature field saved every $0.5\tau_*$, forming a data set of 48 independent snapshots.

Sim. B2

The quasi-steady state has been reached after about $8\tau_*$. After that time, the simulation has been advanced in time for $24\tau_*$ more and the simulated potential-temperature field saved every $0.5\tau_*$, forming a data set of 48 independent snapshots.

4.7 Analysis of results and discussions

4.7.1 Statistics of large temperature fluctuations

I shall start this statistical analysis from the large temperature fluctuations. With a small change in the notation, with respect to section § 4.2, I shall denote the PDF of temperature differences as $P(\Delta_{r;z}\theta)$. The same z -dependence will be added also in α , ζ_∞ and σ (again defined in section § 4.2). This is meant to stress that such quantities might depend on the vertical coordinate z spanning the entire mixed layer. The CBL being homogeneous in the x - y planes, no dependence on x and y is expected (which is actually confirmed, *a posteriori*, from the analysis).

In order to verify the presence of intermittency saturation, one has to verify whether or not the laws (4.3) and (4.4) emerge from the data analysis. Starting from (4.4), for the saturation to occur, I recall that such cumulative probability has to behave as a power law with exponent ζ_∞ . Such behaviour is indeed observed and shown in figures 4.3 (Sim. B), 4.4 (Sim. 1) and 4.5 (Sim. SB1) for different elevations within the mixed layer. From these figures one can easily identify the inertial range of scales (which extends over about half decade) where I measured the best-fit slopes, ζ_∞ (straight lines). For all simulations and analysed elevations, I found $\zeta_\infty \sim 0.6$. I can provide an estimation of the error bar on such an exponent by comparing, for Sim. B, best fits at the two resolutions 128^3 and 256^3 . The maximum variation (from 128^3 to 256^3) of ζ_∞ found within the mixed layer is about 30% of its value.

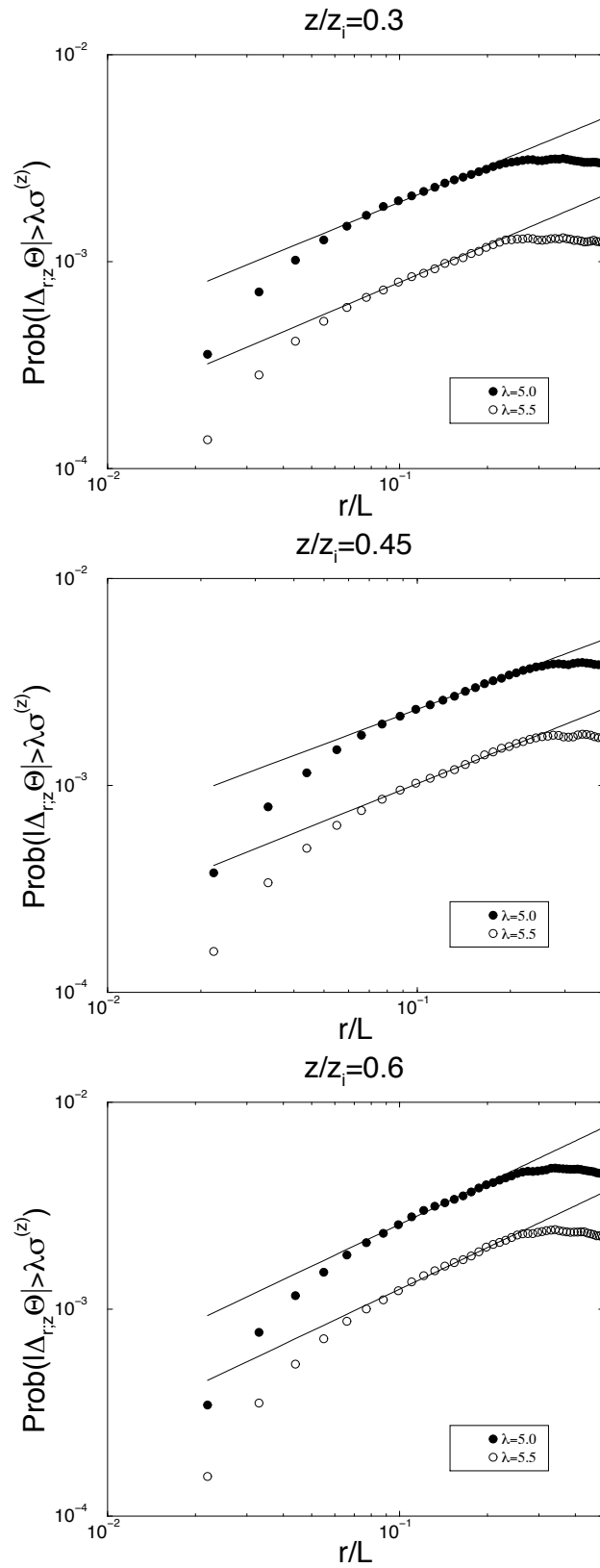


Figure 4.3: For Sim. B, the cumulative probabilities $\text{Prob}[|\Delta_{r;z}\theta| > \lambda\sigma^{(z)}]$ for two values of λ are shown for (a): $z/z_i = 0.3$, (b): $z/z_i = 0.45$ and (c): $z/z_i = 0.6$. The slopes of these curves (continuous line) are compatible with the exponent $\zeta_\infty \sim 0.6$.

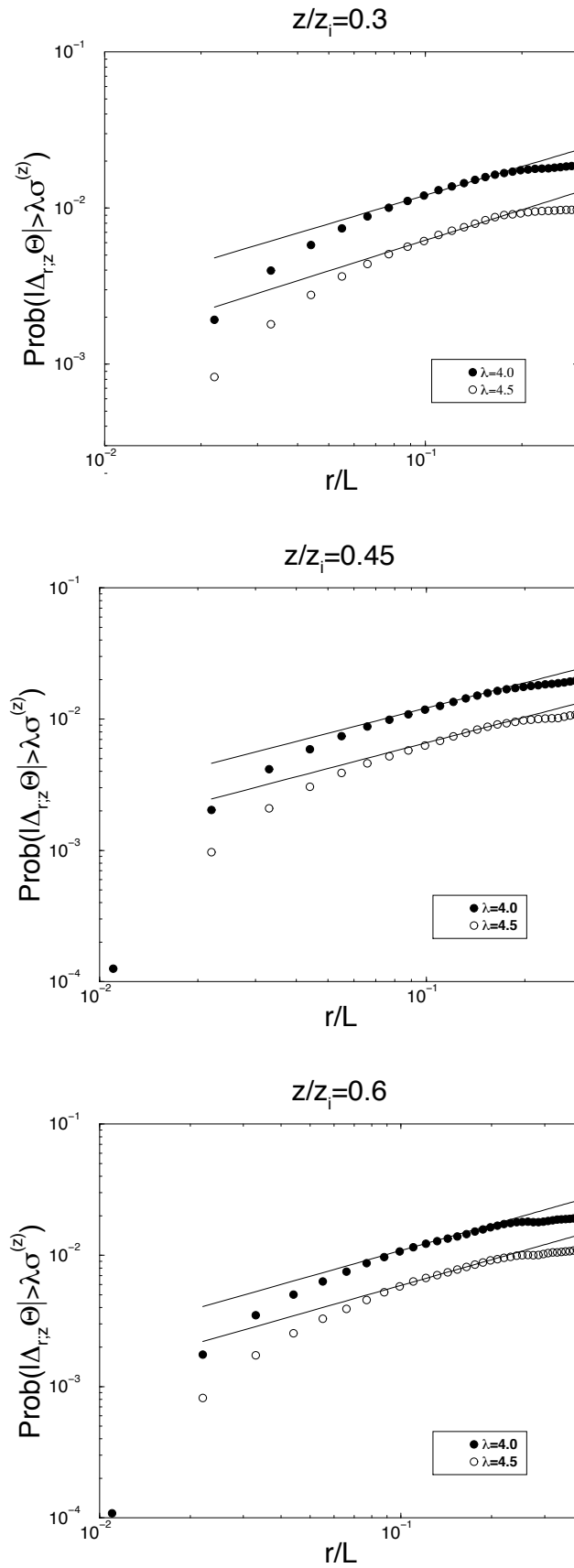


Figure 4.4: As in figure 4.3 but for Sim. 1

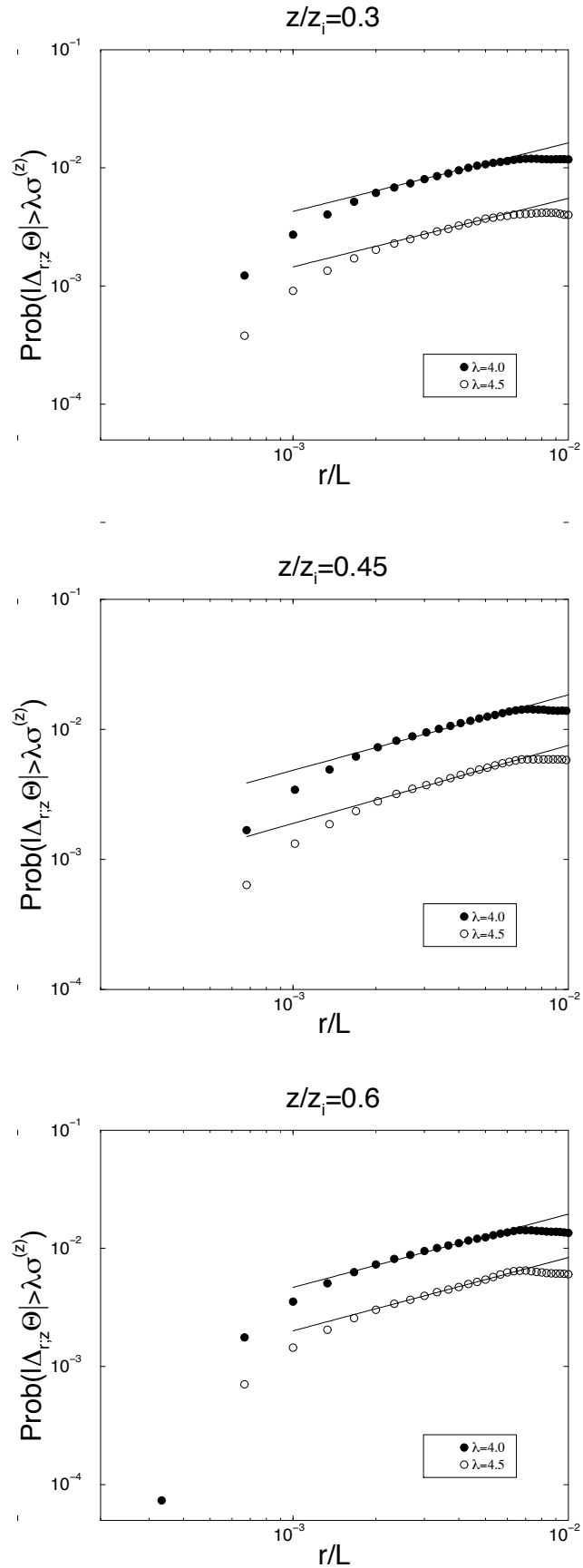


Figure 4.5: As in figure 4.3 but for Sim. SB1

I now pass to corroborate the above scenario by searching for the scaling behaviour given by (4.3). In figures 4.6, 4.7 and 4.8 I reported the behaviour of $P(\Delta_{r,z}\theta)$ (with and without rescaling) relative to Sim. B, for three different elevations from the bottom boundary ($z = 0.3z_i$, $z = 0.45z_i$ and $z = 0.6z_i$). Pictures (a) are relative to the PDF's without rescaling while in pictures (b) the rescaling (4.3) has been exploited (pictures (c) will be described later). The data collapse occurring on the PDF tails means the validity of (4.3), which amounts to prove the presence of intermittency saturation. The exponent ζ_∞ , found to obtain the best data collapse for all separations r falling in the inertial range of scales, is, within the error bar, $\zeta_\infty \sim 0.6$.

A similar good-quality tail data collapse is also observed for the other simulations Sim. 1 and Sim. SB1. Results are reported in figures 4.9, 4.10 and 4.11 (for Sim. 1), and in figures 4.12, 4.13 and 4.14 (for Sim. SB1). In both simulations, the value of ζ_∞ used to obtain the best data collapse of the tails is compatible with $\zeta_\infty \sim 0.6$. Within the error bars, such value is the same of Sim. B.

It is worth observing that, for all simulations, the measured ζ_∞ shows only very slight (order of 10%) variations with the elevation, z , within the mixed layer. It thus appears to be a property of the entire mixed layer. As I shall show later, the dependence on the elevation is contained in the sole function Q .

The fact that ζ_∞ does not show appreciable variations with z can be easily explained as a consequence of the efficient mixing characterizing the layer under investigation. In the strong convective case (Sim. 1) the mixing is due to the action of buoyancy forces, in the less convective case (Sim. SB1) it is induced preferentially by shear. Both mechanisms are present (although shear production is weaker than buoyant production) in Sim. B. Such results seem to be a reminiscence of the universality scenario presented in [81, 76, 92] with respect to the mechanisms sustaining turbulent activity into the system.

What seems to change both with the elevation and by changing the degree of convection is the strength (with respect to σ at that elevation) of the temperature jumps across a plume. The function Q , related to the probability of having a strong jump on a separation r , provided that the latter is crossing a plume (see discussions following (4.3)), shows indeed variations both with z and from one simulation to the other. The behaviour of the function Q is shown in figures 4.15 ((a): Sim. B, (b): Sim. 1, (c): Sim. SB1). In each figure I reported two curves which are relative to the elevations $z = 0.3z_i$ and $z = 0.6z_i$, respectively. Note that Q is defined on the sole tails of the

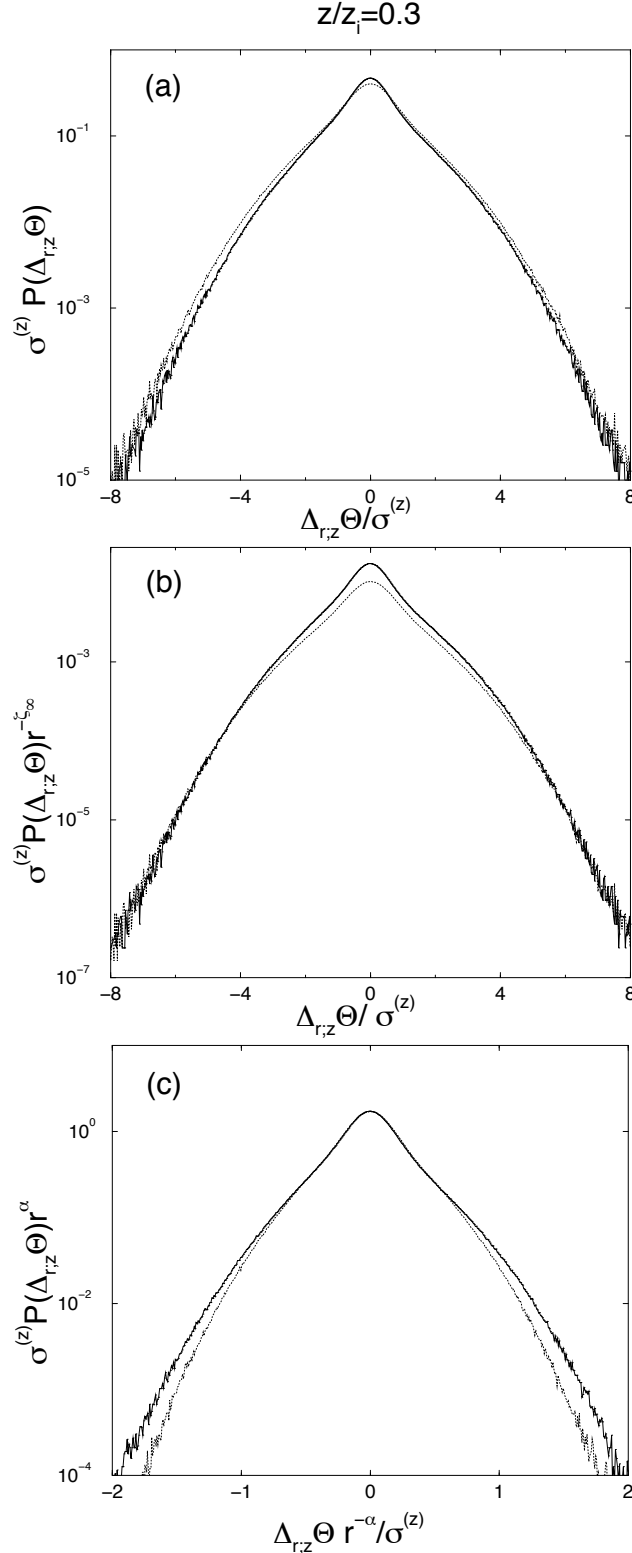


Figure 4.6: The PDF's $P(\Delta_{r;z}\theta)$, for two values of r inside the inertial range of scales ($r/L = 0.22$ and $r/L = 0.11$, L being the side of the (squared) simulation domain) and $z/z_i = 0.3$, z_i being the elevation of the mixed-layer top. (a): PDF's are shown without any r -dependent rescaling; (b) PDF's are multiplied by the factor $\sigma^{(z)}r^{-\zeta_\infty}$ with $\zeta_\infty \sim 0.6$: the collapse of the curve indicates the asymptotic behavior $P(\Delta_{r;z}\theta) \sim r^{\zeta_\infty}$ for large $\Delta_{r;z}\theta$, that means saturation of temperature scaling exponents. (c): PDF's are multiplied by the factor r^α while $\Delta_{r;z}\theta$ by $r^{-\alpha}$: the collapse of PDF cores indicates the validity of (4.2) that is equivalent to the linear behaviour of low-order temperature scaling exponents.

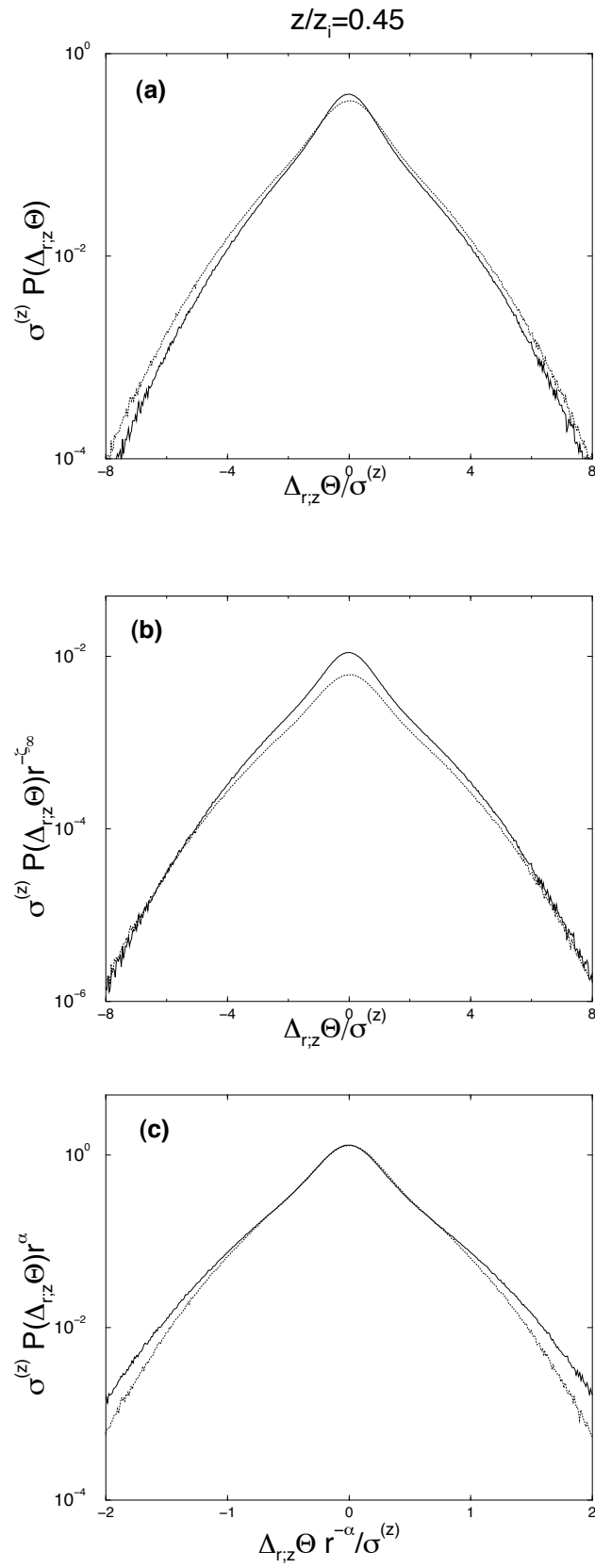
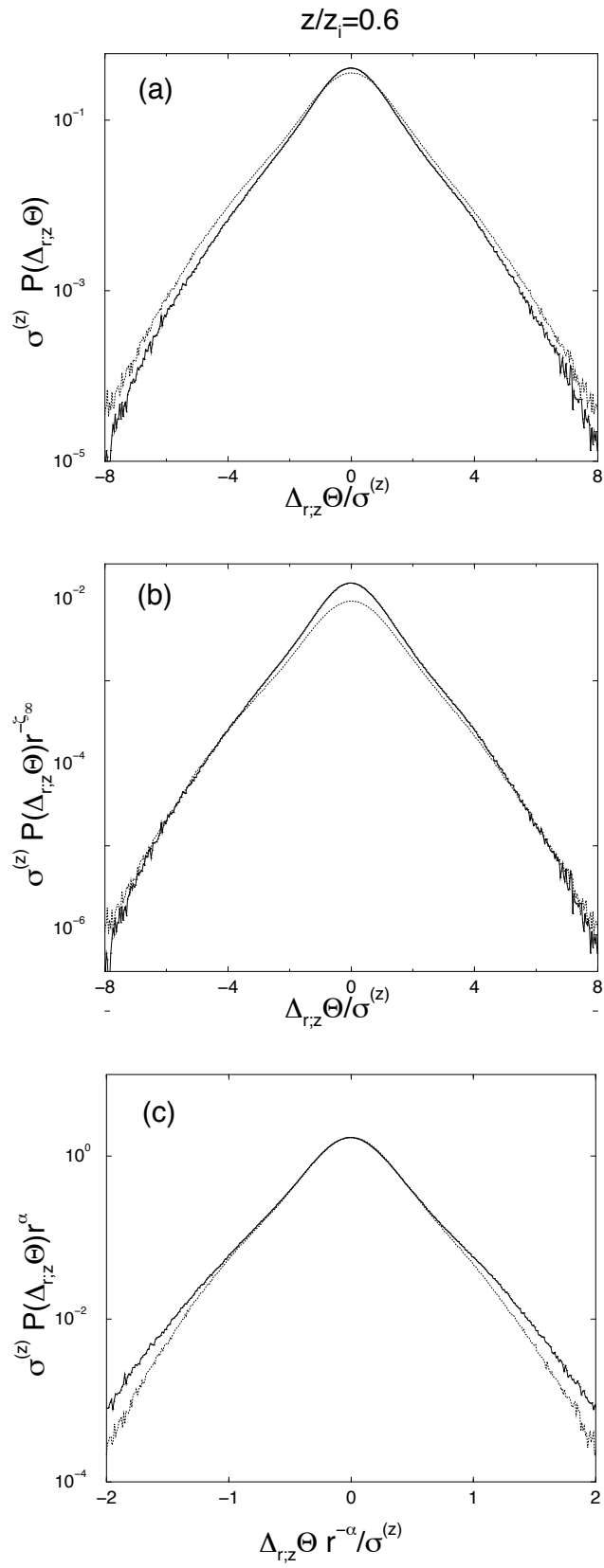


Figure 4.7: As in figure 4.6 but for $z/z_i = 0.45$.

Figure 4.8: As in figure 4.6 but for $z/z_i = 0.6$.

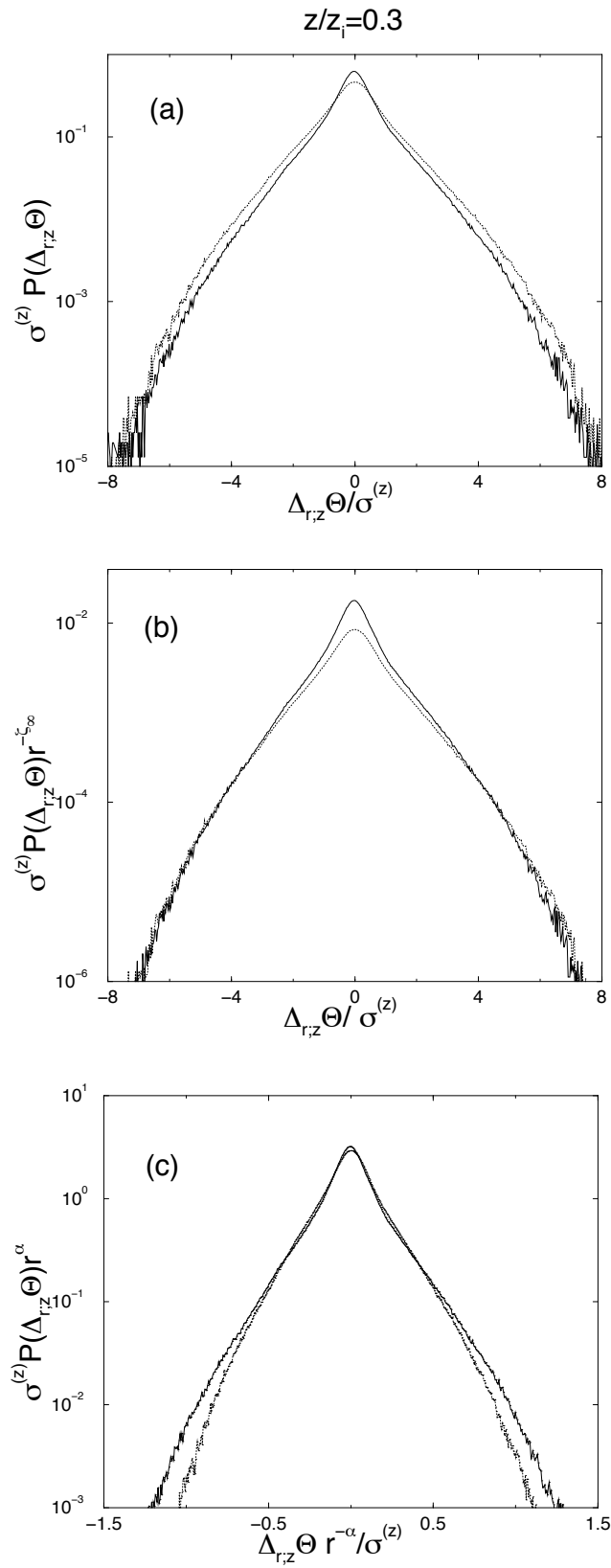


Figure 4.9: As in figure 4.6 but for Sim. 1.

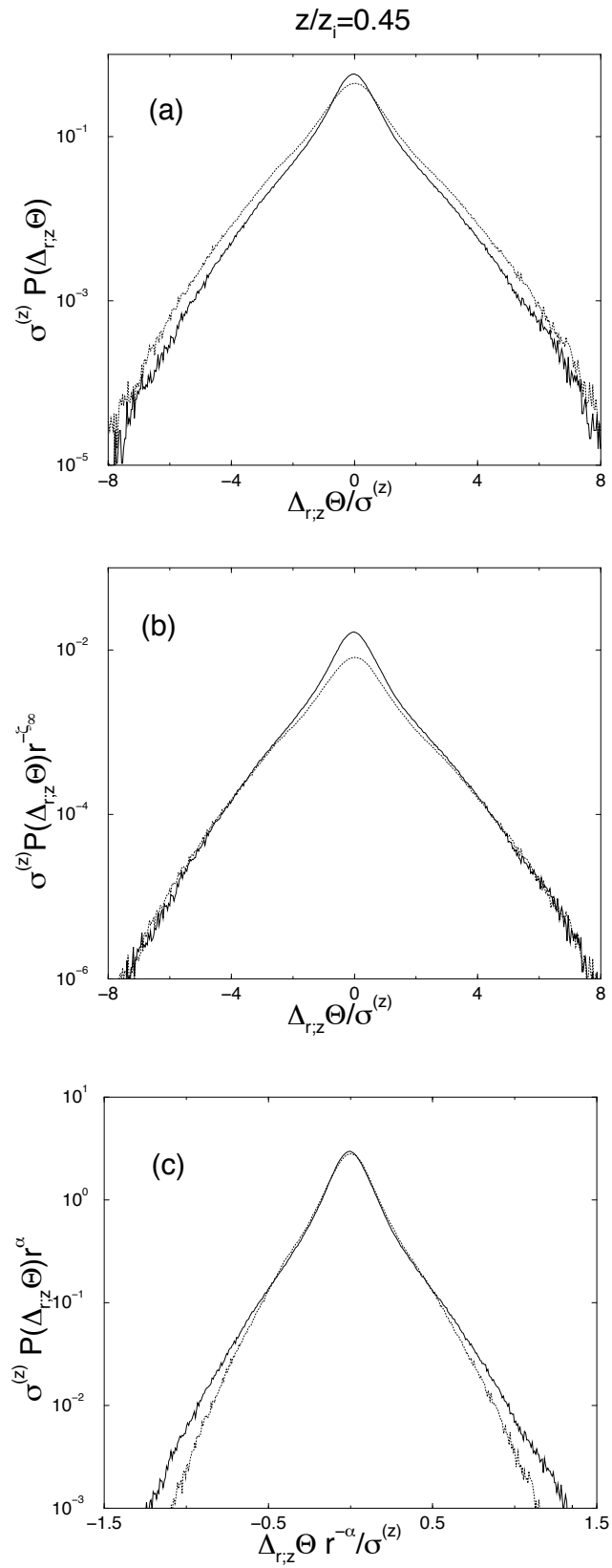


Figure 4.10: As in figure 4.7 but for Sim. 1.

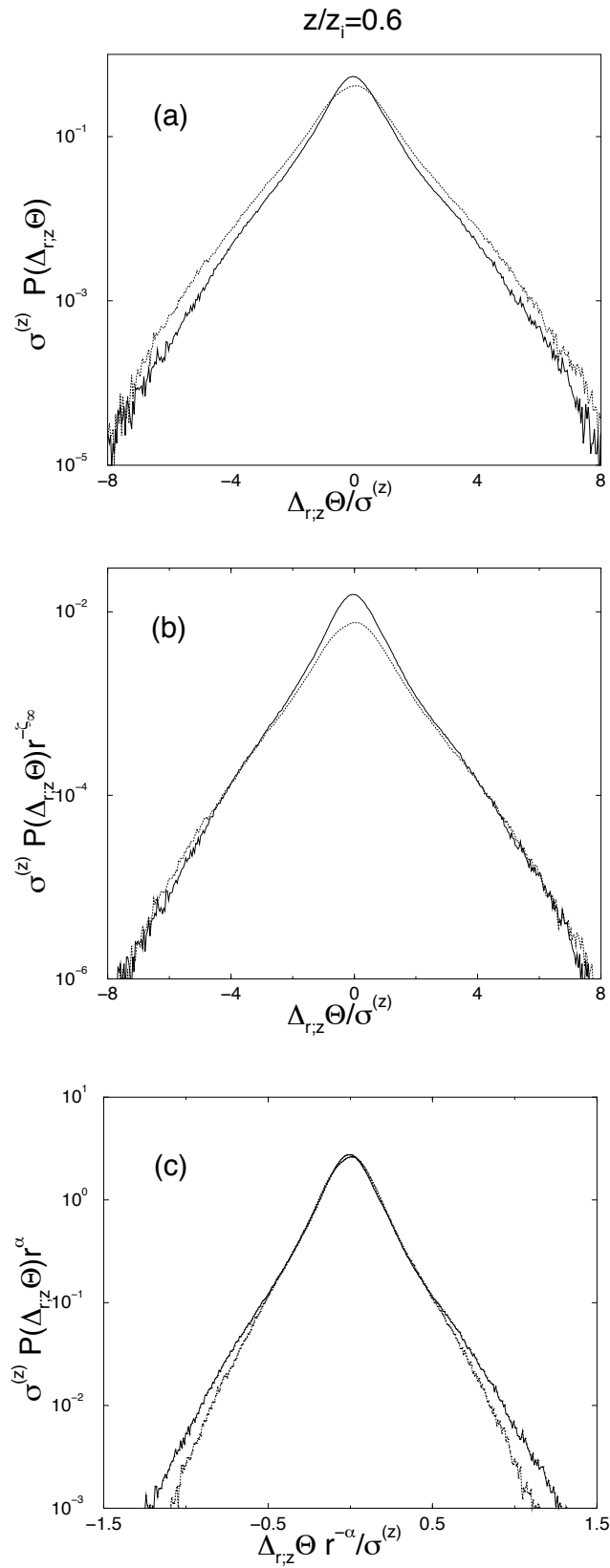


Figure 4.11: As in figure 4.8 but for Sim. 1.

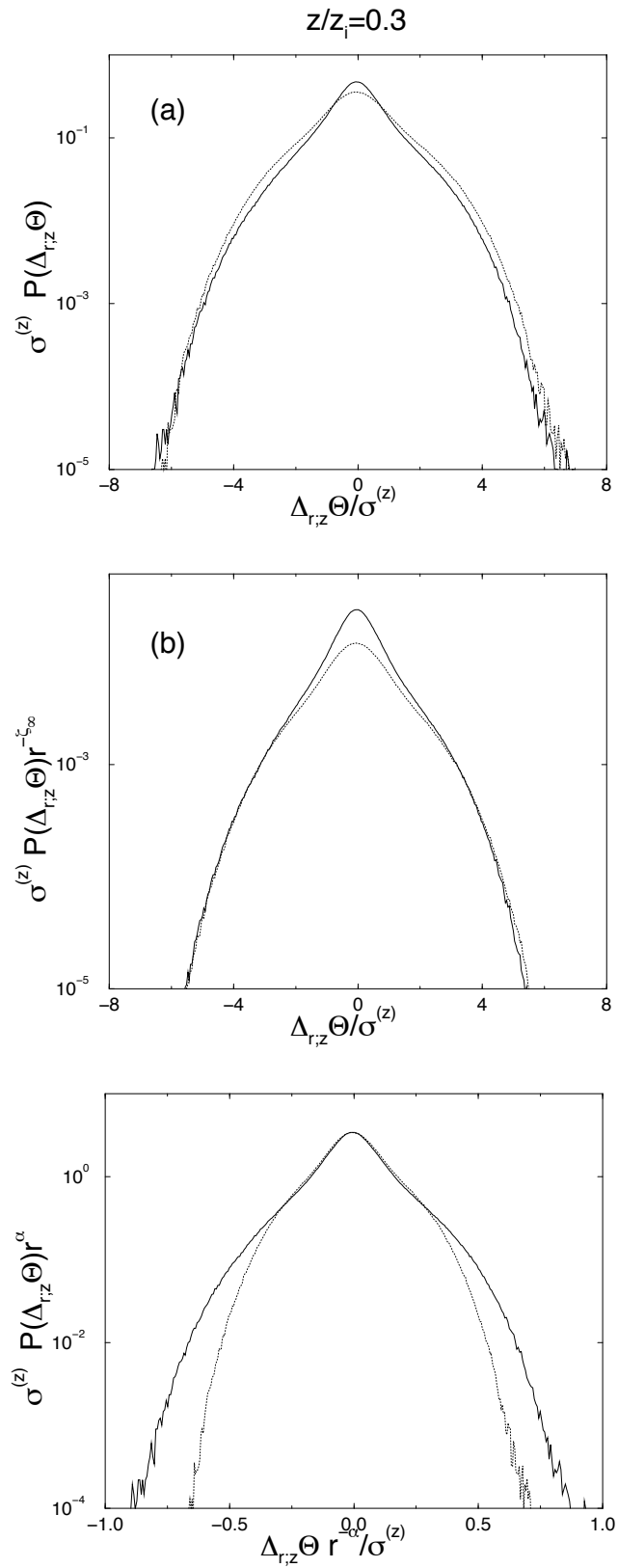


Figure 4.12: As in figure 4.6 but for Sim. SB1 and separation $r/L = 7 \times 10^{-3}$ and $r/L = 3 \times 10^{-3}$.

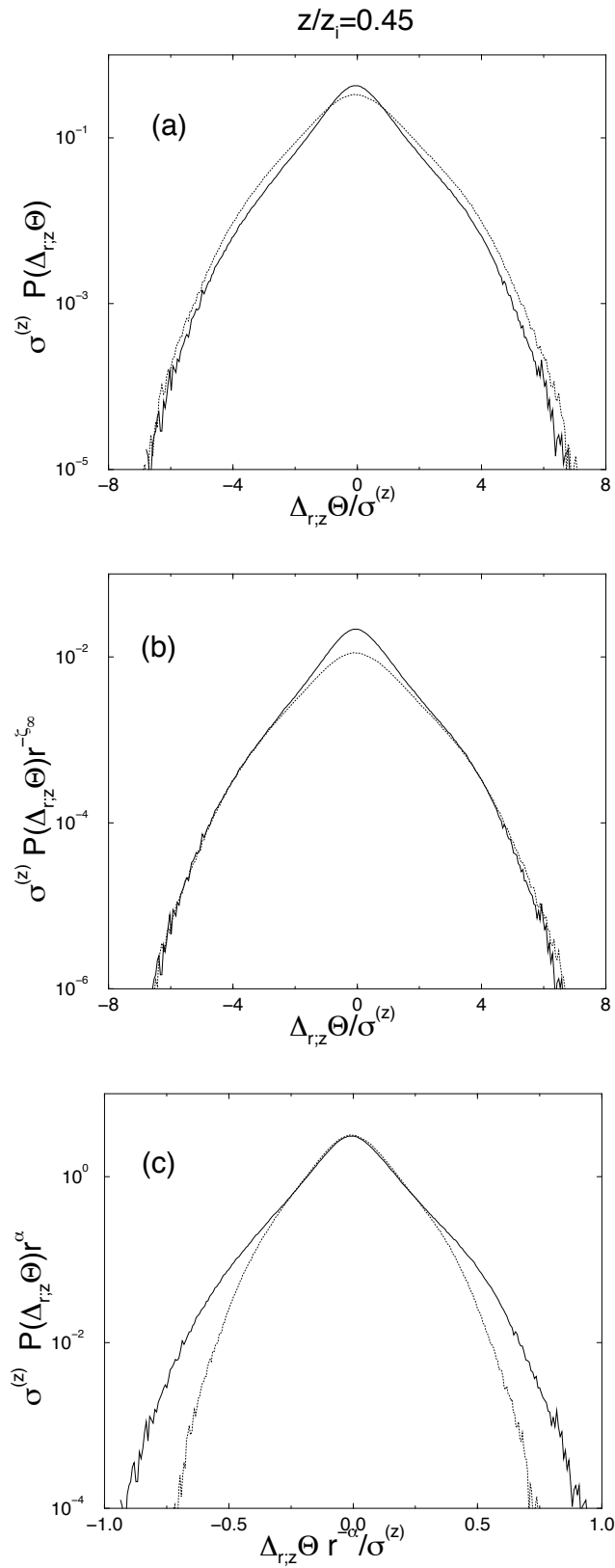


Figure 4.13: As in figure 4.7 but for Sim. SB1 and separation $r/L = 7 \times 10^{-3}$ and $r/L = 3 \times 10^{-3}$.

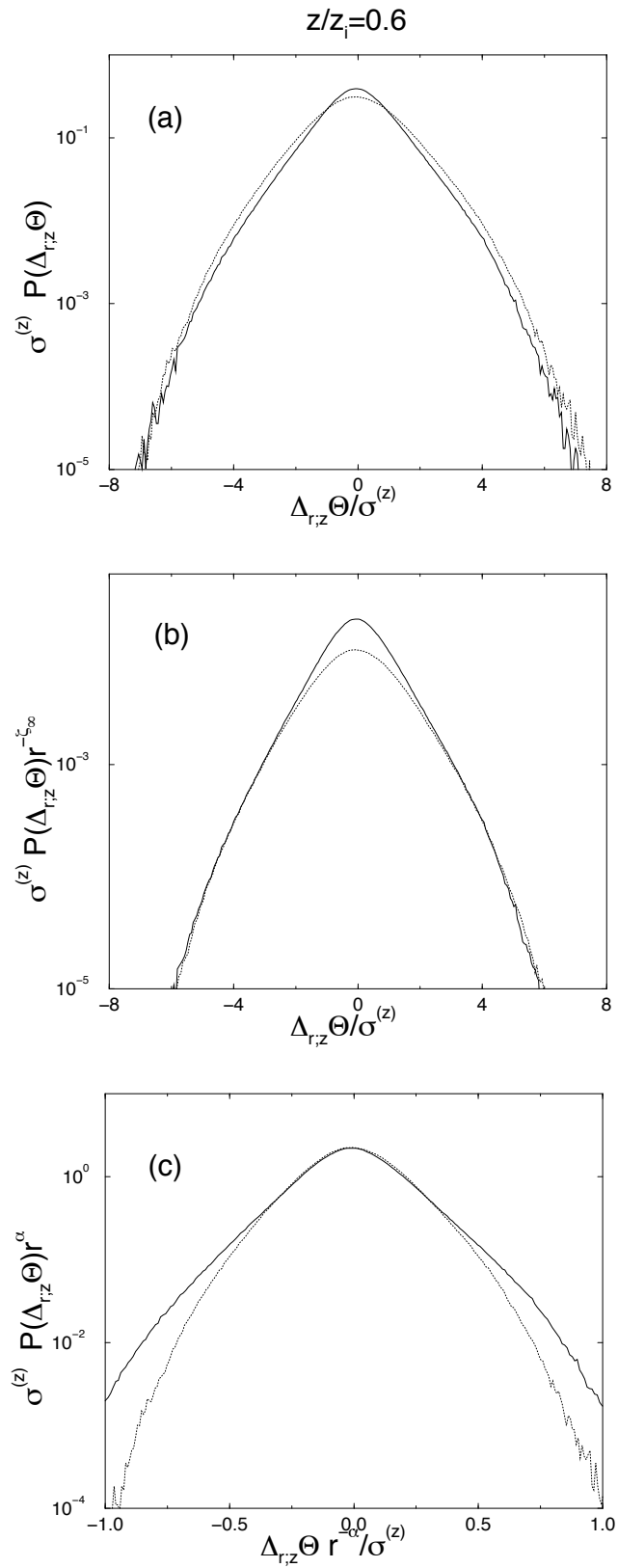


Figure 4.14: As in figure 4.8 but for Sim. SB1 and separation $r/L = 7 \times 10^{-3}$ and $r/L = 3 \times 10^{-3}$.

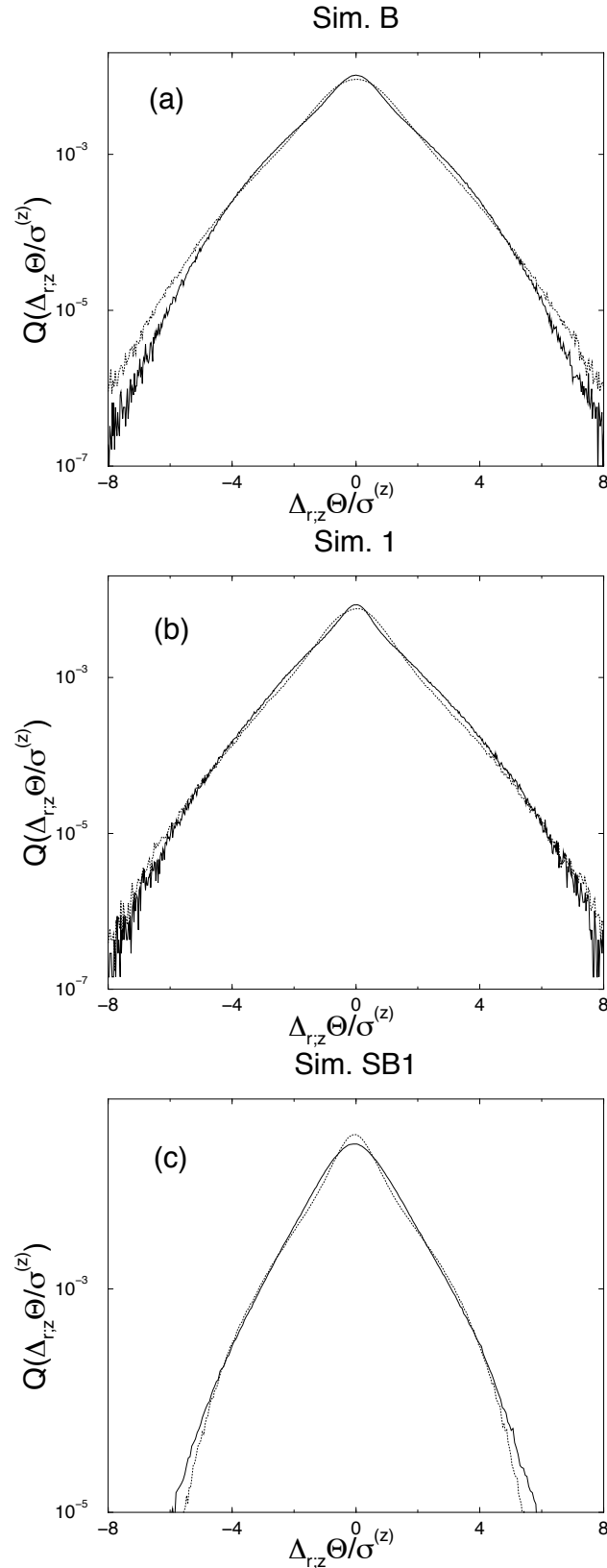


Figure 4.15: The function Q defined in (4.3) are shown, for the three simulations, for two different values of z within the mixed layer: $z/z_i = 0.3$ and $z/z_i = 0.6$. Differences in the shape of these two curves reveal that Q contains a dependence both on the elevation, z , and on the degree of convection.

PDF. Although reported in the figures, the region corresponding to small fluctuations (i.e. the cores) is thus meaningless.

From the inspection of these figures it stems how the dependence on z is practically absent for the most convective simulation (Sim. 1) and more pronounced for the case of weakest convection (Sim. SB1) and in the presence of a relatively small shear (Sim. B). This seems to suggest that the function Q is sensitive to the different degrees of mixing eventually present in different ABL's.

To conclude this section, I note that with the method exploited here to extract the value of ζ_∞ (i.e. via the PDF rescaling) I do not have access to the order of the structure function at which saturation takes place. To have this information, I looked at the structure function scaling exponents and I found evidence of saturation at an order between six and eight. With the present statistics, it turns out very difficult to have insights on the possible dependence on the degree of convection of the order at which saturation occurs.

4.7.2 Dominance of nonmature fronts

In section § 4.3 I addressed the question on the geometrical structure of the fronts responsible for the observed intermittency saturation. As explained in that section, the decomposition of the probability of observing a front in an interval of size r expressed in the form

$$\text{Prob}(\{\text{front}\}) = \text{Prob}(\{\text{front, mature}\}) + \text{Prob}(\{\text{front, nonmature}\})$$

permits to answer the question on whether intermittency saturation is due to steep objects (i.e. mature fronts) or, rather, to fluctuations present on all scales, where the dominant contribution is carried by temperature excursions having just r as a support.

Which of these two options takes place can be perceived from figure 4.16, where the three probabilities are reported (in log-log scale) vs the ratio r/L for the three simulated boundary layers. The fact that the scaling exponent (i.e. the slope inside the scaling region) relative to the total probability and the one relative to the probability of nonmature fronts are approximately the same, is the footprint of dominance of nonmature fronts for the intermittency saturation. Such a conclusion is in agreement with recent experimental results of turbulent convection by Zhou and Xia [93].

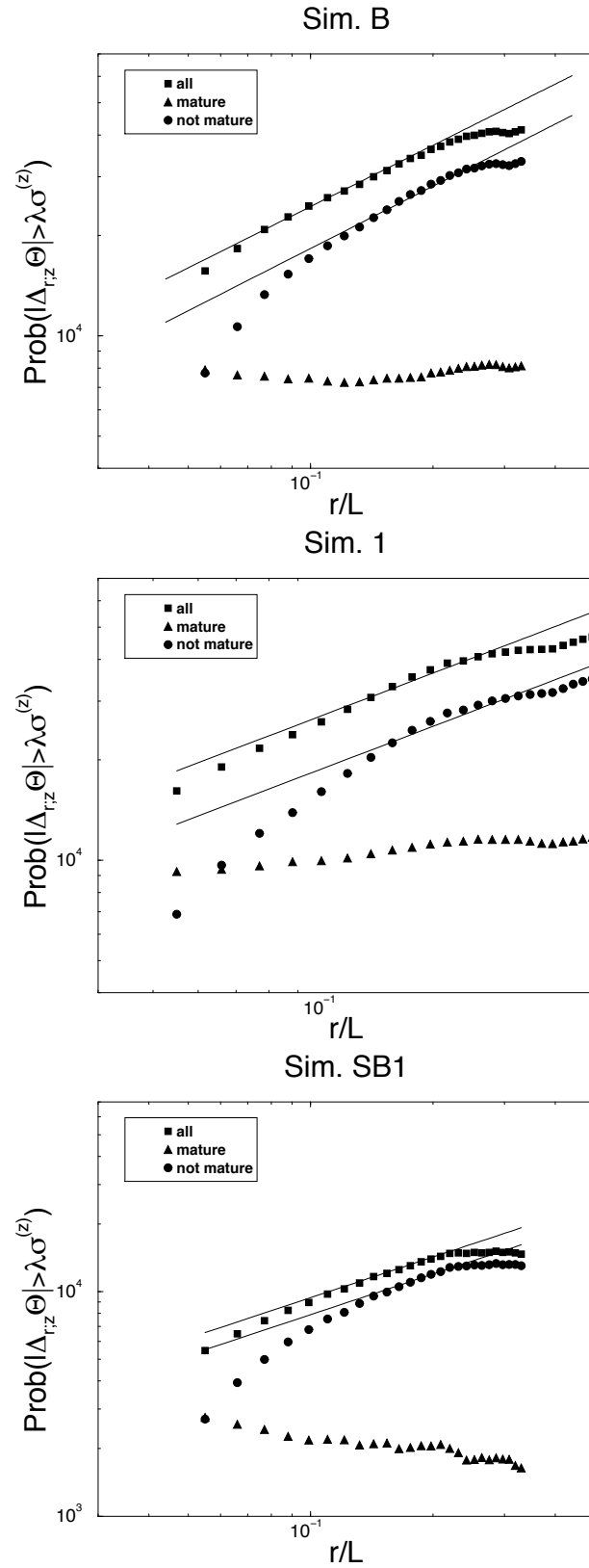


Figure 4.16: For the three analysed simulations, the three cumulative probabilities $\text{Prob}[|\Delta_{r;z}\theta| > \lambda\sigma^{(z)}]$, for $\lambda = 5$, are shown for mature fronts, nonmature fronts and both of them. The two slopes correspond to the exponent $\zeta_\infty \sim 0.6$. Such an exponent is carried by nonmature fronts, mature fronts being clearly subdominant.

4.7.3 Statistics of weak temperature fluctuations

I shall now pass to investigate the statistics of well-mixed regions of the temperature field, corresponding to the inner parts of plumes that are likely to be present in CBL's.

In these regions, fluctuations turn out to be very gentle and, as an immediate consequence, statistics is expected to be characterized by single-scale fluctuations (see section § 4.2). The best candidate for a statistical characterization of weak fluctuations is thus the rescaling form given by (4.2).

To investigate whether or not this is the case, I search for the exponent α (*a priori* dependent on the elevation z within the mixed layer) such that, looking at $r^\alpha P(\Delta_{r;z}\theta)$ vs $\Delta_{r;z}\theta/r^\alpha$ for different values of r , all curves collapse one on the other for each value of z . This would amount to prove the validity of the rescaling law (4.2).

My data turned out to be compatible with such a behaviour. This can be seen for Sim. B in figures 4.6 (c), 4.7 (c) and 4.8 (c); for Sim. 1 in figures 4.9 (c), 4.10 (c) and 4.11 (c); for Sim. SB1 in figures 4.12 (c), 4.13 (c) and 4.14 (c). In all cases, results are relative to three different elevations, z , from the ground, well inside the mixed layer.

The values of α giving the best overlapping of PDF's relative to different separations r turn out to be z -independent and indistinguishable from one simulation to the others. My estimated values is $\alpha \sim 0.2$ with a relative error of about 15%. As for ζ_∞ , such an error bar has been estimated by comparing best fits of Sim. B at the two resolutions 128^3 and 256^3 . Note that the value of α is surprisingly close to the well-known Bolgiano scaling [94]. At the present stage of knowledge, it is not known if this is just a coincidence or a signal of something of physically interesting.

Also note that, similarly to what was observed for ζ_∞ , the exponent α appears weakly dependent on the degree of convection (at least in the range of degrees of convection analysed here) and also seems to characterizes the entire mixed layer.

4.7.4 Characterizing weak temperature excursions

In this section I focus my attention on the geometrical structure of weak scalar excursions which characterize the PDF cores of scalar differences.

As discussed in section § 4.4 the probability of having a weak temperature jump between two points separated by a distance r , can be decomposed in

the form:

$$\begin{aligned} \text{Prob}(\{\text{weak event}\}) &= \text{Prob}(\{\text{weak event, with cancellation}\}) \\ &+ \text{Prob}(\{\text{weak event, without cancellation}\}) . \end{aligned} \quad (4.10)$$

The point is now to understand whether or not there exists a typical separation, r_p , below which

$$\begin{aligned} &\text{Prob}(\{\text{weak event, with cancellation}\}) \\ &< \text{Prob}(\{\text{weak event, without cancellation}\}) . \end{aligned}$$

If this is the case, r_p should provide a measure for the typical horizontal size of the plumes. For $r < r_p$, temperature excursions can be associated to fluctuations occurring in the inner part of the plume, while for $r > r_p$ weak events are formed via successive cancellations of fronts whose support is smaller than r .

In order to answer this question, I computed the three probabilities involved in (4.10) for the three analysed simulations. Results, relative to the elevation $z = z_i/2$, are reported in figure 4.17. A rough estimation of r_p is $r_p \sim L/5$, in qualitative agreement with what one can estimate from the analysis of snapshots of temperature fields at different times (not shown).

4.8 Sensitivity test at higher resolution

In this section I address the question relative to the possible influence of SGS terms on the obtained results. Two different tests might be performed for such a purpose. The first consists in performing simulations with different closure schemes; the second is to increase the resolution and thus to push the effect of SGS parameterizations at smaller and smaller scales. The second option has been chosen, also in view of the fact that with an increased resolution one can control other spurious effects as, e.g., those induced by the used numerical methods.

To be more specific, I repeated Sim. B at the increased resolution 256^3 (I shall refer to it as Sim. B2), maintaining the full set of parameters (geometrical and dynamical) as in Sim. B performed at the resolution 128^3 . On the SP4-IBM SP Power4 platform, the time necessary to advance in time one hour of simulation was around one hour. With the augmented resolution such time became around eight times larger.

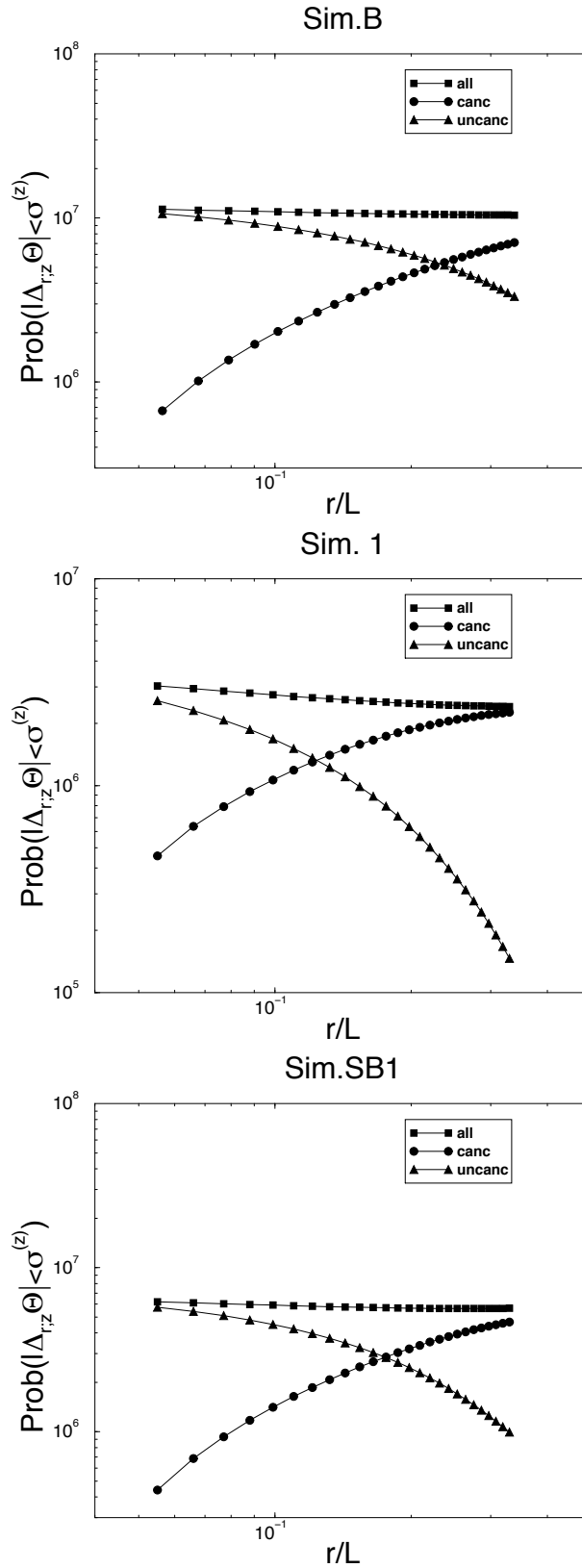


Figure 4.17: For the three analysed simulations, the three cumulated probabilities $\text{Prob}[|\Delta_{r;z}\theta| < \lambda\sigma^{(z)}]$, for $\lambda = 1$, are shown for the weak events with cancellation (canc) and those without cancellation (uncanc). The two curves cross each other for a certain distance, which defines the typical size of the plumes.

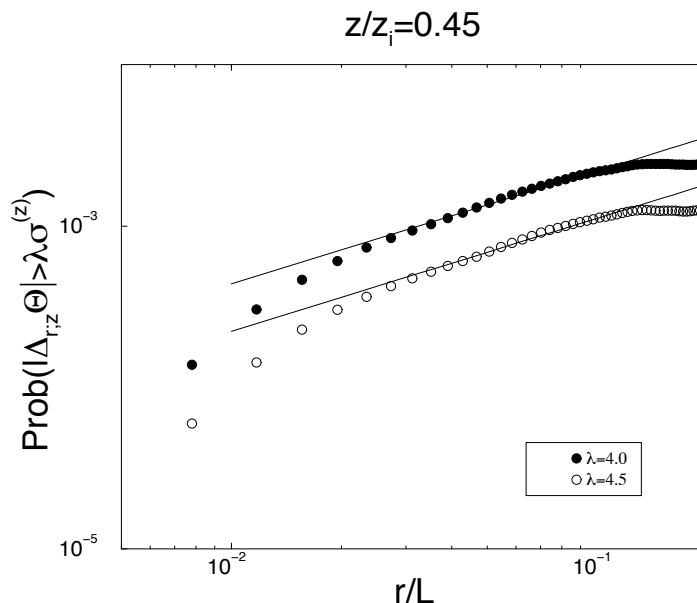
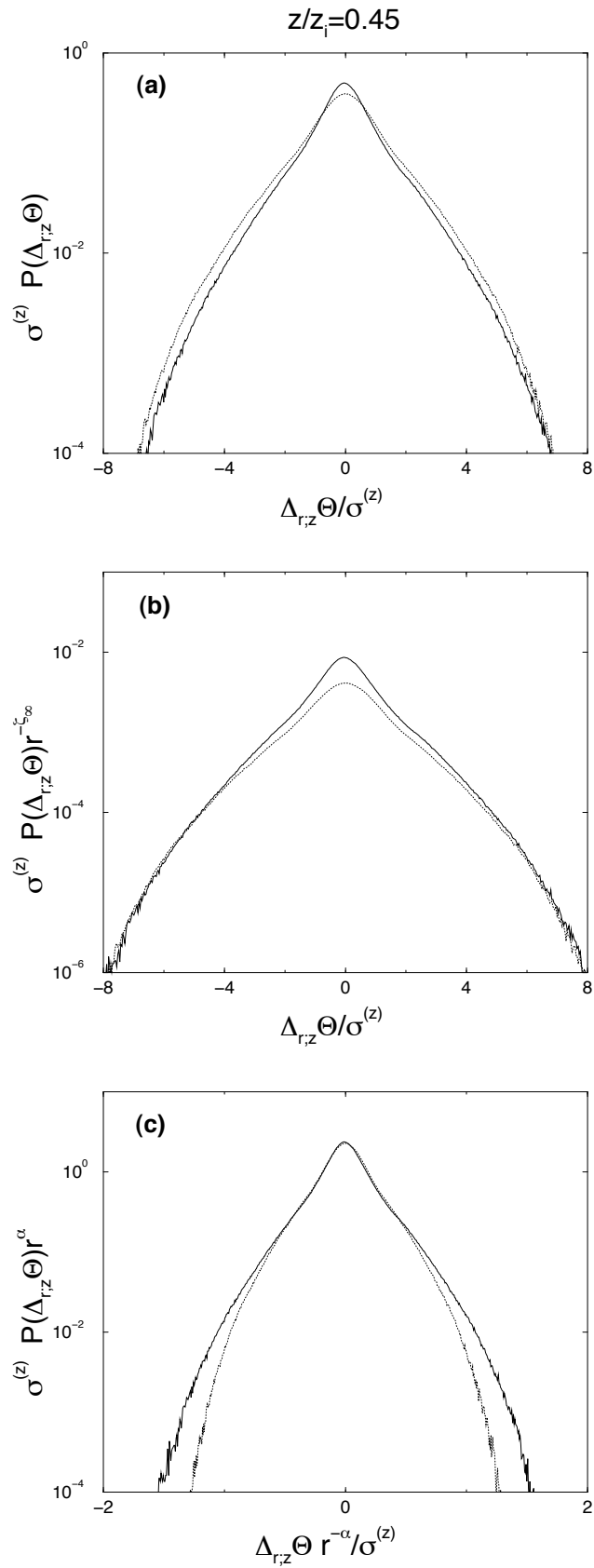


Figure 4.18: For Sim. B simulated at the resolution 256^3 , the cumulative probabilities $\text{Prob}[|\Delta_{r,z}\theta| > \lambda\sigma^{(z)}]$ for two values of λ are shown for $z/z_i = 0.45$. The slopes of these curves (continuous line) are compatible with the exponent $\zeta_\infty \sim 0.6$ measured at the lower resolution (see, for comparison, figure 4.3).

The results are reported in Fig. 4.18 where the cumulative probabilities are shown. As in the corresponding lower-resolution simulations, they present a power-law behaviour which defines the inertial range of scales. The maximum deviation (within the entire mixed layer) of the best-fit exponents with respect to the low resolution simulation, Sim. B, is about 30% of the estimated value $\zeta_\infty \sim 0.6$. Such a variability has been taken as a definition of the error bar on the saturation exponent.

To have a further confirmation of the reliability of the results obtained with the lower resolution 128^3 , in figure 4.19 I show the behaviour of the PDF's for strong and weak fluctuations at the elevations, taken, in way of example, $z = 0.45z_i$. All PDF's in the mixed layer exhibit, for all separations belonging to the inertial range of scales, the same rescaling properties of Sim. B without significant differences in the rescaling exponents.

The exponent $\alpha \sim 0.2$ is measured from such a simulation. The maximum deviation, of about 15% of its value, from the low-resolution simulation Sim. B,

Figure 4.19: As in figure 4.6 but for $z/z_i = 0.45$ and resolution 256^3 .

defines the error bar.

In the above sensitivity test I fixed the geometrical parameters which characterize Sim. B and I increased the resolution. The robustness of these results can be actually argued by means of the following simple considerations.

The first point is that the uncertainties produced in a LES model owing to the SGS terms contaminate the LES fields in regions where small eddies dominate. This happens, e.g., near a wall boundary and in the entrainment zone of the planetary boundary layer. On the contrary, in regions where energy-containing eddies are well-resolved (e.g., within the mixed layer, where the present analysis has been focused), LES fields are known to be weakly dependent on the particular SGS parameterization scheme. Such a dependence becomes even weaker in the case of convective boundary layer, as the one here investigated, where the SGS motion acts as a net energy sink that drains energy from the resolved motion. This is another way to say that energy flows from large scales of motion toward the smallest scales and the cumulative (statistical) effect of the latter can be successfully captured by means of simple eddy-diffusivity/viscosity SGS models.

Moreover, I focused on scales of motion always larger than six/eight grid points, i.e., sufficiently far from the lowest (still resolved) scales that (*a priori*) might be dependent on SGS parameterization schemes. Finally, my conclusions on the dominance of nonmature fronts (i.e. large-scale objects) as the responsible for the intermittency saturation is a further indication of the poor role played by the spatial resolution on these results.

4.9 Conclusions and perspectives

The statistical properties of temperature fluctuations have been analysed in convective boundary layers simulated by means of large-eddy simulations. Three different numerical simulations have been considered, corresponding to different degrees of convection: Sim. 1 is relative to a pure buoyancy-dominated convective regime ($-z_i/L_{MO} = 200$); Sim. B is still relative to a convective regime ($-z_i/L_{MO} = 18$) but it is also affected by a relatively small shear. Finally, Sim. SB1 represents an intermediate case ($-z_i/L_{MO} = 1.5$) between a pure shear and a pure buoyancy-dominated boundary layer.

The main aim of this chapter was to characterize, from a statistical point of view, the fluctuations (weak and strong) of the temperature field within

the mixed layer, where an efficient mixing is guaranteed by the combined action of buoyancy and shear. In this chapter the term “fluctuation” was referred to the occurrence of a temperature jump between points separated by a distance, say, r . The presence of thermal plumes chaotically moving within the CBL makes the strength of such fluctuations strongly sensitive to space and time coordinates. For a fixed instant one thus observes a distribution of values of temperature fluctuations spread over five/six times the RMS of the temperature field. Such a spreading provides a strong justification for the use of probabilistic tools to disentangle the intimate structure of temperature fluctuations within the CBL.

The first point to emphasize is that the PDF’s of such temperature fluctuations are strongly non Gaussian. As is well known, the Gaussian distribution has the remarkable property to be completely determined by its mean and its variance. The latter thus provides a typical, representative, fluctuation of the system. On the contrary, non Gaussian PDF’s need the whole set of moments in order to be completely defined. The latter situation is the one occurring in the analysed CBL’s. From a physical point of view, the lack of Gaussianity means that the concept of typical fluctuation does not apply. In defining a fluctuation, one has to define which part of the PDF is currently being sampled.

The emergence of many (in principle infinite) “typical fluctuations” has important applicative consequences related to the long-standing problem of SGS parameterizations. In constructing the latter schemes utilizing probabilistic approaches, one usually assumes the existence of a unique representative fluctuation as a central hypothesis to extrapolate features of the large-scale, resolved field to small scales. One of the best example is the so-called fractal-interpolation technique [77] which uses the sole fractal dimension as a relevant parameter.

My conclusions strongly suggest to exploit, for the SGS modelling of temperature fields, the so-called multifractal-interpolation schemes recently implemented in [78]. Indeed, my results show that for separations in the inertial range of scales one has:

$$\langle (\Delta_r \theta)^n \rangle = A_n r^{\alpha n} \quad \text{for small } n \quad (4.11)$$

$$\langle (\Delta_r \theta)^n \rangle = B_n r^{\zeta_\infty n} \quad \text{for large } n . \quad (4.12)$$

For both small and large orders (which capture weak and strong fluctuations, respectively) one thus has power-law behaviours with (different) exponents

behaving linearly with the order. Rather than a fractal structure (which should be characterized by a unique power law with an exponent linearly behaving with the order), relations (4.11) and (4.12) suggest the simplest form of multifractality to model small-scale motion: a bifractal structure controlled by the two exponents α and ζ_∞ . The question is now on the dependence of the above parameters on the dynamical characteristics of the ABL. This is a practical need if one uses multifractal interpolations for SGS purposes. Indeed, scaling exponents enter in the multifractal analysis and they might, in principle, depend on dynamical properties of the ABL, as for instance the degree of convection. In the present chapter, I addressed such a question in the context of convective boundary layers, by varying the degree of convection. From $-z_i/L_{MO} = 1.5$ to $-z_i/L_{MO} = 200$, I did not find appreciable variations of scaling exponents, which also turned out to be independent on the elevation from the ground, within the mixed layer. They thus appear intrinsic properties of the CBL. A possible explanation of this property might be sought in the zero-mode mechanism (see [46]) invoked in passive scalar turbulence to explain the observed universality of scaling exponents. Whether or not such mechanism is present also in active scalar turbulence is however one among the many open problems in turbulence research.

Dependence on detailed properties of the CBL and on the elevation are contained in the prefactors A_n and B_n , which are thus nonuniversal. Also this point appears to be compatible with a zero-mode mechanism.

An interesting issue left for future research is on whether the same scenery highlighted here in convective boundary layers is present also in neutrally or stably stratified boundary layers. In that case the LES approach appears to be quite questionable. Laboratory experiments or field experiments seem to be the proper strategy to answer such a question.

Once I identified the statistical role played by ζ_∞ , I addressed the question relative to the connection of such an exponent with thermal plumes. Despite the fact that sharp interfaces are likely to be present, and across such interfaces high temperature fluctuations occur, the dominant contribution to large fluctuations is carried by what I called nonmature fronts, i.e. objects still affected by the steepening process. My conclusion is in agreement with recent experimental results of turbulent convection by Zhou and Xia [93].

The open problem to be addressed is on whether the cliff structures recently observed in the velocity field of a uniformly sheared turbulence [95] are present also in a stable, shear dominated, ABL, and if this is the case,

on whether such structures [95] lead to the intermittency saturation of the velocity field.

As far as the exponent α is concerned, I showed that this is related to the weak fluctuations of the temperature field. Such fluctuations may occur in the inner plume region as well as across the plumes. This amounts to saying that a weak fluctuation between points separated by a certain distance, r , may arise from the cancellation of strong temperature jumps occurring inside r or, alternatively, just because the field is really smooth within the interval of size r . For small r the second possibility is the most frequent. When r is large enough the first scenery dominates. The length r where the change of behaviour occurs furnishes a natural definition for the size of the plume.

Finally, the main conclusions drawn in the present paper has been confirmed by the test case performed at the larger resolution 256^3 .

Part III

Toward the turbulence of complex fluids

Chapter 5

The role of inertia: heavy particles and bubbles

In this last part of the manuscript, I describe some features of the dynamics of complex fluids. Specifically, I focus on advection properties of small particles (massive or polymeric), disregarding their feedback on the flow. In this chapter, inertial-particle motion is studied in the Stokes regime. Exploiting multiscale techniques, the long-time behaviour is shown to be of diffusive type, in the frame of reference moving with the particle mean falling velocity. The latter quantity is then investigated by means of a second-quantization algorithm, which allows to write exact analytical equations at any order in the Stokes (response) time. Such equations have been, and still are, object of numerical simulations, showing that the falling velocity, for a specific flow, is increased by inertial effects for heavy particles.

The chapter is organized as follows: in the introductory section § 5.1 I recall the importance of inertial particles and their main features. In section § 5.2 I introduce multiscale techniques and apply them to the basic equations ruling the dynamics of inertial particles. In section § 5.3 I focus on the equation for the particle density in phase space and I recast it by means of a second-quantization algorithm. In section § 5.4 I show the equations resulting from the application of the aforementioned mathematical techniques to the study of falling velocity. Partial conclusions and, above all, future perspectives follow in section § 5.5.

5.1 Introduction

In most of real situations, tracers suspended in fluids cannot be modelled as simple massless point particles. Both drops in gases and bubbles in liquids, and also solid powders in fluids, have a finite size and their density is, generally speaking, different from the one of the advecting fluid. The description of their movement must then take into account the effects of inertia: this is why such objects are usually called *inertial particles*. Understanding the dynamics of these impurities is very relevant in several domains, ranging from geophysics [96, 97, 98, 99, 100] to astrophysics [101, 102], and from industry to biology [103, 104].

Beside the Eulerian approach used in the previous chapters, I will exploit the Lagrangian description of the particles, which analyses their evolution not in terms of fields but rather by following their trajectories. I will moreover consider dilute solutions of inertial particles of very small size, such that their feedback on the advecting velocity field can be considered negligible. The flow can thus be assumed as fixed, and I will consider both laminar and turbulent situations. For example, the velocity may be assumed steady and periodic in space, or as a Gaussian random field in space and time. Focusing on incompressible flows, a key difference with the study of passive tracers (whose density is equal to the one of the fluid and inertial effects are therefore absent) consists in the dissipative character of the dynamics: now the particle density is not a Lagrangian invariant (i.e., it is not conserved along the trajectories) and clustering effects can take place despite incompressibility. This phenomenon of preferential concentration can be recast, in the presence of gravity, by studying the deviation of falling velocity from its original value, and by analysing how this deviation depends on the flow characteristics and on the space dimension: this will represent the main issue of the present chapter.

It is often the case that the velocity field of interest is active at various length and time scales. Consequently, the equations which govern the particle motion are very hard to analyse directly. In such cases an effective equation which governs the behaviour of the particles at long times and large scales compared to those of the fluid velocity is sought. The derivation of such an effective equation is based on multiscale homogenization techniques [105]. This problem has been studied extensively over the last thirty years for passive tracers. It has been shown that, for periodic or random velocity fields with short range correlations, the particles perform an effective Brownian mo-

tion, whose covariance matrix, the effective diffusivity, has been investigated in its various properties. In particular, it has been proved that the diffusivity is always enhanced, over bare molecular diffusion, for incompressible (i.e. solenoidal) flows and generally depleted for potential (i.e. irrotational) flows [106]. It has also been shown that the presence of inertia usually enhances, or depletes, the diffusivity beyond the corresponding enhancement, or depletion, for the passive tracers [107, 108]. However, strong gravity effects are known to reduce heavy-particle diffusion as compared to fluid particles (i.e. particles which follow streamlines), which generally disperse more efficiently: heavy particles or bubbles [109, 110, 111, 112] have indeed their diffusion reduced by the drift along the gravity direction. Extensions of the above results to the case where the molecular diffusivity is modelled as colored noise have also been analyzed [113].

5.2 Basic equations and multiscale technique

Let me consider a small rigid spherical particle of radius b inside an incompressible flow $\mathbf{v}(\mathbf{x}, t)$, which will be assumed periodic or stationary (in the deterministic sense if laminar, or in the statistical one if turbulent). I shall restrict my attention to the so-called Stokes regime, in which the surrounding flow is differentiable on scales of the order of b (either because turbulence is not present, or because b is much smaller than the turbulent Kolmogorov scale, under which viscosity prevails and smooths the flow) and the mean free path is negligible. Because of the small size of the particle, I will moreover neglect its feedback on the surrounding flow, which is therefore given. The motion of the particle is thus influenced by gravity, buoyancy and viscous drag [114], to which Brownian noise should be added in order to take into account the thermal fluctuations of the fluid. The key difference with passive-scalar transport, i.e. with fluid particles (ruled by a differential equation of the first order in time), is that Newton's law must now be written in its full form as a second-order differential equation for the particle trajectory $\mathbf{X}(t)$:

$$\ddot{\mathbf{X}}(t) - \beta \dot{\mathbf{v}}(\mathbf{X}(t), t) = -\frac{1}{\tau} [\dot{\mathbf{X}}(t) - \mathbf{v}(\mathbf{X}(t), t)] + (1 - \beta) \mathbf{g} + \frac{\sqrt{2\kappa}}{\tau} \boldsymbol{\eta}(t), \quad (5.1)$$

where \mathbf{g} is the gravity acceleration and $\boldsymbol{\eta}(t)$ represents the standard white noise associated to the particle diffusivity κ :

$$\langle \eta_\mu(t) \rangle = 0, \quad \langle \eta_\mu(t) \eta_\nu(t') \rangle = \delta_{\mu\nu} \delta(t - t').$$

Indicating with ρ_p and ρ_f the densities of the particle and of the fluid, respectively, the adimensional coefficient appearing in (5.1) is defined as $\beta \equiv 3\rho_f/(\rho_f + 2\rho_p)$, and the so-called *Stokes time* has also been introduced as $\tau \equiv b^2/3\nu\beta$. According to the ratio between the two densities, β ranges from 0 (when $\rho_f \ll \rho_p$: heavy particles, like drops in gases) to 3 (when $\rho_f \gg \rho_p$: light particles, like bubbles in liquids) and becomes 1 when the two densities are equal (and inertial effects absent). The latter term on the left-hand side of (5.1) represents the so-called “added-mass contribution”, while analysing the right-hand side one deduces that τ constitutes a *response time* of the particle motion to the surrounding flow: when τ , appearing at denominator, is negligible, the same must be for the numerator; in particular, for fluid particles, $\tau = 0$ and $\dot{\mathbf{X}}$ equals \mathbf{v} , immediately adjusting itself to follow any external perturbation and thus reducing (5.1) from a second-order to a first-order differential equation. For finite τ , it is customary to recast (5.1) as a system of two first-order differential equations, but, in order to avoid dealing with the derivative of the fluid velocity ($\dot{\mathbf{v}}$), one often introduces the *covelocity* $\mathbf{U} \equiv \dot{\mathbf{X}} - \beta\mathbf{v}(\mathbf{X}(t), t)$ and obtains:

$$\begin{cases} \dot{\mathbf{X}} = \mathbf{U} + \beta\mathbf{v}(\mathbf{X}(t), t) \\ \dot{\mathbf{U}} = \frac{(1 - \beta)\mathbf{v}(\mathbf{X}(t), t) - \mathbf{U}}{\tau} + (1 - \beta)\mathbf{g} + \frac{\sqrt{2\kappa}}{\tau}\boldsymbol{\eta} . \end{cases} \quad (5.2)$$

The study can be carried on in the corresponding phase space $(\mathbf{x}, \mathbf{u}, t)$. Let me consider the *propagator* $p(\mathbf{x}, \mathbf{u}, t | \mathbf{x}_0, \mathbf{u}_0, 0)$, which satisfies the *forward Kolmogorov equation* deriving from (5.2):

$$\begin{aligned} \frac{\partial}{\partial t} p &= -\mathcal{L}_\beta^* p \\ &\equiv - \left\{ \frac{\partial}{\partial x_\mu} [u_\mu + \beta v_\mu(\mathbf{x}, t)] + \frac{\partial}{\partial u_\mu} \left[\frac{(1 - \beta)v_\mu(\mathbf{x}, t) - u_\mu}{\tau} + (1 - \beta)g_\mu \right] \right. \\ &\quad \left. - \frac{\kappa}{\tau^2} \frac{\partial^2}{\partial u_\mu \partial u_\mu} \right\} p . \end{aligned} \quad (5.3)$$

I now introduce a multiscale expansion [105] for the space and time variables, i.e. I define a set of *slow* variables $\tilde{\mathbf{x}} = \epsilon\mathbf{x}$, $\tilde{t} = \epsilon^2 t$, which are to be considered independent from the corresponding *fast* variables \mathbf{x} and t ; thus, $\partial_{x_\mu} \mapsto \partial_{x_\mu} + \epsilon\partial_{\tilde{x}_\mu}$ and $\partial_t \mapsto \partial_t + \epsilon^2\partial_{\tilde{t}}$. Such a rescaling is meant to catch a diffusive behaviour at timescales much longer than those typical of the flow. Moreover,

the variable \mathbf{u} is considered exclusively fast. Developing also

$$p(\mathbf{x}, \check{\mathbf{x}}, \mathbf{u}, t, \check{t}) = \sum_{m=0}^{\infty} \epsilon^m p_m(\mathbf{x}, \check{\mathbf{x}}, \mathbf{u}, t, \check{t})$$

and substituting in (5.3), the zeroth order reads:

$$\left(\frac{\partial}{\partial t} + \mathcal{L}_\beta^* \right) p_0 = 0 .$$

As the operator \mathcal{L}_β^* only involves fast variables, it is convenient to perform the variable separation $p_0(\mathbf{x}, \check{\mathbf{x}}, \mathbf{u}, t, \check{t}) = \rho(\mathbf{x}, \mathbf{u}, t) P(\check{\mathbf{x}}, \check{t})$, thus obtaining

$$\left(\frac{\partial}{\partial t} + \mathcal{L}_\beta^* \right) \rho = 0 . \quad (5.4)$$

The first order (in ϵ) gives:

$$\left(\frac{\partial}{\partial t} + \mathcal{L}_\beta^* \right) p_1 = - \frac{\partial}{\partial \check{x}_\mu} \{ [u_\mu + \beta v_\mu(\mathbf{x}, t)] p_0 \} . \quad (5.5)$$

One must now impose the solvability condition, by integrating (5.5) over the fast variables:

$$\begin{aligned} & \int dt \frac{1}{\mathcal{T}} \int d\mathbf{x} \int d\mathbf{u} \frac{\partial}{\partial \check{x}_\mu} \{ [u_\mu + \beta v_\mu(\mathbf{x}, t)] p_0 \} = 0 \\ \implies & \frac{\partial}{\partial \check{x}_\mu} P(\check{\mathbf{x}}, \check{t}) \int dt \frac{1}{\mathcal{T}} \int d\mathbf{x} \int d\mathbf{u} [u_\mu + \beta v_\mu(\mathbf{x}, t)] \rho(\mathbf{x}, \mathbf{u}, t) = 0 \\ \implies & \int dt \frac{1}{\mathcal{T}} \int d\mathbf{x} \int d\mathbf{u} \mathbf{v}(\mathbf{x}, t) \rho(\mathbf{x}, \mathbf{u}, t) + (1 - \beta) \mathbf{g} \tau = 0 \end{aligned}$$

where \mathcal{T} represents the period of \mathbf{v} (the temporal integration is not performed if \mathbf{v} is time-independent).

Such a condition is automatically verified by substituting the coordinate \mathbf{u} with $\mathbf{u} - \mathbf{u}^*$, where

$$\mathbf{u}^* = \int dt \frac{1}{\mathcal{T}} \int d\mathbf{x} \int d\mathbf{u} [\mathbf{u} + \beta \mathbf{v}(\mathbf{x}, t)] \rho(\mathbf{x}, \mathbf{u}, t) \quad (5.6)$$

is called *renormalized terminal velocity* and, in general, may be different from the “bare” velocity, $(1 - \beta) \mathbf{g} \tau$, for the quantity:

$$\delta \mathbf{u} \equiv \mathbf{u}^* - (1 - \beta) \mathbf{g} \tau = \int dt \frac{1}{\mathcal{T}} \int d\mathbf{x} \int d\mathbf{u} \mathbf{v}(\mathbf{x}, t) \rho(\mathbf{x}, \mathbf{u}, t) . \quad (5.7)$$

In this frame of reference, one thus has

$$\left(\frac{\partial}{\partial t} + \mathcal{L}_\beta^* \right) p_1 = - [u_\mu + \beta v_\mu(\mathbf{x}, t)] \rho(\mathbf{x}, \mathbf{u}, t) \frac{\partial}{\partial \check{x}_\mu} P(\check{\mathbf{x}}, \check{t}),$$

which simplifies to the so-called *auxiliary equation*

$$\left(\frac{\partial}{\partial t} + \mathcal{L}_\beta^* \right) \chi_\mu(\mathbf{x}, \mathbf{u}, t) = - [u_\mu + \beta v_\mu(\mathbf{x}, t)] \rho(\mathbf{x}, \mathbf{u}, t), \quad (5.8)$$

after another variable separation:

$$p_1(\mathbf{x}, \check{\mathbf{x}}, \mathbf{u}, t, \check{t}) = \chi_\mu(\mathbf{x}, \mathbf{u}, t) \frac{\partial}{\partial \check{x}_\mu} P(\check{\mathbf{x}}, \check{t}).$$

At the second order in ϵ one gets:

$$\left(\frac{\partial}{\partial t} + \mathcal{L}_\beta^* \right) p_2 = - \frac{\partial}{\partial \check{x}_\mu} \{ [u_\mu + \beta v_\mu(\mathbf{x}, t)] p_1 \} - \frac{\partial}{\partial \check{t}} p_0.$$

The corresponding solvability condition reads:

$$\begin{aligned} \frac{\partial}{\partial \check{t}} P(\check{\mathbf{x}}, \check{t}) &= - \int dt \frac{1}{\mathcal{T}} \int d\mathbf{x} \int d\mathbf{u} [u_\mu + \beta v_\mu(\mathbf{x}, t)] \frac{\partial}{\partial \check{x}_\mu} p_1 \\ &= - \int dt \frac{1}{\mathcal{T}} \int d\mathbf{x} \int d\mathbf{u} [u_\mu + \beta v_\mu(\mathbf{x}, t)] \chi_\nu(\mathbf{x}, \mathbf{u}, t) \frac{\partial^2}{\partial \check{x}_\mu \partial \check{x}_\nu} P(\check{\mathbf{x}}, \check{t}). \end{aligned}$$

An effective-diffusion matrix, satisfying

$$\frac{\partial}{\partial \check{t}} P(\check{\mathbf{x}}, \check{t}) = \mathcal{K}_{\mu\nu}^{\text{eff}} \frac{\partial^2}{\partial \check{x}_\mu \partial \check{x}_\nu} P(\check{\mathbf{x}}, \check{t}),$$

thus arises, and is given by

$$\mathcal{K}_{\mu\nu}^{\text{eff}} = - \frac{1}{2} \int dt \frac{1}{\mathcal{T}} \int d\mathbf{x} \int d\mathbf{u} \{ [u_\mu + \beta v_\mu(\mathbf{x}, t)] \chi_\nu(\mathbf{x}, \mathbf{u}, t) + \text{symm.} \}.$$

5.3 Second-quantization algorithm

I shall now focus on the equation (5.4) for the phase-space density $\rho(\mathbf{x}, \mathbf{u}, t)$

$$\begin{aligned} 0 &= \left(\frac{\partial}{\partial t} + \mathcal{L}_\beta^* \right) \rho \\ &= \left\{ \frac{\partial}{\partial t} + \frac{\partial}{\partial x_\mu} [u_\mu + \beta v_\mu(\mathbf{x}, t)] + \frac{\partial}{\partial u_\mu} \left[\frac{(1-\beta)v_\mu(\mathbf{x}) - u_\mu}{\tau} + (1-\beta)g_\mu \right] \right. \\ &\quad \left. - \frac{\kappa}{\tau^2} \frac{\partial^2}{\partial u_\mu \partial u_\mu} \right\} \rho \end{aligned} \quad (5.9)$$

and I introduce the adimensional variable $\mathbf{y} = \sqrt{\tau/2\kappa}\mathbf{u}$. In the space $(\mathbf{x}, \mathbf{y}, t)$, the operator acting on the density in equation (5.9) becomes:

$$\begin{aligned} \left(\frac{\partial}{\partial t} + \mathcal{L}_\beta^* \right) &= \frac{\partial}{\partial t} + \sqrt{\frac{2\kappa}{\tau}} y_\mu \frac{\partial}{\partial x_\mu} + \beta v_\mu(\mathbf{x}, t) \frac{\partial}{\partial x_\mu} + \sqrt{\frac{1}{2\kappa\tau}} (1 - \beta) v_\mu(\mathbf{x}, t) \frac{\partial}{\partial y_\mu} \\ &\quad - \frac{1}{\tau} \frac{\partial}{\partial y_\mu} y_\mu + \sqrt{\frac{\tau}{2\kappa}} (1 - \beta) g_\mu \frac{\partial}{\partial y_\mu} - \frac{1}{2\tau} \frac{\partial^2}{\partial y_\mu \partial y_\mu} \\ &= -\tau^{-1} A_0 + \tau^{-1/2} A_1 + \tau^0 A_2 + \tau^{1/2} A_3 . \end{aligned}$$

The operators A_0 , A_1 , A_2 and A_3 are defined as:

$$\left\{ \begin{array}{l} A_0 = \frac{\partial}{\partial y_\mu} y_\mu + \frac{1}{2} \frac{\partial^2}{\partial y_\mu \partial y_\mu} \\ A_1 = \sqrt{2\kappa} y_\mu \frac{\partial}{\partial x_\mu} + \frac{1}{\sqrt{2\kappa}} (1 - \beta) v_\mu(\mathbf{x}, t) \frac{\partial}{\partial y_\mu} \\ A_2 = \frac{\partial}{\partial t} + \beta v_\mu(\mathbf{x}, t) \frac{\partial}{\partial x_\mu} \\ A_3 = \frac{1}{\sqrt{2\kappa}} (1 - \beta) g_\mu \frac{\partial}{\partial y_\mu} \end{array} \right. .$$

At this point a Hermitian reformulation is convenient. I define $\rho_0(\mathbf{y})$ such that

$$A_0 \rho_0 = 0 \Leftrightarrow \rho_0 = e^{-y^2}$$

and I decompose ρ in

$$\rho(\mathbf{x}, \mathbf{y}, t) = \rho_0^{1/2}(\mathbf{y}) \psi(\mathbf{x}, \mathbf{y}, t) \Leftrightarrow A_0 \rho = -\rho_0^{1/2} K_0 \psi ,$$

where

$$K_0 = \frac{1}{2} \left(y^2 - \frac{\partial^2}{\partial y_\mu \partial y_\mu} - d \right) .$$

A second-quantization algorithm thus spontaneously appears. One can indeed introduce the operators of creation and annihilation

$$a_\mu^\pm = y_\mu \mp \frac{\partial}{\partial y_\mu} ,$$

in terms of which

$$y_\mu = \frac{1}{2} (a_\mu^+ + a_\mu^-) , \quad \frac{\partial}{\partial y_\mu} = \frac{1}{2} (a_\mu^- - a_\mu^+) ,$$

and

$$K_0 = \frac{1}{2}a_\mu^+a_\mu^- = N$$

can be interpreted as the occupation number. The following commutation relations hold:

$$[K_0, a_\mu^\pm] = \pm a_\mu^\pm, \quad [a_\mu^-, a_\nu^+] = 2\delta_{\mu\nu}, \quad [a_\mu^+, a_\nu^+] = 0 = [a_\mu^-, a_\nu^-].$$

One can also analogously rewrite

$$A_1\rho = -\rho_0^{1/2}K_1\psi, \quad A_2\rho = -\rho_0^{1/2}K_2\psi, \quad A_3\rho = -\rho_0^{1/2}K_3\psi,$$

where

$$K_1 = \alpha_\mu a_\mu^+ + \gamma_\mu a_\mu^-, \quad K_2 = -\frac{\partial}{\partial t} - \beta v_\mu(\mathbf{x}, t) \frac{\partial}{\partial x_\mu}, \quad K_3 = \delta_\mu a_\mu^+$$

and

$$\alpha_\mu = \frac{1}{\sqrt{2\kappa}}(1-\beta)v_\mu(\mathbf{x}, t) - \sqrt{\frac{\kappa}{2}} \frac{\partial}{\partial x_\mu}, \quad \gamma_\mu = -\sqrt{\frac{\kappa}{2}} \frac{\partial}{\partial x_\mu}, \quad \delta_\mu = \frac{1}{\sqrt{2\kappa}}(1-\beta)g_\mu.$$

The following step consists in a development at small τ , i.e. I consider particles deviating little from the fluid-particle behaviour. In particular, I write

$$\psi(\mathbf{x}, \mathbf{y}, t) = \sum_{n=0}^{\infty} \tau^{n/2} \psi_n(\mathbf{x}, \mathbf{y}, t)$$

and I study the equation arising at every (integer and half-odd) order in τ :

$$K_0\psi_n = \begin{cases} 0 & \text{for } n = 0 \\ K_1\psi_{n-1} & \text{for } n = 1 \\ K_1\psi_{n-1} + K_2\psi_{n-2} & \text{for } n = 2 \\ K_1\psi_{n-1} + K_2\psi_{n-2} + K_3\psi_{n-3} & \text{for } n \geq 3. \end{cases} \quad (5.10)$$

Such relations can be solved recursively by exploiting the simple inversion formula

$$K_0\Xi = a_{\mu_k}^+ \cdots a_{\mu_1}^+ |0\rangle \Rightarrow \Xi = \frac{1}{k} a_{\mu_k}^+ \cdots a_{\mu_1}^+ |0\rangle,$$

$|0\rangle$ representing the empty state. Therefore, one obtains

$$\psi_n(\mathbf{x}, \mathbf{y}, t) = \psi_n^\emptyset(\mathbf{x}, t)|0\rangle + \psi_n^{\mu_1}(\mathbf{x}, t)a_{\mu_1}^+|0\rangle + \dots + \frac{1}{n!} \psi_n^{\mu_1 \cdots \mu_n}(\mathbf{x}, t)a_{\mu_n}^+ \cdots a_{\mu_1}^+ |0\rangle,$$

where

$$\psi_n^{\mu_1 \dots \mu_k}(\mathbf{x}, t) = \begin{cases} \alpha_{\mu_k} \psi_{n-1}^{\mu_1 \dots \mu_{k-1}} + \frac{2}{k} \langle \gamma_{\mu_{k+1}} \psi_{n-1}^{\mu_1 \dots \mu_{k+1}} \rangle + \delta_{\mu_k} \psi_{n-3}^{\mu_1 \dots \mu_{k-1}} \\ -\frac{1}{k} \left[\frac{\partial}{\partial t} + \beta v_\mu(\mathbf{x}, t) \frac{\partial}{\partial x_\mu} \right] \psi_{n-2}^{\mu_1 \dots \mu_k} & \text{for } k = 1, \dots, n-2 \\ \alpha_{\mu_k} \psi_{n-1}^{\mu_1 \dots \mu_{k-1}} & \text{for } k = n-1, n \end{cases} \quad (5.11)$$

and $\langle \dots \rangle$ implies a symmetrization on the repeated index (i.e. the sum of the possible permutations of the repeated index, divided by the number of such terms). At each step one must also impose the corresponding solvability condition, which forbids the presence of states proportional to $|0\rangle$ on every right-hand side of expressions (5.10), in order to avoid inversion problems. These constraints give:

$$2\gamma_\mu \psi_n^\mu - \left[\frac{\partial}{\partial t} + \beta v_\mu(\mathbf{x}, t) \frac{\partial}{\partial x_\mu} \right] \psi_{n-1}^\emptyset = 0 \quad \forall n \geq 1. \quad (5.12)$$

Together with the normalization condition $\int d\mathbf{x} \psi_n^\emptyset \propto \delta_{n0}$, expressions (5.12) are to be interpreted as equations for the quantities ψ_n^\emptyset , which can be solved recursively (analytically or numerically) once the incompressible flow $\mathbf{v}(\mathbf{x}, t)$ is given. I write hereafter some of these equations, considering only velocity fields possessing odd parity with respect to reflections in the vertical direction. In other words, indicating with $\check{\mathbf{x}}$ the point having the same coordinates of \mathbf{x} except for the vertical one (which is its opposite), I focus on velocities satisfying $\mathbf{g} \cdot \mathbf{v}(\check{\mathbf{x}}, t) = -\mathbf{g} \cdot \mathbf{v}(\mathbf{x}, t)$. Such flows are significant to analyse the particle fall velocity (or, better, its deviation from the bare value $(1 - \beta)\mathbf{g}\tau$) because no mean contribution is present and every (eventual) nonzero result is to be interpreted as due to preferential concentration in areas of rising or falling fluid. Considering the “even” and “odd” parts of the scalar fields ψ_n^\emptyset (i.e. their symmetric and antisymmetric parts for reflections in the vertical direction), here are the first few equations deriving from (5.12):

$$\begin{aligned} \left[\partial_t + v_\mu(\mathbf{x}, t) \frac{\partial}{\partial x_\mu} - \kappa \frac{\partial^2}{\partial x_\mu \partial x_\mu} \right] \psi_0^\emptyset = 0 &\Rightarrow \psi_0^\emptyset = \text{const.} = \left(\int d\mathbf{x} \right)^{-1} \\ \left[\partial_t + v_\mu(\mathbf{x}, t) \frac{\partial}{\partial x_\mu} - \kappa \frac{\partial^2}{\partial x_\mu \partial x_\mu} \right] \psi_1^\emptyset = 0 &\Rightarrow \psi_1^\emptyset = \text{const.} = 0 \end{aligned}$$

$$\begin{aligned}
& \left[\partial_t + v_\mu(\mathbf{x}, t) \frac{\partial}{\partial x_\mu} - \kappa \frac{\partial^2}{\partial x_\mu \partial x_\mu} \right] \psi_2^\emptyset = (1 - \beta)^2 \frac{\partial v_\mu}{\partial x_\nu} \frac{\partial v_\nu}{\partial x_\mu} \psi_0^\emptyset \Rightarrow \psi_2^\emptyset = \psi_2^{\emptyset(\text{even})} \\
& \left[\partial_t + v_\mu(\mathbf{x}, t) \frac{\partial}{\partial x_\mu} - \kappa \frac{\partial^2}{\partial x_\mu \partial x_\mu} \right] \psi_3^\emptyset = (1 - \beta)^2 \frac{\partial v_\mu}{\partial x_\nu} \frac{\partial v_\nu}{\partial x_\mu} \psi_1^\emptyset = 0 \Rightarrow \psi_3^\emptyset = 0 \\
& \left\{ \begin{aligned} & \left[\partial_t + v_\mu(\mathbf{x}, t) \frac{\partial}{\partial x_\mu} - \kappa \frac{\partial^2}{\partial x_\mu \partial x_\mu} \right] \psi_4^{\emptyset(\text{odd})} = -(1 - \beta) g_\mu \frac{\partial}{\partial x_\mu} \psi_2^\emptyset \\ & \left[\partial_t + v_\mu(\mathbf{x}, t) \frac{\partial}{\partial x_\mu} - \kappa \frac{\partial^2}{\partial x_\mu \partial x_\mu} \right] \psi_4^{\emptyset(\text{even})} = \dots \end{aligned} \right. \\
& \left\{ \begin{aligned} & \left[\partial_t + v_\mu(\mathbf{x}, t) \frac{\partial}{\partial x_\mu} - \kappa \frac{\partial^2}{\partial x_\mu \partial x_\mu} \right] \psi_5^{\emptyset(\text{odd})} = -(1 - \beta) g_\mu \frac{\partial}{\partial x_\mu} \psi_3^\emptyset = 0 \\ & \left[\partial_t + v_\mu(\mathbf{x}, t) \frac{\partial}{\partial x_\mu} - \kappa \frac{\partial^2}{\partial x_\mu \partial x_\mu} \right] \psi_5^{\emptyset(\text{even})} = \dots = 0 \\ & \Rightarrow \psi_5^{\emptyset(\text{even})} = \text{const.} = 0 \ \& \ \psi_5^{\emptyset(\text{odd})} = \text{const.} = 0, \Rightarrow \psi_5^\emptyset = 0. \end{aligned} \right. \\
& \left\{ \begin{aligned} & \left[\partial_t + v_\mu(\mathbf{x}, t) \frac{\partial}{\partial x_\mu} - \kappa \frac{\partial^2}{\partial x_\mu \partial x_\mu} \right] \psi_6^{\emptyset(\text{odd})} = \dots \\ & \dots \end{aligned} \right.
\end{aligned}$$

5.4 Equations for the falling velocity

In this section I focus on heavy particles, i.e. $\beta = 0$. The terminal velocity (5.6) is thus given by:

$$\begin{aligned}
u_\mu^* &= \int dt \frac{1}{\mathcal{T}} \int d\mathbf{x} \int d\mathbf{u} u_{\mu\rho}(\mathbf{x}, \mathbf{u}, t) = \sqrt{\frac{2\kappa}{\tau}} \int dt \frac{1}{\mathcal{T}} \int d\mathbf{x} \int d\mathbf{y} y_{\mu\rho}(\mathbf{x}, \mathbf{y}, t) \\
&= \sqrt{\frac{2\kappa}{\tau}} \sum_{n=1}^{\infty} \tau^{n/2} \int dt \frac{1}{\mathcal{T}} \int d\mathbf{x} \psi_n^\mu(\mathbf{x}, t), \tag{5.13}
\end{aligned}$$

where the last equality has been obtained by exploiting the orthogonality relation of Hermite polynomials and shows that, at any order n , the corresponding function $\psi_n(\mathbf{x}, \mathbf{u}, t)$ enters only via its one-index coefficient $\psi_n^\mu(\mathbf{x}, t)$. Analysing the structure of these latter functions (5.11), it is easy to show that the integrals in (5.13) vanish for $n = 1$, for all even orders and for any non-vertical component μ . The first nonzero contribution thus comes from $n = 3$ and gives $\mathbf{u}^* = \mathbf{g}\tau + \mathcal{O}(\tau^2)$, as one would expect. The deviation from the

bare velocity $g\tau$ (5.7) is thus expressed by

$$\delta \mathbf{u} = \sum_{m=0}^{\infty} \tau^{2+m} \int dt \frac{1}{\mathcal{T}} \int d\mathbf{x} \mathbf{v}(\mathbf{x}, t) \psi_{4+2m}^{\theta(\text{odd})}(\mathbf{x}, t),$$

therefore one reduces to compute the spatial integral (and possibly the temporal average) of the odd parts of the even-order functions ψ_n^θ , which satisfy the equations listed at the end of section § 5.3. In particular, the first correction (involving $\psi_4^{\theta(\text{odd})}$) has been computed numerically, by solving the coupled system for ψ_2^θ and $\psi_4^{\theta(\text{odd})}$, for two special situations of stationary, incompressible, cellular flows: the three-dimensional so-called ABC flow [67],

$$\begin{cases} v_1 = A \sin(2\pi x_3) + C \cos(2\pi x_2) \\ v_2 = B \sin(2\pi x_1) + A \cos(2\pi x_3) \\ v_3 = C \sin(2\pi x_2) + B \cos(2\pi x_1), \end{cases}$$

and its two-dimensional restriction (BC flow)

$$\begin{cases} v_1 = C \cos(2\pi x_2) \\ v_2 = B \sin(2\pi x_1). \end{cases}$$

In the former case, I obtained a hint of *increased* falling velocity (with respect to $g\tau$), but this result still has to be verified accurately. However, the same indication arose in the latter case, where it was possible to simulate some low-Péclet-number flows. Specifically, considering the unit-side cubic cell with $B = C = 1$ and $g = 9.8$, I simulated $\kappa = 1$ ($Pe \simeq 1$) and $\kappa = 0.1$ ($Pe \simeq 10$) and I obtained downward deviations from the bare velocity of 0.031 and 15.89, respectively. Some higher-Péclet-number flows were also simulated, showing a further increase in falling velocity, but also such results still have to be verified, because of limited computation power: this prevented the simulation from reaching times long enough to be considered steady states, and from using a spatial resolution sufficient for correctly capturing all oscillations.

5.5 Future work

The results of section § 5.4 provide a hint in the direction of falling-velocity enhancement by inertial effects for heavy particles, but I stress again that more accurate simulations have to be performed with more powerful computers. Moreover, it would be interesting to take into account also the second

correction away from the bare velocity, i.e. the one due to $\psi_6^{\theta(\text{odd})}$. The equation for the latter quantity has already been found (it has not been written here for the sake of simplicity) and it involves both $\psi_4^{\theta(\text{odd})}$ and $\psi_4^{\theta(\text{even})}$ as source terms. A system of four equations should thus be solved, for ψ_2^θ , $\psi_4^{\theta(\text{odd})}$, $\psi_4^{\theta(\text{even})}$ and $\psi_6^{\theta(\text{odd})}$. Such an issue has already been attacked by Lagrangian simulations, and this will constitute future work. An interesting (and unavoidable) extension of the previous results to the opposite situation of very light particles is also in order.

In the second part of this chapter I focused exclusively on the analysis of the falling velocity. However, it was shown, at the end of section § 5.2, that at the following order in ϵ an effective-diffusivity equation holds. Such a subject could represent the object of a future analysis in the same spirit of the one presented here. The starting point, instead of (5.4), would be provided by the auxiliary equation (5.8).

A completely different approach would be needed if, on the contrary, one wanted to investigate the feedback of the particles on the surrounding fluid, thus considering them as active. However, such an issue is not pertinent with the guideline of the present work. Therefore, in the next chapter, I will move to the study of polymers, but, for the sake of continuity, always from a “passive” point of view.

Chapter 6

Polymer relaxation time in FENE model

Polymer stretching in random smooth flows is investigated within the framework of the FENE dumbbell model. The advecting flow is Gaussian and short-correlated in time. The stationary PDF of polymer extension is derived exactly. The characteristic time needed for the system to attain the stationary regime is computed as a function of the Weissenberg number and the maximum length of polymers. The transient relaxation to the stationary regime is predicted to be exceptionally slow in the proximity of the coil-stretch transition.

The chapter is organized as follows: introductory section § 6.1 recalls the main features of polymers. In section § 6.2 I introduce the model and present the main results. The stationary PDF of the elongation and the transient relaxation time are computed in sections § 6.3 and § 6.4, respectively. In the concluding section § 6.5 I discuss the relevance of these analytical results for experiments and numerical simulations.

6.1 Introduction

Polymers are (usually very long) chains of simple molecules, called monomers. Their structure may be very complex, as is the case for the DNA. The ability of polymers to considerably change the large-scale statistics of the advecting flow has important practical applications, drag reduction being one of the most relevant ones [115]. It is known indeed, and actually exploited for industrial purposes (like oil transport in submarine ducts), that adding small quantities of polymers (few parts per million in mass) can reduce the drag up to 80%. Polymers affect the dynamics of the advecting velocity field only if they are highly elongated. Understanding how a single polymer chain is stretched by a random flow is thus the first issue to address in the study of hydrodynamical properties of polymer solutions.

At equilibrium, the radial shape of coiled polymers is spherical due to their entropy. When placed in an inhomogeneous flow, polymers are deformed and stretched by the gradients of the velocity. The product of the longest relaxation time of polymers and the characteristic rate of deformation is called the Weissenberg number Wi . For small Wi , the entropic force prevails and polymers are in the coiled state. When Wi exceeds a critical value, the molecules become highly elongated and their extension sharply increases. This phenomenon is called coil-stretch transition and the critical Weissenberg number is known to be approximately one.

I investigate the statistics of polymer extension in the finite extensible nonlinear elastic (FENE) dumbbell model [116]. Such a model looks appropriate to describe synthetic molecules above all, while biological ones (like DNA) are usually modelled as “worm-like chains” [117]. In FENE, a polymer is described as two beads joined by an elastic spring. This model can be seen as a restriction of the Rouse model, which takes into account several small masses connected by springs: analysing the motion in terms of linear oscillation modes, I substantially focus on the fundamental mode. However, the elastic force diverges as the elongation of polymers attains its maximum value, R_m , and this gives a large-extension cutoff. Consequently, the stationary regime exists however strong the velocity gradients are.

Since attention is directed only to the dynamics of a single molecule, the feedback on the advecting flow is disregarded. It is worth noticing that, in the highly-stretched state, the energy exchange between the flow and the polymer (kinetic and elastic energies, respectively), which is responsible for drag reduction and similar effects, is very strong and can be taken into ac-

count by considering an additional term in the stress tensor appearing in NS equation: this is the domain of *non-Newtonian* (or viscoelastic) fluids, whose study is not among the aims of the present work.

Anyway, no matter how stretched the polymer is, its end-to-end separation is always much smaller than the turbulent Kolmogorov scale (at which viscous and advective effects are comparable), thus a strict analogy with the previous chapter holds, in the sense that the flow is still assumed differentiable on scales typical of the polymer. In particular, to allow analytical progress, the random flow is chosen to have the Batchelor–Kraichnan (BK) statistics. This means that the considered flow is Gaussian, white in time and linear in space. The BK model is a fully-solvable model for passive turbulent transport which can provide useful connections between theory and real behaviours (for a review on the applications to scalar and magnetic fields, see [46]). The results should be intended as a qualitative description of real polymer dynamics. I derive the complete form of the stationary PDF of polymer extension and describe how the statistics of polymer stretching changes with increasing velocity gradients. Concerning the statistics at finite times, I compute the typical time needed for the system to reach the steady state and predict how this depends on the maximum length of polymers and on the stretching by the flow. My analysis shows that the coil-stretch transition of polymers is characterized by an anomalous dynamics in time.

The coil-stretch transition was predicted in 1974 for shear and hyperbolic flows [118] and has been widely studied experimentally for such flows [119, 120, 121, 122]. In contrast, the experimental study of polymer dynamics in random flows is a very recent achievement. This is due to the difficulty in generating a flow that is random at scales comparable with the size of polymers (about $100\ \mu\text{m}$). This difficulty can be overcome thanks to the elastic turbulence discovered by Groisman and Steinberg [123]; the flow of a highly elastic polymer solution at low Reynolds numbers, but large Wi , has all the main properties of fully-developed turbulence. Therefore, in solutions of sufficiently elastic polymers it is possible to excite turbulent motion in exceedingly small volumes. Exploiting elastic turbulence in polymer solutions, the stretching and the deformation of a single DNA molecule in a three-dimensional random flow was thus investigated [124].

Theoretical studies concerning the coil-stretch transition in random flows focused mainly on the Hookean dumbbell model [125, 126, 127]. This model is suitable only for the coiled state ($Wi < 1$), since the linear force, in principle, allows infinite extensions and for large Wi polymers can become more

and more elongated under the action of velocity gradients. For $Wi \geq 1$ a stationary PDF of the extension no longer exists and this behaviour was conjectured to coincide with the coil-stretch transition. To overcome this oversimplification, the maximum length of polymers must be taken into account. One possibility is to replace the Hookean force by a nonlinear elastic force. The large-value tail of the stationary PDF of the extension, for a general inharmonic force, was obtained by Chertkov [125]; such an approximate analysis was subsequently applied by Thiffeault to the FENE model [128]. Here I exactly derive the complete statistics of polymer stretching within the context of the FENE dumbbell model at general Wi .

Concerning the statistics at finite times, preliminary results were obtained for the Hookean model in [127]. There, the relaxation time to the stationary regime could be defined only in the coiled state, so the behaviour of the relaxation time for very small Wi was derived and a divergence for $Wi = 1$ was observed; this suggested a critical behaviour close to the coil-stretch transition. I present the first prediction of the complete dependence of the transient relaxation time on Wi and R_m with the more realistic FENE model.

6.2 Coil-stretch transition

In elastic dumbbell models a polymer is described as two beads connected by a spring. The beads represent the ends of the molecule and their separation is a measure of the extension. The beads experience: (a) a hydrodynamic drag force modelled by the Stokes law; (b) a Brownian force due to thermal fluctuations of the fluid; (c) an elastic force due to the spring connecting one bead to the other. I consider two-dimensional and three-dimensional flows indifferently, the dimension of the flow being denoted by d . Since in physical applications the elongation of polymers is always smaller than the viscous scale of the flow, the dumbbell is assumed to move in a linear velocity field $\mathbf{v}(\mathbf{r}, t) = \mathbf{v}_0(t) + \mathbf{r} \cdot \boldsymbol{\partial}\mathbf{v}(t)$. Inertial effects and hydrodynamic interactions between the beads are neglected. Consequently, the separation vector between the beads, \mathbf{R} , evolves according to the stochastic differential equation [116]

$$d\mathbf{R} = (\mathbf{R} \cdot \boldsymbol{\partial}\mathbf{v})dt - \frac{\mathbf{F}(\mathbf{R})}{\tau}dt + \sqrt{\frac{2R_0^2}{\tau}}d\mathbf{W}, \quad (6.1)$$

where R_0 is the equilibrium length of the polymer, τ is its relaxation time in the absence of flow, and \mathbf{W} is a d -dimensional Brownian motion which accounts for thermal noise. In the FENE dumbbell model, the elastic force $\mathbf{F}(\mathbf{R})$ takes the form $\mathbf{F}(\mathbf{R}) = \mathbf{R}/(1 - R^2/R_m^2)$, where R_m denotes the maximum extension of the molecule. In physical applications the ratio R_m/R_0 usually lies between 10 and 100 [116]. The length of the vector \mathbf{R} is a measure of the extension of the polymer.

Within the Kraichnan model [36, 37], I recall that $\mathbf{v}(\mathbf{x}, t)$ is a statistically stationary, homogeneous and isotropic Gaussian field with zero mean and second-order correlation

$$\langle v_\mu(\mathbf{x}, t)v_\nu(\mathbf{x} + \mathbf{r}, t') \rangle = \delta(t - t')D_{\mu\nu}^{(v)}(\mathbf{r}) .$$

In the so-called Batchelor regime, the flow is assumed to be smooth in space. If one further imposes incompressibility, the tensor $D_{\mu\nu}^{(v)}(\mathbf{r})$ must take the form [56]

$$D_{\mu\nu}^{(v)}(\mathbf{r}) = D_0\delta_{\mu\nu} - D_1r^2 \left[(d+1)\delta_{\mu\nu} - 2\frac{r_\mu r_\nu}{r^2} \right] .$$

In random flows the Weissenberg number can be defined as $Wi = \lambda\tau$, where λ is the maximum Lyapunov exponent of the flow, that is the average logarithmic growth rate of nearby fluid particle separations. The maximum Lyapunov exponent of the BK flow has asymptotically a Gaussian PDF with mean value $\lambda = d(d-1)D_1$ and variance $\Delta = 2\lambda/d$ [129].

6.2.1 Stationary regime

The statistics of polymer elongation is described by the PDF of the norm of \mathbf{R} averaged over velocity realizations¹: $\mathcal{P}(R, t) = \int d\Phi \langle P(\mathbf{R}, t) \rangle R^{d-1}$, where $d\Phi$ denotes integration over angular variables. When the flow \mathbf{v} has the BK statistics, $\mathcal{P}(R, t)$ obeys a one-dimensional Fokker–Planck (FP) equation with nontrivial drift and diffusion coefficients (see section § 6.3). Under reflecting boundary conditions (the probability does not flow outside the domain of definition) the system reaches a steady state for all Wi : this should be contrasted with the Hookean model, where the stationary regime does not exist for $Wi \geq 1$ [125, 126, 128, 127]. The stationary PDF of the

¹Because of the statistical homogeneity of \mathbf{v} , the average PDF of the elongation does not depend on the point of application of the vector \mathbf{R} .

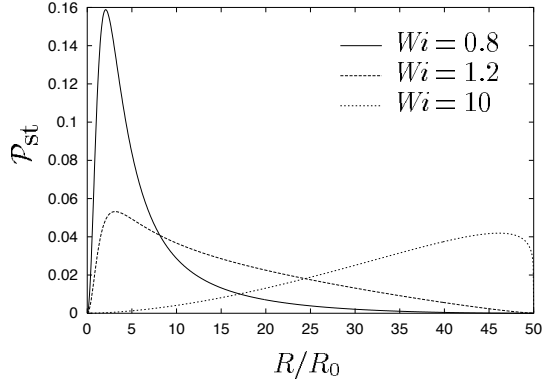


Figure 6.1: Stationary PDF of polymer elongation for the three-dimensional FENE model at different Weissenberg numbers Wi ($R_m/R_0 = 50$).

elongation, $\mathcal{P}_{\text{st}}(R) = \lim_{t \rightarrow \infty} \mathcal{P}(R, t)$, has the form (see section § 6.3)

$$\mathcal{P}_{\text{st}}(R) = NR^{d-1} \left(1 + \frac{Wi R^2}{d R_0^2}\right)^{-h} \left(1 - \frac{R^2}{R_m^2}\right)^h \quad 0 \leq R \leq R_m, \quad (6.2)$$

where $h = [2(R_0^2/R_m^2 + Wi/d)]^{-1}$ and N is the normalization coefficient (see equation (6.8) below). The stationary PDF is shown in figure 6.1 for different Wi . For elongations small if compared to the equilibrium length, $\mathcal{P}_{\text{st}}(R)$ scales as R^{d-1} ; this result holds for a general elastic force since the left tail of \mathcal{P}_{st} comes from the events where the elastic force dominates and equation (6.1) reduces to a d -dimensional Langevin equation (for physically meaningful elastic interactions $\mathbf{F}(\mathbf{R})$ should scale as \mathbf{R} for $R \rightarrow 0$). For intermediate extensions, $R_0 \ll R \ll R_m$, the stationary PDF is proportional to the power law R^{d-1-2h} in accordance with the prediction of [126]. For large elongations, $\mathcal{P}_{\text{st}}(R)$ scales as $(R_m^2 - R^2)^h$ and vanishes for $R = R_m$. In practical applications, $R_0/R_m \ll 1$, the exponent h is approximatively $d/(2Wi)$, as predicted in [128]. Obviously, when $R_m \rightarrow \infty$ and $Wi < 1$, $\mathcal{P}_{\text{st}}(R)$ tends to the stationary solution of the Hookean model [127].

The maximum of the PDF, R_* , determines the fraction of polymers which are highly stretched. The graph of R_* as a function of Wi is shown in figure 6.2. When Wi is smaller than one, R_* is of the order of R_0 and most of polymers have the coiled equilibrium configuration. With increasing Wi the most probable elongation R_* grows slowly until Wi exceeds $d/(d-1)$. Then, a sharp transition occurs to a strongly elongated state. This can

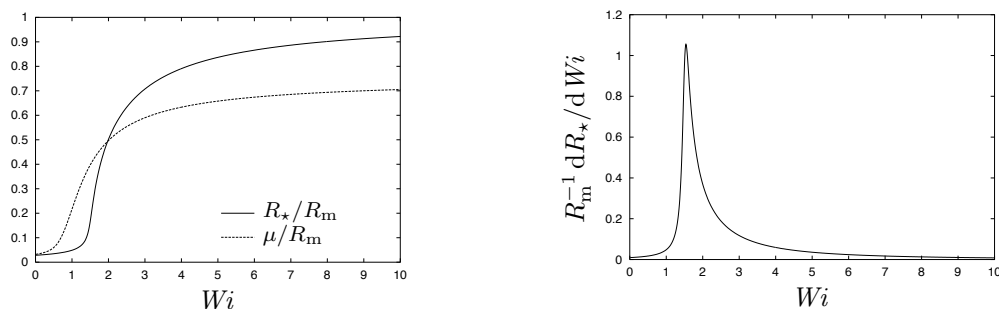


Figure 6.2: Left: most probable rescaled elongation R_*/R_m and average rescaled extension μ/R_m as functions of the Weissenberg number Wi ($d = 3$, $R_m = 50$, $R_0 = 1$). Right: first derivative of R_*/R_m with respect to Wi .

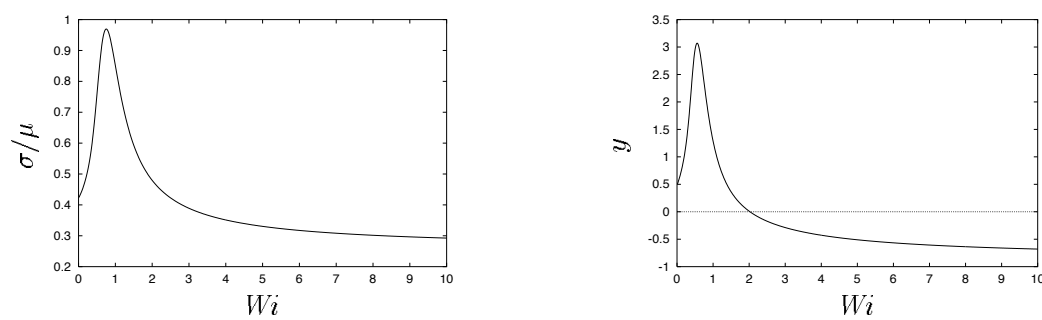


Figure 6.3: Left: normalized root mean square σ/μ as a function of the Weissenberg number Wi ($d = 3$, $R_m = 50$, $R_0 = 1$). Right: skewness y vs Wi for the same values of the parameters.

be appreciated from the behaviour of the first-order derivative of R_* as a function of Wi (figure 6.2). As Wi becomes very large, R_* approaches R_m . The same analysis holds for the average extension μ , apart from the fact that it starts increasing for a smaller Wi and its limiting value is $(3/4)R_m$ (see figure 6.2). It is worth noticing that the coil-stretch transition becomes sharper and sharper with increasing R_m (not plotted).

The normalized RMS value of the extension, σ/μ , with $\sigma^2 = \int dR (R - \mu)^2 \mathcal{P}_{st}(R)$, is represented in figure 6.3. It increases at low Wi until it reaches a maximum value; then σ is compensated by the sharp increase in μ and at large Wi the rescaled RMS eventually relaxes to the constant value $1/\sqrt{15}$.

The skewness $y = [\int dR (R - \mu)^3 \mathcal{P}_{st}(R)]/\sigma^3$ is positive for small Wi and becomes negative at large Wi (figure 6.3) accordingly with the qualitative

behaviour of the stationary PDF (figure 6.1). The maximum of skewness in the neighbourhood of the coil-stretch transition can be easily understood as follows. At low Wi the PDF is peaked at R_0 and the skewness is positive. With increasing Wi the right tail starts raising, but μ is still of the order of R_0 : the skewness, therefore, increases and achieves its maximum value. Beyond the coil-stretch transition, μ starts moving towards the maximum extension and the skewness decreases until it becomes negative at large Wi , that is when the PDF has a long left tail. The limiting value of y for $Wi \rightarrow \infty$ is $-(2/3)\sqrt{5/3}$.

6.2.2 Relaxation to the stationary regime

I now turn to the time dependence of the PDF of the elongation. Starting from an initial condition peaked at R_0 , the system relaxes to the stationary regime described by (6.2). The time needed to reach the stationary regime, T , is solution of a transcendental equation which involves continued fractions (see section § 6.4).

For small Weissenberg numbers, $0 \leq Wi \lesssim d/(d+4)$, the transient relaxation time T behaves according to the prediction of the linear model [127]:

$$T/\tau = (1/2)[1 - Wi(d+2)/d]^{-1}, \quad (6.3)$$

independently of R_m (see inset in figure 6.4). In the proximity of the coil-stretch transition T displays a maximum as a function of the Wi . The relaxation is exceptionally slow in this range of Wi because the stationary regime results from the competition between the coiled state and the highly-stretched state. The position and the value of the maximum relaxation time, T_m , depend on the cutoff R_m (figure 6.4). As the maximum allowed extension of polymers increases, T_m is closer and closer to $Wi = 1$ and grows; at large R_m , the FENE model should indeed match the Hookean model, where T diverges as Wi tends to one [127].

For very large Weissenberg numbers, the stretching time is small, if compared to τ , and the molecules are expected to rapidly reach the highly stretched configuration. Hence, T vanishes as Wi tends to infinity. A numerical fit shows that T scales as Wi^{-1} at large Wi .

In the next sections I explicitly derive (6.2) and the equation for T .

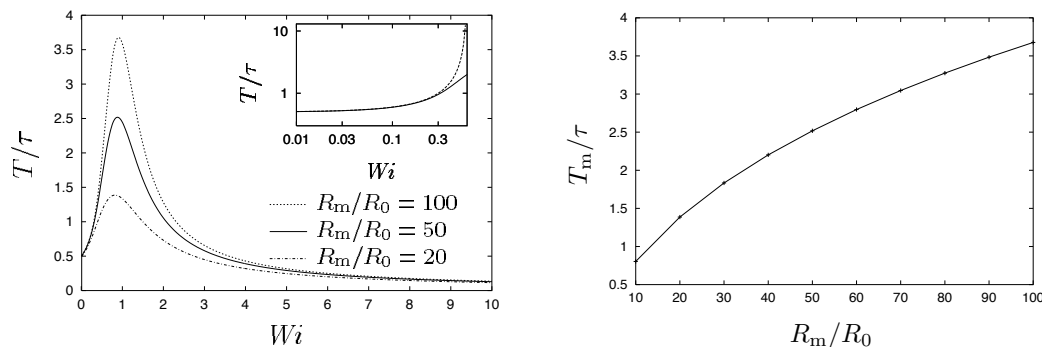


Figure 6.4: Left: rescaled time of relaxation to the stationary regime, T/τ , as a function of the Weissenberg number Wi for three different values of R_m/R_0 ($d = 3$). The inset shows the linear-model approximation given by equation (6.3) (dashed line) for $R_m/R_0 = 50$: the agreement is good up to $d/(d+4) \simeq 0.4$. Right: dependence of the maximum rescaled relaxation time T_m/τ on the maximum relative extension of polymers R_m/R_0 .

6.3 Fokker–Planck equation

For a fixed realization of the velocity field, the PDF of the end-to-end vector, $P(\mathbf{R}, t)$, satisfies the FP equation associated with (6.1) [74]:

$$\partial_t P + \partial \cdot \left[\left(\mathbf{R} \cdot \partial \mathbf{v} - \frac{\mathbf{F}(\mathbf{R})}{\tau} \right) P \right] = \frac{R_0^2}{\tau} \partial^2 P. \quad (6.4)$$

To obtain an equation for $\mathcal{P}(R, t)$, one has to average the above equation over the velocity realizations and to integrate the result over angular variables. The terms of the type $\langle v_i P \rangle$, in general, do not lead to a closed form for the mean PDF and a closed equation cannot be deduced from ((6.4)). The Gaussianity and the δ -correlation in time of the BK model provide an exact closure. Exploiting FND's formula [130], one obtains: $\langle (\partial_\mu v_\nu) P \rangle = C_{\mu\nu\kappa\lambda} \partial_{R_\lambda} [R_\kappa \langle P \rangle]$, with $C_{\mu\nu\kappa\lambda} = D_1 [(d+1)\delta_{\mu\kappa}\delta_{\nu\lambda} - \delta_{\mu\nu}\delta_{\kappa\lambda} - \delta_{\mu\lambda}\delta_{\nu\kappa}]$. One can thus derive, from (6.4), a one-dimensional FP equation for $\mathcal{P}(R, t)$:

$$\partial_s \mathcal{P}(R, s) = -\partial_R [A(R) \mathcal{P}(R, s)] + \partial_R^2 [B(R) \mathcal{P}(R, s)], \quad (6.5)$$

where time has been rescaled with τ , $s = t/\tau$, and the drift and diffusion coefficients have the form

$$A(R) = \frac{(d+1)Wi}{d} R - F(R) + (d-1) \frac{R_0^2}{R}, \quad B(R) = \frac{Wi}{d} R^2 + R_0^2. \quad (6.6)$$

The coefficients A and B are time independent, due to the stationarity of the advecting flow. If R_0 is set to zero, then equation (6.5) reduces to the approximate equation for the large-value tail of the PDF derived by Chertkov [125].

To solve (6.5), reflecting boundary conditions must be imposed, which amounts to saying that the probability current associated with the solution, $J(R, s) = A(R)\mathcal{P}(R, s) - \partial_R[B(R)\mathcal{P}(R, s)]$, vanishes in $R = 0$ and $R = R_m$ for all $s \geq 0$. This means that there is no flow of probability through the boundaries of the domain. Under these conditions the stationary PDF of the elongation takes the form [74]

$$\mathcal{P}_{\text{st}}(R) = \frac{C}{B(R)} e^{\int_{R_1}^R dx A(x)/B(x)}, \quad (6.7)$$

where the constant C and the lower integration limit R_1 are fixed by the normalization condition. The above formula holds for a general elastic force of the form $\mathbf{F}(\mathbf{R}) = f(R)\mathbf{R}$. Replacing the force of the FENE model into (6.7), one thus obtains (6.2) with

$$N = \frac{2\Gamma(d/2 + h + 1)}{R_m^d \Gamma(d/2)\Gamma(h + 1) {}_2F_1(d/2, h; d/2 + h + 1; -WiR_m^2/dR_0^2)}. \quad (6.8)$$

6.4 Relaxation time

The time-dependent solution of the FP (6.5) can be obtained by separation of variables [74]. In other words, $\mathcal{P}(R, s)$ can be sought in the form

$$\mathcal{P}(R, s) = \mathcal{P}_{\text{st}}(R) + \sum_{k=1}^{\infty} c_k e^{-\mu_k s} p_k(R), \quad (6.9)$$

where the coefficients c_k are fixed by the initial condition $\mathcal{P}(R, 0)$ and μ_k , $p_k(R)$ are respectively the eigenvalues and the eigenfunctions of the ordinary differential equation

$$\frac{d^2}{dR^2}[B(R)p_k(R)] - \frac{d}{dR}[A(R)p_k(R)] + \mu_k p_k(R) = 0 \quad (6.10)$$

(without sum over k). The above equation should be solved with reflecting boundary conditions: $J_k(0) = \lim_{R \rightarrow R_m} J_k(R) = 0$, J_k being the probability current associated with the eigenfunction p_k . It can be shown that the

eigenvalues μ_k are real and non-negative, $\mathcal{P}_{\text{st}}(R)$ belonging to the eigenvalue $\mu_0 = 0$ [74]. As it will be seen, the eigenvalues form a countable set and may be arranged in ascending order: $0 < \mu_1 < \mu_2 < \dots$. The reciprocal of μ_1 , therefore, is the time of relaxation to the stationary regime rescaled by τ .

Equation (6.10) is a second-order linear differential equation with four regular singularities in the complex plane. By the change of dependent and independent variables $z = (R/R_m)^2$, $p_k(z) = z^{(d-1)/2}(1-z)^h w_k(z)$, this equation can be transformed into a standard Heun equation for the function $w_k(z)$ [131]:

$$\frac{d^2 w_k}{dz^2} + \left(\frac{\gamma}{z} + \frac{\delta}{z-1} + \frac{\epsilon}{z-a} \right) \frac{dw_k}{dz} + \frac{\alpha\beta z - q}{z(z-1)(z-a)} w_k = 0, \quad (6.11)$$

where

$$\begin{aligned} a &= -\frac{d}{Wi} \frac{R_0^2}{R_m^2}, & q &= \frac{d}{2} \left(h + \frac{\mu_k}{2Wi} \right) \\ \alpha &= h + \frac{d}{4} - \frac{1}{4} \sqrt{d \left(d - \frac{4\mu_k}{Wi} \right)}, & \beta &= h + \frac{d}{4} + \frac{1}{4} \sqrt{d \left(d - \frac{4\mu_k}{Wi} \right)} \\ \gamma &= \frac{d}{2}, & \delta &= h, & \epsilon &= 1 + h, \end{aligned}$$

with $h = [2(R_0^2/R_m^2 + Wi/d)]^{-1}$. Reflecting boundary conditions for p_k map into the following limiting conditions for w_k :

$$\lim_{z \rightarrow 0} z^{\gamma-1} w_k(z) = 0, \quad \lim_{z \rightarrow 1} (1-z)^{\delta-1} w_k(z) = 0. \quad (6.12)$$

The Heun equation is the general Fuchsian equation with four singularities. In the standard form (6.11), the singular points are 0, 1, a and ∞ . Let z_0 be a generic singularity of (6.11). From the theory of Fuchsian equations, the local behaviour of $w_k(z)$ near z_0 is specified by the characteristic exponents ρ_1 and ρ_2 associated with z_0 [132]. If $\rho_1 - \rho_2$ is not integer, in a neighbourhood of z_0 (which excludes the nearest other singularity) $w_k(z)$ can be written in the form $b_1(z-z_0)^{\rho_1} \Psi(z-z_0) + b_2(z-z_0)^{\rho_2} \psi(z-z_0)$, where b_1, b_2 are constant and Ψ, ψ are analytic functions such that $\Psi(z_0) \neq 0 \neq \psi(z_0)$. If $\rho_1 - \rho_2$ is integer and $\rho_1 \geq \rho_2$, the function ψ can be no longer analytic in z_0 and involve the function $\log(z-z_0)$.

The singularity $z = 0$ has characteristic exponents 0 and $1 - \gamma$; the singularity $z = 1$ has characteristic exponents 0 and $1 - \delta$. In physical applications,

one can exclude the situation where δ is integer. On the contrary, $1 - \gamma$ is zero when $d = 2$.

Consider first the case $d = 3$, where there are not logarithmic singularities in $z = 0$. To fulfill conditions (6.12), w_k must be simultaneously a local solution about $z = 0$ and $z = 1$, in both cases belonging to the exponent 0. Such a solution is called a Heun function of class I relative to the points 0 and 1, and exists only for a countable set of values of q and hence of μ_k [131]. The condition for the aforementioned Heun function to exist leads to a transcendental equation for the eigenvalues μ_k [133]:

$$L_0 - \frac{M_0 K_1}{L_1 - \frac{M_1 K_2}{L_2 - \dots}} = 0, \quad (6.13)$$

where

$$K_i = \frac{(i + \alpha - 1)(i + \beta - 1)(i + \gamma - 1)(i + \omega - 1)}{(2i + \omega - 1)(2i + \omega - 2)},$$

$$L_i = q + a\varpi - \frac{\epsilon\varpi(\gamma - \delta) + [\varpi + \alpha\beta][2\varpi + \gamma(\omega - 1)]}{(2i + \omega - 1)(2i + \omega + 1)},$$

$$M_i = \frac{(i + 1)(i + \omega - \alpha + 1)(i + \omega - \beta + 1)(i + \delta)}{(2i + \omega + 1)(2i + \omega + 2)},$$

with $\omega = \gamma + \delta - 1$ and $\varpi = i(i + \omega)$. The rescaled relaxation time T/τ is then the reciprocal of the lowest non-zero solution of (6.13). In the case $d = 2$ the conclusions are unchanged since the solution involving a logarithm in the neighbourhood of $z = 0$ should be discarded.

I solved (6.13) numerically: the continued fraction was computed by the modified Lentz method and the first non-zero solution was evaluated by the “root false position” method (better known as *regula falsi*) [134].

6.5 Summary and discussion

The goal of this chapter was to investigate polymer stretching in a turbulent flow within the context of a fully-solvable model. The statistical features of the BK flow allow one to derive the complete form of the stationary PDF of polymer elongation for a general elastic force. When specializing to finitely extensible polymers, I recover the main properties of polymer dynamics in

real turbulent flows and compute the time of relaxation to the stationary regime.

It should be noted that the velocity field considered here is statistically isotropic. Together with the δ -correlation in time, this is a key assumption in order to derive a fully-analytical solution of the problem. In the experimental setup of [124] the elastic turbulent flow is superimposed to a mean shear flow. The long-time statistics of polymer extension in the presence of a mean shear has been recently considered [135, 136, 137, 138].

The main result of my study is the behaviour of the relaxation time to the steady state as a function of Wi . The transient relaxation time is an increasing function of Wi at low Wi , is maximum close to the coil-stretch transition and eventually tends to zero with increasing Wi . Knowing the dependence of the transient time on Wi is relevant both for numerical simulations and experiments. For example, in the former case, the time required for uncorrelated polymer chains that are suddenly exposed to the same flow to correlate is (implicitly) related to the sharpness of stress gradients one can expect in the flow. Hence, the prediction of the transient time in my study is useful to estimate the required grid spacing to fully resolve those gradients. In the latter case, the fact that the transient relaxation time is especially long just below the coil-stretch transition implies that, within such a range of Wi , experimental measures are more sensitive to statistical fluctuations.

Experiments concerning the transient relaxation to the stationary regime can investigate the time dependence of the conditional PDF $\mathcal{P}(R, t|R_0, 0)$, which corresponds to the initial condition peaked at the equilibrium size: $\mathcal{P}(R, 0|R_0, 0) = \delta(R - R_0)$. Such an initial condition can be fixed experimentally as follows. The PDF of the extension is constructed by following the motion of different polymer molecules and collecting $R(t)$ for each molecule: one should then start counting time only when the length of the corresponding polymer is approximatively R_0 . This is equivalent to selecting the initial state where all molecules have the equilibrium extension, $R(0) = R_0$.

As for the transient relaxation time, this can be measured directly from the time behaviour of the conditional moments of the extension: $\overline{R^n}(t) = \int dR R^n \mathcal{P}(R, t|R_0, 0)$, where n is a positive integer. The conditional PDF can indeed be expanded as in (6.9) and the order of series and integral can be interchanged in the definition of $\overline{R^n}$ due to the integrability of $R^n p_k(R)$ and to the uniform convergence of series (6.9) [139]. Therefore, all the moments of the extension converge to their stationary value with the same rate as the PDF of the extension.

To conclude, it is believed that the results obtained for the nonlinear dumbbell model are relevant for the comprehension of polymer dynamics in turbulent flows at any Weissenberg number. Moreover, this study may stimulate new experiments directed to investigate the transient relaxation to the stationary regime.

Bibliography

- [1] FRISCH, U. 1995 *Turbulence*. Cambridge University Press, Cambridge.
- [2] KOLMOGOROV, A. N. 1941 The local structure of turbulence in incompressible viscous fluid for very large Reynolds number. *Dokl. Akad. Nauk SSSR* **30**, 299–303.
- [3] LANOTTE, A. & MAZZINO, A. 1999 Anisotropic nonperturbative zero modes in passively advected magnetic fields. *Phys. Rev. E* **60**, R3483–R3486.
- [4] ANTONOV, N. V., LANOTTE, A. & MAZZINO, A. 2000 Persistence of small-scale anisotropies and anomalous scaling in a model of magnetohydrodynamics turbulence. *Phys. Rev. E* **61**, 6586–6605.
- [5] ANTONOV, N. V., HONKONEN, Y., MAZZINO, A. & MURATORE-GINANNESCHI, P. 2000 Manifestation of anisotropy persistence in the hierarchies of magnetohydrodynamical scaling exponents. *Phys. Rev. E* **62**, R5891–R5894.
- [6] ADZHEMYAN, L. T., ANTONOV, N. V., MAZZINO, A., MURATORE-GINANNESCHI, P. & RUNOV, A. V. 2001 Pressure and intermittency in passive vector turbulence. *Europhys Lett.* **55**, 801–806.
- [7] HNATICH, M., HONKONEN, J., JURCISIN, M., MAZZINO, A. & SPRINC, S. 2005 Anomalous scaling of passively advected magnetic field in the presence of strong anisotropy. *Phys. Rev. E* **71**, 066312.
- [8] PARISI, G. & FRISCH, U. 1985 On the singularity structure of fully developed turbulence. In *Turbulence and Predictability in Geophysical Fluid Dynamics* (eds. Ghil, M., Benzi, R. & Parisi, G.). Proceedings

- of the International School of Physics “Enrico Fermi” (1983), 84–87, North-Holland, Amsterdam.
- [9] BENZI, R., PALADIN, G., PARISI, G. & VULPIANI, A. 1984 On the multifractal nature of fully developed turbulence and chaotic systems. *J. Phys. A* **17**, 3521–3531.
- [10] OBUKHOV, A. M. 1962 Some specific features of atmospheric turbulence. *J. Fluid Mech.* **13**, 77–81.
- [11] KOLMOGOROV, A. N. 1962 A refinement of previous hypotheses concerning the local structure of turbulence in a viscous incompressible fluid at high Reynolds numbers. *J. Fluid Mech.* **13**, 82–85.
- [12] YAGLOM, A. M. 1966 Effect of fluctuations in energy dissipation rate on the form of turbulence characteristics in the inertial subrange. *Dokl. Akad. Nauk SSSR* **166**, 49–52.
- [13] MANDELBROT, B. 1974 Intermittent turbulence in self-similar cascades: divergence of high moments and dimension of the carrier. *J. Fluid Mech.* **62**, 331–358.
- [14] CRAMÉR, H. 1938 Sur un nouveau théorème-limite de la théorie des probabilités. *Actualités Scientifiques et Industrielles* **736**, 5–23.
- [15] KOLMOGOROV, A. N. 1941 Dissipation of energy in locally isotropic turbulence. *Dokl. Akad. Nauk SSSR* **32**, 16–18.
- [16] HARTE, D. 2001 *Multifractals Theory and Applications*. Chapman & Hall / CRC, Boca Raton (FL).
- [17] LANFORD, O. E. 1973 Entropy and equilibrium states in classical mechanics. In *Statistical Mechanics and Mathematical Problems* (ed. Lenard, A.). Lecture Notes in Physics **20**, 1–113, Springer, Berlin.
- [18] FELLER, W. 1968 *An Introduction to Probability Theory and its Applications, Third edition*. Vol. 1, Wiley, New York (NY).
- [19] BENDER, C. M. & ORSZAG, S. A. 1978 *Advanced Mathematical Methods for Scientists and Engineers*. McGraw-Hill, New York (NY).

-
- [20] MANDELBROT, B. 1991 Random multifractals: negative dimensions and the resulting limitations of the thermodynamic formalism. *Proc. R. Soc. Lond. A* **434**, 79–88.
- [21] BOUCHAUD, J. P. & POTTERS M. 2000 *Theory of Financial Risks*. Cambridge University Press, Cambridge.
- [22] VARADHAN, S. R. S. 1984 *Large Deviations and Applications*. SIAM, Philadelphia (PA).
- [23] ELLIS, R. S. 1985 *Entropy, Large Deviations and Statistical Mechanics*. Springer–Verlag, New York (NY).
- [24] ZOHAR, G. 1999 Large deviations formalism for multifractals. *Stoch. Proc. Appl.* **79**, 229–242.
- [25] BAHADUR, R. R. & RANGA RAO, R. 1960 On deviations of the sample mean. *Ann. Math. Stat.* **31**, 1015–1027.
- [26] DEMBO, A. & ZEITOUNI, O. 1998 *Large Deviations Techniques and Applications, Second edition*. Springer–Verlag, New York (NY).
- [27] NOVIKOV, E. A. & STEWART, R. W. 1964 The intermittency of turbulence and the spectrum of energy dissipation. *Izv., Akad. Nauk SSSR, Ser. Geoffiz.*, no. 3, 408–413.
- [28] MENEVEAU, C. & SREENIVASAN K.R. 1989 Measurement of $f(\alpha)$ from scaling of histograms, and applications to dynamical systems and fully developed turbulence. *Phys. Lett. A* **137**, 103–112.
- [29] VAN DE WATER, W. & SCHRAM, P. 1988 Generalized dimensions from near-neighbor information. *Phys. Rev. A* **37**, 3118–3125.
- [30] HOSOKAWA, I. 1991 Intrinsic Probability of a Multifractal Set. *J. Phys. Soc. Jpn.* **60**, 3983–3985.
- [31] HOSOKAWA, I. 1992 Fundamental Properties of “Homogeneous” Multifractals. *J. Phys. Soc. Jpn.* **61**, 1831–1833.
- [32] YAKHOT, V. 2005 Probability Densities in Strong Turbulence. arXiv: physics/0512102.

-
- [33] CHEKHLOV, A. & YAKHOT, V. 1995 Kolmogorov turbulence in a random-force-driven Burgers equation: anomalous scaling and probability density functions. *Phys. Rev. E* **52**, 5681–5684.
- [34] MITRA, D., BEC, J., PANDIT, R. & FRISCH U. 2005 Is multiscaling an artifact in the stochastically forced Burgers equation? *Phys. Rev. Lett.* **94**, 194501.
- [35] BIFERALE, L. & PROCACCIA, I. 2005 Anisotropy in turbulent flows and in turbulent transport. *Phys. Rep.* **414**, 43–164.
- [36] KRAICHNAN, R. H. 1968 Small-scale structure of a scalar field convected by turbulence. *Phys. Fluids* **11**, 945–953.
- [37] KRAICHNAN, R. H. 1994 Anomalous scaling of a randomly advected passive scalar. *Phys. Rev. Lett.* **72**, 1016–1019.
- [38] SREENIVASAN, K. R. & ANTONIA, R. 1997 The phenomenology of small-scale turbulence. *Ann. Rev. Fluid. Mech.* **29**, 435–472.
- [39] ARNEODO, A., BAUDET, C., BELIN, F., BENZI, R., CASTAING, B., CHABAUD, B., CHAVARRIA, R., CILIBERTO, S., CAMUSSI, R., CHILLÀ, F., DUBRULLE, B., GAGNE, Y., HEBRAL, B., HERWEIJER, J., MARCHAND, M., MAURER, J., MUZY, J. F., NAERT, A., NOULLEZ, A., PEINKE, J., ROUX, F., TABELING, P., VAN DE WATER, W. & WILLAIME, H. 1996 Structure functions in turbulence, in various flow configurations, at Reynolds number between 30 and 5000, using extended self-similarity. *Europhys. Lett.* **34**, 411–416.
- [40] KURIEN, S. & SREENIVASAN, K. R. 2000 Anisotropic scaling contributions to high-order structure functions in high-Reynolds-number turbulence. *Phys. Rev. E* **62**, 2206–2212.
- [41] WARHAFT, Z. & SHEN, X. 2002 On the higher order mixed structure functions in laboratory shear flow. *Phys. Fluids* **14**, 2432–2438.
- [42] ARAD, I., DHRUVA, B., KURIEN, S., L'VOV, V. S., PROCACCIA, I. & SREENIVASAN, K. R. 1998 Extraction of Anisotropic Contributions in Turbulent Flows. *Phys. Rev. Lett.* **81**, 5330–5333.

- [43] BIFERALE, L. & TOSCHI, F. 2001 Anisotropic Homogeneous Turbulence: Hierarchy and Intermittency of Scaling Exponents in the Anisotropic Sectors. *Phys. Rev. Lett.* **86**, 4831–4834.
- [44] BIFERALE, L., CALZAVARINI, E., TOSCHI, F. & TRIPICCIONE, R. 2003 Universality of anisotropic fluctuations from numerical simulations of turbulent flows. *Europhys. Lett.* **64**, 461–467.
- [45] GAWĘDZKI, K. & KUPIAINEN A. 1995 Anomalous scaling of the passive scalar. *Phys. Rev. Lett.* **75**, 3834–3837.
- [46] FALKOVICH, G., GAWĘDZKI, K. & VERGASSOLA, M. 2001 Particles and fields in fluid turbulence. *Rev. Mod. Phys.* **73**, 913–975.
- [47] FALKOVICH, G. & FOUXON, A. 2005 Anomalous Scaling of a Passive Scalar in Turbulence and in Equilibrium. *Phys. Rev. Lett.* **94**, 214502.
- [48] CELANI, A. & SEMINARA, A. 2005 Large-Scale Structure of Passive Scalar Turbulence. *Phys. Rev. Lett.* **94**, 214503.
- [49] FRISCH, U., MAZZINO, A. & VERGASSOLA, M. 1998 Intermittency in passive scalar advection. *Phys. Rev. Lett.* **80**, 5532–5537.
- [50] FRISCH, U., MAZZINO A. & VERGASSOLA, M. 1999 Lagrangian dynamics and high-order moments intermittency in passive scalar advection. *Phys. Chem. Earth* **24**, 945–951.
- [51] FRISCH, U., MAZZINO, A., NOULLEZ, A. & VERGASSOLA, M. 1999 Lagrangian method for multiple correlations in passive scalar advection. *Phys. Fluids* **11**, 2178–2186.
- [52] FURUTSU, K. 1963 On the statistical theory of electromagnetic waves in a fluctuating medium. *J. Res. Nat. Bur. Standards D* **67**, 303–323.
- [53] NOVIKOV, E. A. 1965 Functionals and the random-force method in turbulence theory. *Sov. Phys. JETP* **20**, 1290–1294.
- [54] DONSKER, M. D. 1964 On function space integrals. In *Proceedings of a Conference on the Theory and Applications of Analysis in Function Space* (eds. Martin, W. T. & Segal, I.), June 9–13, 1963, Dedham (MA). Ch. 2, pp. 17–30, MIT Press, Cambridge (MA).

- [55] CHERTKOV, M., FALKOVICH, G., KOLOKOLOV, I. & LEBEDEV, V. 1995 Normal and anomalous scaling of the fourth-order correlation function of a randomly advected passive scalar. *Phys. Rev. E* **52**, 4924–4941.
- [56] MONIN, A. S. & YAGLOM, A. M. 1975 *Statistical Fluid Mechanics*. MIT Press, Cambridge (MA).
- [57] SHRAIMAN, B. I. & SIGGIA, E. D. 1998 Anomalous scaling for a passive scalar near the Batchelor limit. *Phys. Rev. E* **57**, 2965–2977.
- [58] CHERTKOV, M. & FALKOVICH, G. 1996 Anomalous Scaling Exponents of a White-Advected Passive Scalar. *Phys. Rev. Lett.* **76**, 2706–2709.
- [59] ARAD, I., L'VOV, V. S. & PROCACCIA, I. 1999 Correlation functions in isotropic and anisotropic turbulence: The role of the symmetry group. *Phys. Rev. E* **59**, 6753–6765.
- [60] GRADSHTEYN, I. S. & RYZHIK, I. M. 1965 *Table of integral series and products*. Academic Press, New York (NY).
- [61] COURANT, R. & HILBERT, D. 1953 *Methods of Mathematical Physics*. Vol. 1, Interscience Publishers, New York (NY).
- [62] YAKHOT, V. & SREENIVASAN, K. R. 2005 Anomalous Scaling of Structure Functions and Dynamic Constraints on Turbulence Simulations. [arXiv: nlin.CD/0506038](https://arxiv.org/abs/nlin.CD/0506038).
- [63] MENEVEAU, C. & KATZ, J. 2000 Scale-Invariance and Turbulence Models for Large-Eddy Simulation. *Annu. Rev. Fluid Mech.* **32**, 1–32.
- [64] MCCOMB, W. D. 1992. *The Physics of Fluid Turbulence*. Oxford University Press, Oxford.
- [65] SHRAIMAN, B. I. & SIGGIA, E. D. 2000 Scalar Turbulence. *Nature* **405**, 639–646.
- [66] LESIEUR, M. 1997 *Turbulence in Fluids: Third revised and enlarged edition*. Kluwer Academic Publishers, Dordrecht.

-
- [67] BIFERALE, L., CRISANTI, A., VERGASSOLA M. & VULPIANI A. 1995 Eddy diffusivities in scalar transport. *Phys. Fluids* **7**, 2725–2734.
- [68] MAZZINO, A. 1997 Effective correlation times in turbulent scalar transport. *Phys. Rev. E* **56**, 5500–5510.
- [69] MAZZINO, A., MUSACCHIO, S. & VULPIANI, A. 2005 Multiple-scale analysis and renormalization for preasymptotic scalar transport. *Phys. Rev. E* **71**, 011113.
- [70] LEONARD, A. 1974 Energy cascade in large-eddy simulation of turbulent flows. *Adv. Geophys.* **18**, 237–248.
- [71] HORIUTI, K. 1997 A new dynamic two-parameter mixed model for large-eddy simulation. *Phys. Fluids* **9**, 3443–3464.
- [72] BORUE, V. & ORSZAG, S. A. 1998 Local energy flux and subgrid-scale statistics in three-dimensional turbulence. *J. Fluid Mech.* **366**, 1–31.
- [73] KANG, H. S. & MENEVEAU, C. 2001 Passive scalar anisotropy in a heated turbulent wake: new observations and implications for largeeddy simulations. *J. Fluid Mech.* **442**, 161–170.
- [74] RISKEN, H. 1989 *The Fokker–Planck Equation: Methods of Solutions and Applications, Second Edition*. Springer–Verlag, Berlin.
- [75] GARDINER, C. W. 1985 *Handbook of Stochastic Methods: for Physics, Chemistry and the Natural Sciences, Second Edition*. Springer–Verlag, Berlin.
- [76] CELANI, A., LANOTTE, A., MAZZINO, A. & VERGASSOLA, M. 2001 Fronts in passive scalar turbulence. *Phys. Fluids* **13**, 1768–1783.
- [77] SCOTTI, A. & MENEVEAU, C. 1997 Fractal model for coarse grained non linear partial differential equation. *Phys. Rev. Lett.* **78**, 867–870.
- [78] BASU, S., FOUFOULA-GEORGIU, E. & PORTÉ-AGEL, F. 2004 Synthetic Turbulence, Fractal Interpolation and Large-Eddy Simulation. *Phys. Rev. E* **70**, 026310.

-
- [79] ZINN-JUSTIN, J. 1989 *Quantum field theory and critical phenomena*, Oxford Academic Press, Oxford.
- [80] BALKOVSKY, E. & LEBEDEV, V. 1998 Instanton for the Kraichnan passive scalar problem. *Phys. Rev. E* **58**, 5776–5795.
- [81] CELANI, A., LANOTTE, A., MAZZINO, A. & VERGASSOLA, M. 2000 Universality and saturation of intermittency in passive scalar turbulence. *Phys. Rev. Lett.* **84**, 2385–2388.
- [82] CELANI, A., MAZZINO, A. & VERGASSOLA, M. 2001 Thermal plume turbulence. *Phys. Fluids* **13**, 2133–2135.
- [83] ANTONELLI, M., MAZZINO, A. & RIZZA, U. 2003 Statistics of temperature fluctuation in a buoyancy-dominated boundary layer flow simulated by a Large-Eddy Simulation model. *J. Atmos. Sci.* **60**, 215–224.
- [84] MOENG, C.H. & SULLIVAN, P. P. 1994 A comparison of shear and buoyancy driven Planetary Boundary Layer flows. *J. Atmos. Sci.* **51**, 999–1021.
- [85] MOENG, C. H. 1984 A large-eddy-simulation model for the study of planetary boundary-layer turbulence. *J. Atmos. Sci.* **41**, 2052–2062.
- [86] SULLIVAN, P. P., MCWILLIAMS, J. C. & MOENG, C. H. 1994 A subgrid-scale model for large-eddy simulation of planetary boundary layer flows. *Bound. Layer Meteorol.* **71**, 247–276.
- [87] MOENG, C. H. & WYNGAARD, J. C. 1989 Evaluation of turbulent transport and dissipation closures in second-order modeling. *J. Atmos. Sci.* **46**, 2311–2330.
- [88] ANDRÉN, A. & MOENG, C. H. 1993 Single-point closure in a neutrally stratified boundary layer. *J. Atmos. Sci.* **50**, 3366–3379.
- [89] NIEUWSTADT, F. T. M. & BROST, R. A. 1986 The decay of convective turbulence. *J. Atmos. Sci.* **43**, 532–546.
- [90] GARRAT, J. R. 1992 *The atmospheric boundary layer*. Cambridge University Press, Cambridge.

-
- [91] DEARDORFF, J. W. 1972 Numerical investigation of the planetary boundary layer with an inversion lid. *J. Atmos. Sci.* **29**, 91–115.
- [92] CELANI, A., MATSUMOTO, T., MAZZINO, A. & VERGASSOLA, M. 2002 Scaling and Universality in turbulent convection. *Phys. Rev. Lett.* **88**, 054503.
- [93] ZHOU, S. Q. & XIA, K. Q. 2002 Plume statistics in thermal turbulence: mixing of an active scalar. *Phys. Rev. Lett.* **89**, 184502.
- [94] BOLGIANO, R. 1959 Turbulent spectra in a stably stratified atmosphere. *J. Geophys. Res.* **64**, 2226–2229.
- [95] STAICU, A. & VAN DE WATER, W. 2003 Small scale velocity jumps in shear turbulence. *Phys. Rev. Lett.* **90**, 094501.
- [96] BALKOVSKY, E., FALKOVICH, G. & FOUXON, A. 2001 Intermittent distribution of inertial particles in turbulent flows. *Phys. Rev. Lett.* **86**, 2790–2793.
- [97] FALKOVICH, G., FOUXON, A. & STEPANOV, M. G. 2002 Acceleration of rain initiation by cloud turbulence. *Nature* **419**, 151–154.
- [98] FALKOVICH, G. & PUMIR, A. 2004 Intermittent distribution of heavy particles in a turbulent flow. *Phys. Fluids* **16**, L47–L50.
- [99] FALKOVICH, G., STEPANOV, M. & VUCELJA, M. 2005 Rain initiation time in turbulent warm clouds. *arXiv: physics/0411201*.
- [100] CELANI, A., FALKOVICH, G., MAZZINO, A. & SEMINARA, A. 2005 Droplet condensation in turbulent flows. *Europhys. Lett.* **70**, 775–781.
- [101] BRACCO, A., CHAVANIS, P. H., PROVENZALE, A. & SPIEGEL, E. A. 1999 Particle aggregation in a turbulent Keplerian flow. *Phys. Fluids* **11**, 1120–2287.
- [102] MATARRESE, S. & MOHAYEE, R. 2002 The growth of structure in the intergalactic medium. *Mon. Not. R. Astr. Soc.* **329**, 37–60.
- [103] KÁROLYI, G., PÉNTÉK, Á., SCHEURING, I., TÉL, T. & TOROZKAI, Z. 2000 Chaotic flow: the physics of species coexistence. *Proc. Natl. Acad. Sci.* **97**, 13661–13665.

-
- [104] RUIZ, J., MACÍAS, D. & PETERS, P. 2004 Turbulence increases the average settling velocity of phytoplankton cells. *Proc. Natl. Acad. Sci.* **101**, 17720–17724.
- [105] BENSOUSSAN, A., LIONS, J. L. & PAPANICOLAOU, G. 1978 *Asymptotic Analysis of Periodic Structures*. North-Holland, Amsterdam.
- [106] VERGASSOLA, M. & AVELLANEDA, M. 1997 Scalar transport in compressible flow. *Physica D* **106**, 148–166.
- [107] PAVLIOTIS, G. A., STUART, A. M. & BAND, L. 2005 Monte Carlo Studies of Effective Diffusivities for Inertial Particles. In *Proceedings of MC2QMC2004* (ed. Talay, D.), June 7–10, 2004, Juan-les-Pins. Springer-Verlag, Berlin.
- [108] PAVLIOTIS, G. A. & STUART, A. M. 2005 Periodic homogenization for inertial particles. *Physica D* **204**, 161–187.
- [109] SPELT, P. D. M. & BIESHEUVEL, A. 1997 On the motion of gas bubbles in homogeneous isotropic turbulence. *J. Fluid Mech.* **336**, 221–244.
- [110] SPELT, P. D. M. & BIESHEUVEL, A. 1998 Dispersion of Gas Bubbles in Large-Scale Homogeneous Isotropic Turbulence. *Appl. Sci. Res.* **58**, 463–482.
- [111] POORTE, R. E. G. & BIESHEUVEL, A. 2002 Experiments on the motion of gas bubbles in turbulence generated by an active grid. *J. Fluid Mech.* **461**, 127–154.
- [112] MAZZITELLI, I. M. & LOHSE, D. 2004 Lagrangian statistics for fluid particles and bubbles in turbulence. *New J. Phys.* **6**, no. 203, pp. 1–28.
- [113] CASTIGLIONE, P. & CRISANTI, A. 1999 Dispersion of passive tracers in a velocity field with non- δ -correlated noise. *Phys. Rev. E* **59**, 3926–3934.
- [114] MAXEY, M. R. & RILEY, J. J. 1983 Equation of motion for a small rigid sphere in a nonuniform flow. *Phys. Fluids* **26**, 883–889.
- [115] GYR, A. & BEWERSDORFF, H. W. 1995 *Drag reduction of turbulent flows by additives*. Kluwer Academic Publishers, Dordrecht.

- [116] BIRD, R. B., HASSAGER, O., ARMSTRONG, R. C. & CURTISS, C. F. 1977 *Dynamics of Polymeric Liquids, Kinetic Theory*. Vol. 2, Wiley, New York.
- [117] MARKO, J. F. & SIGGIA, E. D. 1995 Stretching DNA. *Macromolecules* **28**, 8759–8770.
- [118] DE GENNES, P. G. 1974 Coil-stretch transition of dilute flexible polymer under ultra-high velocity gradients. *J. Chem. Phys.* **60**, 5030–5042.
- [119] PERKINS, T. T., SMITH, D. E. & CHU, S. 1997 Single Polymer Dynamics in an Elongational Flow. *Science* **276**, 2016–2021.
- [120] SMITH, D. E., BABCOCK, H. P. & CHU, S. 1999 Single-Polymer Dynamics in Steady Shear Flow. *Science* **283**, 1724–1727.
- [121] HUR, J. S., SHAQFEH, E. S., BABCOCK, H. P. & CHU, S. 2002 Dynamics and configurational fluctuations of single DNA molecules in linear mixed flows. *Phys. Rev. E* **66**, 011915.
- [122] BABCOCK, H. P., TEIXEIRA, R. E., HUR, J. S., SHAQFEH, E. S. & CHU, S. 2003 Visualization of Molecular Fluctuations near the Critical Point of the Coil-stretch Transition in Polymer Elongation. *Macromolecules* **36**, 4544–4548.
- [123] GROISMAN, A. & STEINBERG, V. 2000 Elastic turbulence in a polymer solution flow. *Nature* **405**, 53–55.
- [124] GERASHCHENKO, S., CHEVALLARD, C. & STEINBERG, V. 2005 Single polymer dynamics: coil-stretch transition in a random flow. *Europhys. Lett.* **71**, 221–227.
- [125] CHERTKOV, M. 2000 Polymer Stretching by Turbulence. *Phys. Rev. Lett.* **84**, 4761–4764.
- [126] BALKOVSKY, E., FOUXON, A. & LEBEDEV, V. 2000 Turbulent Dynamics of Polymer Solutions. *Phys. Rev. Lett.* **84**, 4765–4768.
- [127] CELANI, A., MUSACCHIO, S. & VINCENZI, D. 2005 Polymer transport in random flow. *J. Stat. Phys.* **118**, 529–552.

-
- [128] THIFFEAULT, J. L. 2003 Finite extension of polymers in turbulent flow. *Phys. Lett. A* **308**, 445–450.
- [129] KRAICHNAN, R. H. 1974 Convection of a passive scalar by a quasi-uniform random straining field. *J. Fluid Mech.* **64**, 737–762.
- [130] KLYATSKIN, V. I., WOYCZYNSKI, W. A. & GURARIE, D. 1996 Short-time correlation approximations for diffusing tracers in random velocity fields: A functional approach. In *Stochastic Modeling in Physical Oceanography* (ed. Adler, R. J.). Progress in Probability **39**, 221–270, Birkhauser, Basel.
- [131] RONVEAUX, A. 1995 *Heun's Differential Equations*. Oxford University Press, Oxford.
- [132] WHITTAKER, E. T. & WATSON, G. N. 1996 *A Course of Modern Analysis, Fourth Edition*. Cambridge University Press, Cambridge.
- [133] ERDÉLYI, A. 1944 Certain expansions of solutions of the Heun equation. *Q. J. Math. (Oxford Series)* **15**, 62–69.
- [134] PRESS, W. H., FLANNERY, B. P., TEUKOLSKY, S. A. & VETTERLING, W. T. 1993 *Numerical Recipes*. Cambridge University Press, Cambridge.
- [135] CHERTKOV, M., KOLOKOLOV, I., LEBEDEV, V. & TURITSYN K. 2005 Statistics of Polymer Extension in a Random Flow with Mean Shear. *J. Fluid Mech.* **531**, 251–260.
- [136] CELANI, A., PULIAFITO, A. & TURITSYN, K. 2005 Polymers in linear shear flow: a numerical study. *Europhys. Lett.* **70**, 464–470.
- [137] PULIAFITO, A. & TURITSYN, K. 2005 Numerical study of polymer tumbling in linear shear flows *Physica D* **211**, 9–22.
- [138] TURITSYN, K. 2005 Polymer dynamics in chaotic flows with strong shear component. [arXiv: nlin.CD/0501025](https://arxiv.org/abs/nlin.CD/0501025).
- [139] SMIRNOV, V. 1984 *Cours de Mathématiques Supérieures*. Vol. 4, 2nd part. MIR, Moscow.

Summary - Riassunto

This thesis encompasses analytical, and also numerical, work within the general framework of hydrodynamical turbulence. It is divided into three parts. The first part is devoted to the study of the degree of universality and self-similarity at different scales, which is a key point in the classical view of ideal turbulence. Analysis is performed both on the velocity field, investigating its scaling exponents, and on passive scalars advected by it, in the presence of “nonideal” (e.g. inhomogeneous, even point-like) sources: comparisons with the corresponding homogeneous situations are performed, in order to verify a possible small-scale restoration of homogeneity, i.e. of ideality.

The second part moves to a large-scale study of turbulence. First, large-eddy simulation closures for the passive scalar are derived systematically from first principles in the Kraichnan advection model. Subsequently, they are applied to the numerical study of a practical situation (the atmospheric boundary layer), also in order to verify some of the issues raised in the previous part. In the third part, I analyse the dynamics of complex particles, which (despite disregarding their feedback on the flow) do not fit the passive-scalar description. More specifically, I focus on the falling velocity of inertial particles (for which inertia, gravity and advection interact in a nontrivial way) in the Stokes regime and on the study of relaxation time of probability density functions of polymers in the FENE model for Batchelor–Kraichnan flows.

Modelli analitici di turbolenza: dalle piccole alle grandi scale, e oltre

Questa tesi raccoglie studi analitici, e numerici, svolti nell’ambito della turbolenza fluidodinamica. Essa è divisa in tre parti.

La prima parte riguarda lo studio del grado di universalità e autosimilarità

alle diverse scale, cardine dello scenario classico della turbolenza. Ho analizzato sia il campo di velocità, studiando i suoi esponenti di scala, sia il trasporto di scalare passivo, in presenza di sorgenti non ideali (in particolare disomogenee, come la sorgente puntiforme): la verifica di un possibile ripristino a piccola scala dell'omogeneità, cioè dell'idealità, è stata svolta mediante un costante paragone con la controparte omogenea.

Nella seconda parte mi sono concentrato sullo studio delle grandi scale in turbolenza. Dapprima, ho sistematicamente derivato dai principi primi le chiusure LES nel modello di avvezione di Kraichnan per lo scalare passivo. Successivamente, ho applicato la tecnica LES allo studio di una situazione di notevole interesse pratico, lo strato limite atmosferico, anche per verificare alcuni degli argomenti costituenti la parte precedente.

Nell'ultima parte, ho analizzato la dinamica di particelle complesse, che non rientrano nella modellizzazione di scalare passivo (pur avendo trascurato la loro retroazione sul flusso). In particolare, ho studiato la velocità di caduta di particelle inerziali (per cui inerzia, gravità e trasporto interagiscono in modo non banale) nel regime di Stokes e il tempo di rilassamento delle PDF di molecole polimeriche nel modello FENE per flussi di Batchelor–Kraichnan.